Investigating the onset of insulin resistance and non-alcoholic fatty liver disease in obesity-induced cardiac dysfunction

Anél W Boshoff

Thesis presented in fulfilment of the requirements for the degree of
Master of Medical Science (Medical Physiology)
Division of Medical Physiology, Faculty of Medicine and Health Sciences,
Stellenbosch University

Supervisor: Dr Rabia Johnson
Co-supervisor: Prof Barbara Huisamen
Co-supervisor: Dr Kwazi Gabuza

April 2019

Declaration

By submitting this thesis electronically, I declare that the entirety of the work contained therein is my own, original work, that I am the sole author thereof (save to the extent explicitly otherwise stated), that reproduction and publication thereof by Stellenbosch University will not infringe any third party rights and that I have not previously in its entirety or in part submitted it for obtaining any qualification.

Date: April 2019

Acknowledgements

I would like to thank the following individuals and institutions for their valuable contributions to the completion of this project:

The Biomedical Research and Innovation Platform of the South African Medical Research Council, for use of facilities and financial support, as well as Prof Johan Louw and Prof Christo Muller for giving me the opportunity and resources to complete this project. The National Research Foundation for financial support (Thuthuka Grant IUD 107261). And the Division of Medical Physiology, Stellenbosch University, for academic support.

My supervisor, Dr Rabia Johnson, for your endless patience and willingness to give guidance where needed. I have grown a great deal while under your supervision and appreciate everything you did for me and this project. My co-supervisors, Prof Barbara Huisamen and Dr Kwazi Gabuza, for always being available to provide a fresh perspective on technical or theoretical questions. The Cardiometabolism group, Xolisa Nxele, Ebrahim Samodien and Lawrence Mabasa, for always being willing to assist. Ruzayda van Aarde, Charna Chapman and Samira Ghoor for technical support. Sandi Bowles and Nireshni Chellan for moral support and great conversation.

My dearest friends, Dani Millar and Simoné Nel, for always being there, for all the proof-reading and wine-drinking and scientific banter. My Mam and my sister, for your unending love and support, and for always being eager to learn about what it is that I do. My Paps, for inspiring me to be curious and tenacious in the pursuit of knowledge. My Buddy, Anton Huysamer, your unwavering positive attitude has never failed to make me smile. Every day with you is filled with adventure and sunshine and pure happiness.

Outputs during the study

1. Symposia

- **Boshoff, A.W.,** Huisamen, B., Gabuza, K. & Johnson, R. Understanding the liver to protect the heart: the role that non-alcoholic fatty liver disease plays in the disease progression of diabetes-induced cardiac dysfunction. **Oral presentation**, Biomedical Research and Innovation Platform, Annual Research Symposium, Cape Town, South Africa, October 2017

- **Boshoff, A.W.,** Huisamen, B., & Johnson, R. Investigating the onset of insulin resistance and non-alcoholic fatty liver disease in obesity-induced myocardial dysfunction. **Oral presentation**, Biomedical Research and Innovation Platform, Annual Research Symposium, Cape Town, South Africa, October 2018.

2. Conferences

- **Boshoff, A.W.,** Huisamen, B., Lecour, S., Muller, C. & Johnson, R. Understanding the liver to protect the heart: Investigating the link between insulin resistance and non-alcoholic fatty liver disease in obesity-induced myocardial dysfunction. **Poster presentation**, Academic Year Day, Tygerberg Medical Campus, Stellenbosch University, South Africa, August 2018

- **Boshoff, A.W.,** Huisamen, B., Lecour, S., Muller, C. & Johnson, R. Understanding the liver to protect the heart: Investigating the link between insulin resistance and non-alcoholic fatty liver disease in obesity-induced myocardial dysfunction. **Poster presentation**, First Conference of Biomedical and Natural Sciences and Therapeutics, Stellenbosch, South Africa, October 2018

- **Boshoff, A.W.,** Huisamen, B., Muller, C., Lecour, S. & Johnson, R. Investigating the onset of insulin resistance and non-alcoholic fatty liver disease in obesity-induced cardiac dysfunction. **Oral presentation**, Department of Biomedical Sciences Annual Research Day, Tygerberg Medical Campus, Stellenbosch University, South Africa, November 2018

3. Awards

Boshoff, A.W., Huisamen, B., & Johnson, R. Investigating the onset of insulin resistance and non-alcoholic fatty liver disease in obesity-induced myocardial dysfunction. Oral presentation, Biomedical Research and Innovation Platform, Annual Research Symposium, Cape Town, South Africa, October 2018. **Awarded Best MSc Oral Presentation**

4. Publications

- Johnson, R., **Boshoff, A.W.,** Huisamen, B., Lecour, S., Cour, M., Louw, J., Muller, C. Hepatic steatosis: a cause or consequence of muscle insulin resistance and subsequent cardiac dysfunction in a leptin receptor-deficient db/db mice model. **Submitted manuscript**. International Journal of Molecular Sciences. Manuscript ID: ijms-400575. Received: 18 November 2018 (Appendix C)

Contents

List of Abbreviations

°C	Degrees Celsius
% EF	Percent ejection fraction
ACTB	Beta-actin
AKT	Protein Kinase B
AGE	Advanced glycation end-products
ALT	Alanine transferase
AMPK	Adenosine monophosphate-activated protein kinase
ANOVA	Analysis of variance
ApoB	Apolipoprotein B
AST	Aspartate transaminase
B2M	Beta 2 microglobulin
BAT	Brown adipose tissue
BMI	Body mass index
BSA	Bovine serum albumin
CAMK2	Ca^{2+}/calmodulin dependent protein kinase 2
CD36	Cluster of differentiation 36
cDNA	Complementary deoxyribonucleic acid
CPT1	Carnitine palmitoyl transferase 1
CRP	C-reactive protein
CT	Threshold cycle
CTGF	Connective tissue growth factor
CVD	Cardiovascular disease
DAG	Diacyl glycerol
dH_2O	Distilled water
DNA	Deoxyribonucleic acid
ECL	Enhanced chemiluminescence
ECM	Extracellular matrix
ECRA	Ethics Committee for Research on Animals
ELISA	Enzyme-linked immunosorbent assay
EtOH	Ethanol
FASN	Fatty acid synthase
FFA	Free fatty acid
FHBL	Familial hypobetalipoproteinaemia

GLUT4	Glucose transporter 4
GSK3β	Glycogen synthase kinase 3 beta
HOMA-IR	Homeostasis model assessment of insulin resistance
H&E	Haematoxylin & Eosin
HDL	High-density lipoprotein
HFHS	High-fat, high-sugar
Hmgcr	3-Hydroxy-3-Methylglutaryl-CoA Reductase
HPRT1	Hypoxanthine phosphoribosyl transferase 1
HRP	Horseradish peroxidase
IκBα	Inhibitor of kappa B alpha
IGF-1	Insulin-like growth factor 1
IKKβ	Inhibitor of kappa B kinase beta
IL6	Interleukin6
IRS1	Insulin receptor substrate 1
JNK	Jun N-terminal substrate
kDa	Kilo Dalton
LCFA	Long-chain fatty acid
LDL	Low-density lipoprotein
Lepr$^{db/db}$	Leptin receptor-deficient
LV	Left ventricular
LVDD	Left ventricular diastolic dysfunction
Malonyl-CoA	Malonyl coenzyme A
MetS	Metabolic syndrome
mRNA	Messenger ribonucleic acid
NAFLD	Non-alcoholic fatty liver disease
NASH	Non-alcoholic steatohepatitis
NCD	Non-communicable disease
NCEP	National Cholesterol Education Program
NEFA	Non-esterified fatty acids
NFκB	Nuclear factor κ-B
NOX4	NADPH Oxidase 4
NPPA	Natriuretic peptide precursor A
ORO	Oil red O
PBS	Phosphate buffered saline
PCR	Polymerase chain reaction

PDGF	Platelet-derived growth factor
PKCθ	Protein kinase C theta
PI3K	Phosphoinositide 3-kinase
PNPLA2	Patatin-like phospholipase domain-containing protein 2
PNPLA3	Patatin-like phospholipase domain-containing protein 3
PPARγ	Peroxisome proliferator-activated receptor gamma
PPARα	Peroxisome proliferator-activated receptor alpha
PUDAC	Primate Unit and Delft Animal Centre
PVDF	Polyvinylidene fluoride
qRT-PCR	Quantitative reverse transcription polymerase chain reaction
RAGE	Receptor of AGE
RNA	Ribonucleic acid
SAMRC	South African Medical Research Council
SAT	Subcutaneous adipose tissue
SCD1	Stearoyl-coenzyme A desaturase 1
SEM	Standard error of the mean
Ser	Serine
SERCA	Sarco/endoplasmic reticulum Ca^{2+}-ATPase
SREBF1	Sterol regulatory element binding factor 1
SAT	Subcutaneous adipose tissue
T2DM	Type 2 diabetes mellitus
TBS	Tris-buffered saline
TBS-T	Tris-buffered saline containing Tween 20
TDI	Tissue Doppler Imaging
TGFβ	Tissue growth factor beta
TLR4	Toll-like receptor 4
TNFα	Tumour necrosis factor alpha
TNFR1	TNFα receptor 1
Tyr	Tyrosine
VAT	Visceral adipose tissue
VLDL	Very low-density lipoprotein
WAT	White adipose tissue
WHO	World Health Organization

List of Figures

List of Tables

List of Appendices

Abstract

Introduction: The global obesity epidemic has been associated with various metabolic disorders, including insulin resistance and non-alcoholic fatty liver disease (NAFLD). Insulin resistance is thought be a hallmark of NAFLD, which is an established risk factor for the development of type 2 diabetes mellitus (T2DM) and cardiac dysfunction. Conversely, evidence exists to suggest that NAFLD can develop despite conserved insulin sensitivity, and that it can play a role in the development of insulin resistance. While both insulin resistance and NAFLD are known to contribute to cardiac dysfunction, it is not evident which develops first. With the rising burden of obesity-related heart disease, it is vital to gain a better understanding of the pathophysiology involved in order to better treat or prevent heart failure.

Aim: To investigate the order of onset of NAFLD and insulin resistance in obesity-induced cardiac dysfunction.

Methods: Six- to fifteen-week-old male leptin receptor deficient (*Lepr*$^{db/db}$) mice and their lean littermate controls (*Lepr*$^{db/+}$) were monitored weekly to measure fasting blood glucose and body weight. Heart function was determined weekly using TDI echocardiography, after which 8 animals per group were terminated. Serum was collected to measure lipogram and liver enzymes, while muscle, liver and heart tissue were used to investigate insulin resistance, NAFLD, and cardiac dysfunction, respectively.

Results: Data obtained showed that *Lepr*$^{db/db}$ mice had increased body weight (31.75 g ± 0.71 vs. 20.50 g ± 0.55, $p < 0.001$) and total cholesterol (3.90 mmol/L ± 0.14 vs. 1.90 mmol/L ± 0.04, $p < 0.001$) by 6 weeks of age. Serum AST/ALT ratio (0.76 ± 0.07) indicated hepatic lipid accumulation by 7 weeks and histological analysis confirmed the presence of NAFLD at this time, as well as its progression in severity with age. Gene expression analysis in the liver showed an increase in lipogenic genes *FASN* (1.16 ± 0.18 vs. 0.25 ± 0.05, $p < 0.01$) and *SCD1* (1.03 ± 0.08 vs. 0.20 ± 0.05, $p < 0.001$) by 7 weeks of age. Muscle insulin resistance was not present at the onset of NAFLD, and developed around 10 weeks of age, as confirmed by a decrease in pPI3K and pAKT protein expression (0.17 ± 0.03 vs 0.10 ± 0.01, $p < 0.01$ and 0.23 ± 0.06 vs 0.12 ± 0.03, $p < 0.05$, respectively). Gene expression analysis confirmed an increase in oxidative stress *NOX4* (1.23 ± 0.30 vs. 0.77 ± 0.09, $p < 0.05$), inflammation *NFκB* (1.68 ± 0.09 vs. 0.69 ± 0.04, $p < 0.001$) and apoptosis *CASP3* (1.42 ± 0.10 vs. 1.06 ± 0.06, $p < 0.05$) in the heart of *Lepr*$^{db/db}$ mice by 10 weeks.

Conclusion: Hepatic steatosis preceded muscle insulin resistance in a genetic model of obesity, and likely contributed to the development of insulin resistance and myocardial dysfunction.

Opsomming

Inleiding: Die wêreldwye vetsug epidemie is geassosieer met verskeie metabolies afwykings, insluitend insulien weerstandigheid en nie-alkoholiese vetterige lewer siekte (NAFLD). Insulien weerstandigheid word beskou as 'n kenmerk van NAFLD, wat 'n gevestigde risikofaktor is vir die ontwikkeling van tipe 2 diabetes mellitus (T2DM) en kardiale disfunksie. Daarenteen bestaan bewyse dat NAFLD kan ontwikkel ondanks die behoud van insulien sensitiwiteit, en dat dit 'n rol kan speel in die ontwikkeling van insulien weerstandigheid. Alhoewel beide insulienweerstandigheid en NAFLD bekend is om by te dra tot hartafwykings in vetsug, is dit nie duidelik wat eerste ontwikkel nie. Met die stygende las van vetsugverwante hartsiektes is dit noodsaaklik om die risikofaktore wat betrokke is om hartversaking beter te verstaan en in sodoende, beter te behandel of te voorkom.

Doelstelling: Om die volgorde van aanvang van NAFLD en insulienweerstandigheid in vetsugverwante hartafwykings te ondersoek.

Metodes: Ses tot vyftien week-oue manlike leptien-reseptor-gebrekkige (*Lepr*$^{db/db}$) -muise en hul maer beheerkontroles (Lepr$^{db/+}$) is weekliks gemonitor om bloedglukose en liggaamsgewig te meet. Hartfunksie is weekliks vasgestel met behulp van TDI-ekkokardiografie, waarna 8 diere per groep beëindig is. Serum is ingesamel om lipogram en lewer ensieme te meet, terwyl spier-, lewer- en hartweefsel gebruik is om insulienweerstandigheid, NAFLD en hartafwykings onderskeidelik te ondersoek.

Resultate: Die data wat verkry is, het getoon dat *Lepr*$^{db/db}$-muise hoër gewig (31,75 g ± 0,71 vs. 20,50 g ± 0,55, p <0,001) en totale cholesterol (3,90 mmol / L ± 0,14 teenoor 1,90 mmol / L ± 0,04, p <0,001) gehad het teen 6 weke oud. Serum AST/ALT-verhouding (0.76 ± 0.07) het lewer lipiedakkumulasie teen 7 weke aangedui en histologiese analise het die teenwoordigheid van NAFLD op hierdie tydstip bevestig, sowel as die ontwikkelling daarvan in erns met ouderdom. Gene-ekspressie-analise in die lewer het 'n toename in lipogene gene *FASN* (1.16 ± 0.18 vs. 0.25 ± 0.05, p <0.01) en *SCD1* (1.03 ± 0.08 vs. 0.20 ± 0.05, p <0.001) teen 7 weke oud. Spierinsulienweerstand was nie teenwoordig by die aanvang van NAFLD nie, en ontwikkel ongeveer 10 weke oud, soos bevestig deur 'n afname in pPI3K- en pAKT-proteïenuitdrukking (0.17 ± 0.03 vs 0.10 ± 0.01, p <0.01 and 0.23 ± 0.06 vs 0.12 ± 0,03, p <0,05, onderskeidelik). Gene-ekspressie-analise bevestig 'n toename in oksidatiewe stres *NOX4* (1.23 ± 0.30 vs. 0.77 ± 0.09, p <0.05), inflammasie *NFκB* (1,68 ± 0.09 vs. 0.69 ± 0.04,

p <0.001) en apoptose *CASP3* (1.42 ± 0.10 vs. 1.06 ± 0.06, p <0.05) in die hart van *Lepr*$^{db/db}$ muise teen 10 weke.

Gevolgtrekking: Lewer steatosis kom voor spier insulien weerstandigheid voor in 'n genetiese model van vetsug, en dra waarskynlik by tot die ontwikkeling van insulien weerstand en miokardiale afwykings.

Chapter 1: Literature Review

1.1 Non-communicable diseases

Non-communicable diseases (NCDs) are chronic, non-transmissible and slow-progressing conditions that include cardiovascular disease (CVD), respiratory disease, cancer and diabetes. The World Health Organization (WHO) has identified smoking of tobacco products, excessive alcohol consumption, lack of physical activity and an unhealthy diet as the main risk factors associated with the development of NCDs (WHO, 2017). While these risk factors are largely modifiable, NCDs have continued to increase in prevalence and are now responsible for 71% of all global deaths, far exceeding the number of deaths caused by communicable diseases (Figure 1.1). Of the four main NCDs, CVD is the most prevalent, comprising 44% of NCD cases and causing 17.9 million deaths in 2016 (WHO, 2018).

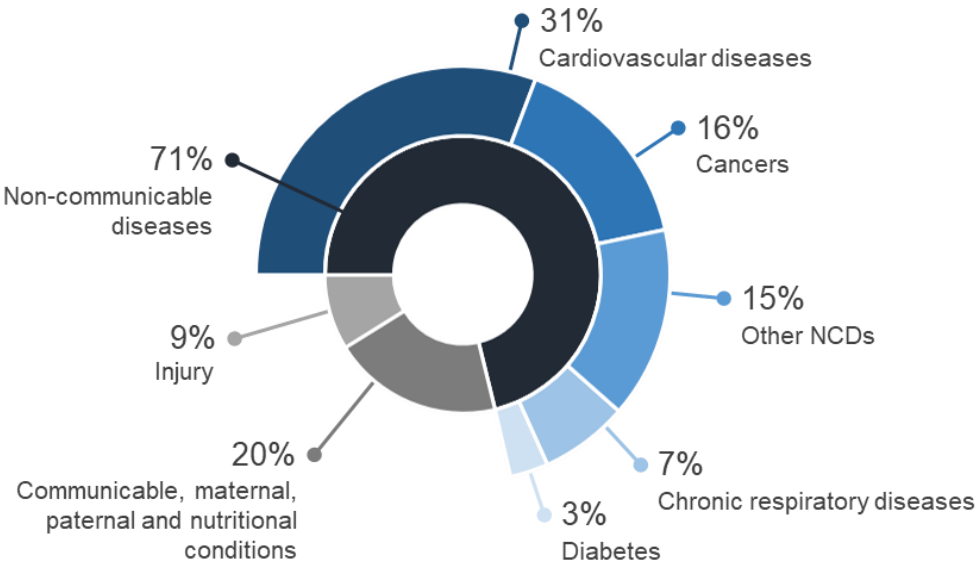

***Figure 1.1: Global causes of death**. Causes of death worldwide as a % of total deaths among all ages and genders in 2016. Adapted from World Health Organization noncommunicable diseases country profiles, 2018*

1.2 Cardiovascular disease

Cardiovascular disease is a term that encompasses a wide range of conditions involving narrowed or blocked heart vessels that can result in heart failure. Of these conditions, atherosclerotic heart disease, such as coronary artery disease and stroke, are widely studied and relatively well-understood (Mandviwala, et al., 2016; Leong, et al., 2017). Additionally, in 1972 Rubler, et al. identified a heart condition that results in structural and functional changes

to the myocardium, in the absence of coronary artery disease or hypertension, as a consequence of metabolic perturbations such as obesity, insulin resistance, and type 2 diabetes mellitus (T2DM). These structural and functional changes, further referred to as cardiac dysfunction, develop slowly and are aggravated due to increased gluco- and lipotoxicity induced by the hyperglycaemic and hyperlipidaemic state. It has been proposed that a shift in substrate preference, due to metabolic inflexibility, plays a central role in the pathophysiology of cardiac dysfunction. This alteration in energy metabolism markedly increases oxidative stress, hypertrophy, and interstitial fibrosis, resulting in myocardial structural modifications with impaired cardiac relaxation and reduced left ventricular ejection fraction (LVEF).

These subtle changes are initially asymptomatic and cannot be detected, except with the use of image modalities such as Tissue Doppler Imaging (TDI) echocardiography or Speckle Tracking echocardiography (Goland, et al., 2006; Stevanovic & Dekleva, 2018). However, early intervention for cardiac dysfunction is difficult, as it only becomes clinically evident late in disease progression when the damage is irreversible (Loncarevic, et al., 2016; Borghetti, et al., 2018). Encouragingly, most CVDs, including cardiac dysfunction, can be prevented by addressing the preceding risk factors (WHO, 2017) and as such, it is important to understand the pathophysiology of these underlying conditions.

1.3 Metabolic syndrome

Metabolic syndrome (MetS) is a term used to describe a cluster of metabolic abnormalities that increases an individual's risk of developing CVD (Reaven, 2011; Rask-Madsen & Kahn, 2012). The exact characterization of MetS differs between countries; however, in 2001 the National Cholesterol Education Program (NCEP) introduced a simple yet reliable clinical definition. According to this definition, MetS is characterized by five risk factors, including; abdominal obesity (waist circumference > 88 cm in women and > 102 cm in men), impaired fasting blood glucose (5.6 - 6.9 mmol/L), increased triglycerides (> 1.7 mmol/L), reduced high-density lipoprotein (HDL) (< 1.3 mmol/L in women and < 1 mmol/L in men), and chronic hypertension (systolic blood pressure > 130 mmHg and diastolic blood pressure > 85 mmHg) (Paschos & Paletas, 2009). The occurrence of one of these conditions increases an individual's risk of developing CVD, while the co-occurrence of three or more conditions results in a diagnosis of MetS and infers a significantly elevated risk of CVD (Gurka, et al., 2018).

More recently, non-alcoholic fatty liver disease (NAFLD) has also been recognized as part of MetS, as individuals with NAFLD exhibit a worsened cardiometabolic phenotype, accompanied by impaired systolic and diastolic function (Fotbolcu, et al., 2010; Karabay, et al., 2014). Non-alcoholic fatty liver disease can be defined as a condition in which excess lipids are accumulated in more than 5% of the liver, in the absence of excess alcohol consumption (Birkenfeld & Shulman, 2014). Not only is NAFLD the most common liver disease in the Western world (Ahmed, 2015), but it is also closely associated with obesity, with an estimated 80 - 90% of obese patients suffering from intrahepatic lipid accumulation (Gaggini, et al., 2013).

1.4 **Obesity**

One of the most prominent conditions associated with MetS is visceral obesity, also known as central or abdominal obesity. Visceral obesity refers to the accumulation of excessive fat stores within and around the abdominal cavity, including fat stores around internal organs such as the heart, liver, and pancreas. According to the WHO, an individual with a body mass index (BMI) > 25 kg/m^2 is classified as overweight, while an individual with a BMI > 30 kg/m^2 is considered obese. Obesity has become a global epidemic and it is estimated that 39% of adults are overweight and 13% are obese, while in South Africa, 53.8% of adults are overweight and 28.3% are obese (WHO, 2018). Furthermore, it is estimated that there will be a 33% increase in obesity worldwide by 2030 (Finkelstein, et al., 2012).

Studies have shown that obese individuals have increased lipid stores. However, lipid stores within the body are not inherently pathological, as a small amount of fat (3 - 5% in men and 12 - 15% in women) is required for normal body function. Lipids such as triglycerides and cholesterol are stored in specialized fat cells called adipocytes and form a key component of adipose tissue, which helps to maintain hormonal balance while supporting thermoregulation and energy homeostasis (Landrier, et al., 2012). Obesity is often associated with excess dietary intake of energy in the form of high-fat high-sugar meals. In times of excess energy availability, glucose can be stored as glycogen in the liver, or substrates can be converted to triglycerides and stored in adipose tissue. In times of high energy demand, triglyceride stores are broken down by lipolysis and transported to peripheral tissues where they are oxidized and used as a source of energy (Turnbull, et al., 2016). Thus, the balance between lipogenesis and lipolysis is crucial and dysregulation thereof may lead to lipid accumulation.

There are two main types of adipose tissue, white adipose tissue (WAT) and brown adipose tissue (BAT). Where BAT is associated with energy expenditure, the main function of WAT is

to store excess energy as triglycerides. In obesity, increased triglyceride storage in adipose tissue results in an increase in adipocyte size (hypertrophy) and number (hyperplasia) (Lessard, et al., 2014). Of the two types, WAT compared to BAT has been more closely linked to the disruption of lipid metabolism, altered adipokine secretion, inflammation and subsequent insulin resistance. In a population-based study using obese women, Michaud, et al. (2016) found a strong positive correlation between enlarged adipocytes (increased WAT) in both visceral and subcutaneous adipose tissues (VAT and SAT), and impaired insulin sensitivity, demonstrating that a link exists between excess fat deposition and deleterious metabolic alterations.

1.4.1 Adipose tissue dysfunction

Adipocytes and pre-adipocytes are embedded in the extracellular matrix (ECM) of adipose tissue, which also contains resident tissue macrophages that assist in the mediation of adipokine secretion as well as the generation and degradation of ECM. During obesity, adipose tissue expansion via adipocyte hypertrophy, can disrupt these functions and result in chronic, low-grade inflammation, insulin resistance and ectopic fat accumulation (Figure 1.2). Adipocyte hypertrophy causes adipose tissue macrophages to produce mediators such as tissue growth factor beta (TGF-β) and platelet derived growth factor (PDGF), which attracts and activates fibroblasts. Fibroblasts initiate fibrogenesis, which alters the expandability of adipose tissue and causes fat to be stored ectopically. According to findings by Lessard, et al. (2014), loss of expandability in SAT leads to visceral fat storage, hypertrophy and multiple metabolic consequences such as insulin resistance and NAFLD. Ectopic fat accumulation in organs such as the liver may therefore interfere with cellular function and hence the development of insulin resistance.

Adipocyte hypertrophy also alters adipokine secretion, causing a decrease in the secretion of adiponectin, an important adipokine with a role in obesity-induced insulin resistance (Kim, et al., 2018). Simultaneously, there is an increase in cytokine secretion, causing macrophages from the circulation to be recruited and activated. Macrophages can either be “classically” activated, taking on a pro-inflammatory M1 phenotype, or they can be “alternatively” activated to take on an anti-inflammatory M2 phenotype. In the case of adipose tissue expansion by hypertrophy, macrophages undergo classical activation, further increasing cytokine release and promoting inflammatory signalling (Luo, et al., 2017), which can lead to local and systemic insulin resistance (Figure 1.3).

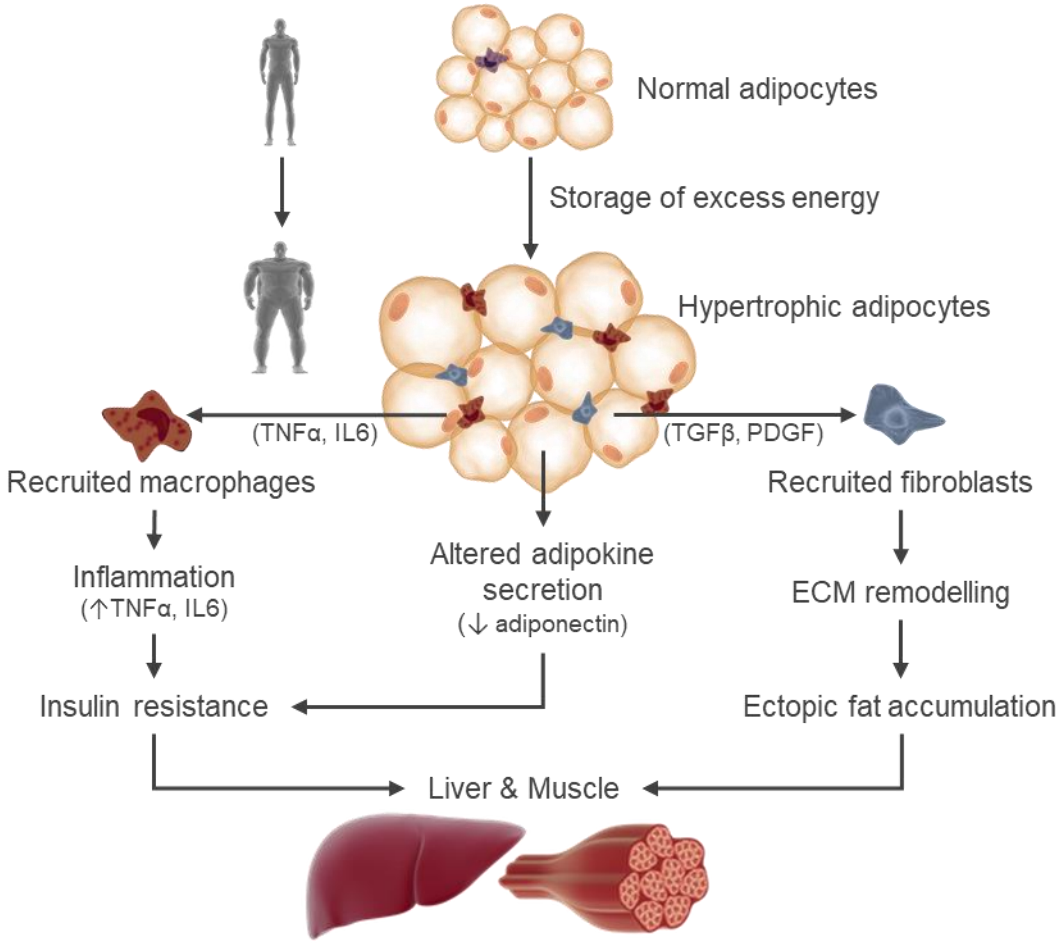

Figure 1.2: Adipose tissue dysfunction in obesity. *Storage of excess energy in the form of triglycerides within adipose tissue can cause adipocyte hypertrophy, leading to inflammation, altered adipokine secretion and remodelling of the extracellular matrix (ECM), culminating in insulin resistance and ectopic fat accumulation. Illustrations created using www.somersault1824.com.*

One of the first, and possibly the most well-studied cytokine in relation to obesity-induced inflammation is tumour necrosis factor alpha (TNFα). Under normal conditions, inhibitor of kappa B alpha (IκBα) sequesters nuclear factor kappa B (NFκB) in the cytosol, inhibiting its translocation. However, TNFα signalling causes phosphorylation of inhibitor of kappa B kinase beta (IKKβ), which then causes IκBα to degrade and release NFκB. The liberated NFκB is then able to translocate to the nucleus and initiate transcription of pro-inflammatory genes (Zhao, et al., 2015). Furthermore, FFAs serve as ligands for the toll-like receptor 4 (TLR4) complex, which activates the classical inflammatory response and promotes recruitment and accumulation of macrophages in the adipose tissue (Bai & Sun, 2015). These macrophages produce large amounts of pro-inflammatory mediators such as TNFα and interleukin 6 (IL6) that causes adipose tissue insulin resistance.

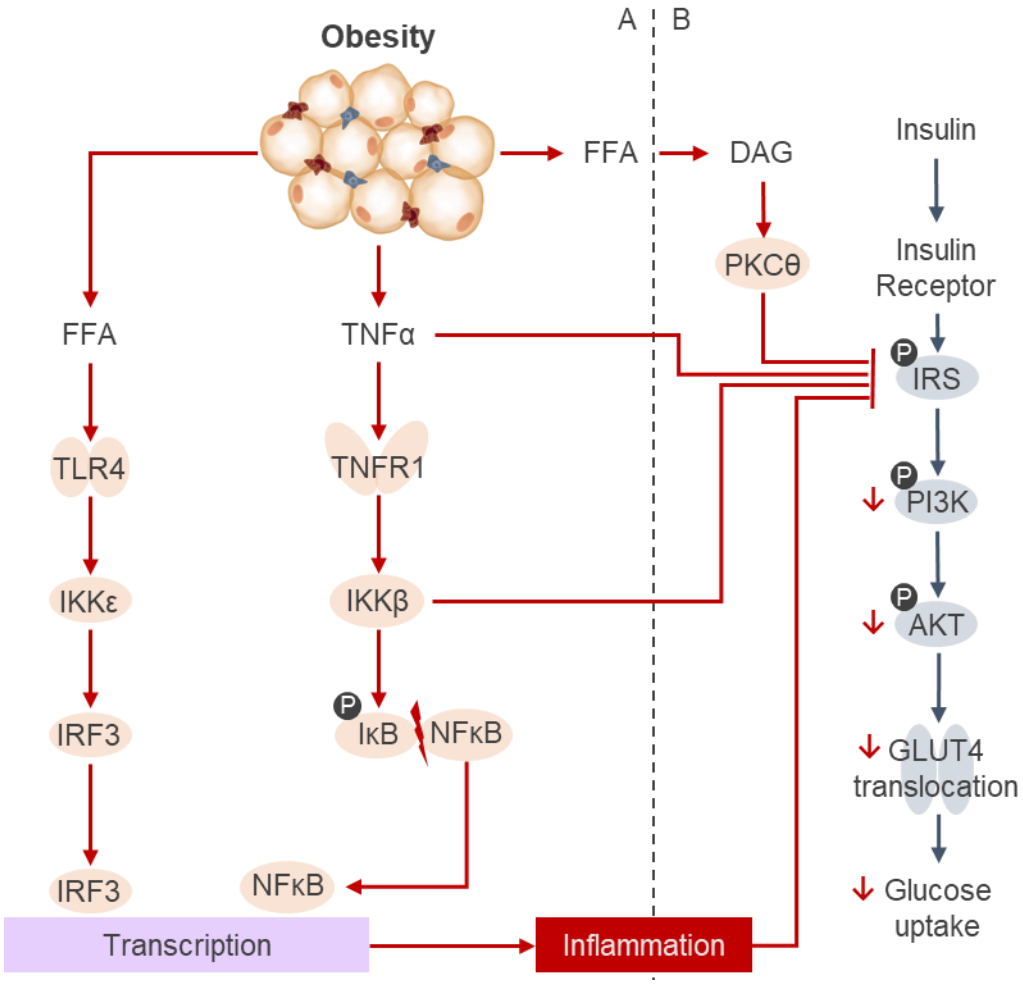

Figure 1.3: Molecular mechanisms of obesity-induced inflammation and insulin resistance*. A) Obesity causes the activation of an immune response and release of pro-inflammatory cytokines such as tumour necrosis factor alpha (TNFα) and interleukin 6 (IL6), initiating transcription of inflammatory genes. B) Under normal conditions (blue arrows) insulin stimulates the translocation of glucose transporter 4 (GLUT4) and uptake of glucose into the cell, while inhibiting lipolysis and gluconeogenesis. In an obese state (red arrows) inflammation and increased free fatty acids disrupt the insulin signalling cascade and inhibit GLUT4 translocation. Illustrations created using www.somersault1824.com.*

In addition to storage of excess energy, adipose tissue fulfils an important endocrine function. Therefore, adipose tissue dysfunction is not dependent entirely on the amount of fat deposition, but also on the altered release of adipokines. Fonseca (2003) showed that improving adipocyte function with a peroxisome proliferator activator γ (PPARγ) agonist improved insulin sensitivity in humans, despite significant gains in fat mass. As an endocrine organ, dysfunction of adipose tissue can result in the activation of a pro-inflammatory response with major consequences for pancreatic β-cell failure, hepatotoxicity, muscle insulin resistance and cardiac dysfunction. This pro-inflammatory state promotes insulin resistance and drives MetS, increasing the risk of heart failure.

1.5 Insulin resistance

Insulin is a hormone that plays a vital role in energy homeostasis and metabolism. It is synthesized and released by pancreatic β-cells in response to an elevation in blood glucose levels. This increase in glucose-stimulated insulin secretion will allow for uptake and subsequent use or storage of glucose in peripheral tissue. In an insulin resistant state, insulin is hyper-secreted which results in the inability of peripheral tissue to utilize glucose effectively, leading to hyperinsulinaemia and hyperglycaemia (Lebovitz, 2001). Furthermore, insulin resistance promotes lipogenesis and causes a positive feedback loop which further exacerbates obesity. Chronic hyperglycaemia and hyperinsulinaemia caused by insulin resistance can also lead to pancreatic β-cell failure and T2DM.

Under normal physiological conditions, the insulin signalling pathway (Figure 1.3 B) is activated when insulin binds to the insulin receptor on the cell membrane, leading to phosphorylation of insulin receptor substrate 1 at Tyr^{618} ($IRS1^{Tyr618}$). A signalling cascade is then initiated by which the phosphorylation of phosphoinositide-dependent protein kinase at Tyr^{688} ($PI3K^{Tyr688}$) leads to the phosphorylation of protein kinase B at Ser^{473} (AKT^{Ser473}). This in turn leads to the translocation of glucose transporter 4 (GLUT4) from the cytosol to the cell membrane, allowing for the active transport of glucose into the cell from the circulation (Brewer, et al., 2014). Insulin resistance occurs when this pathway is inhibited and can be caused by a number of obesity-related factors.

Numerous pre-clinical and clinical studies have implicated obesity-induced chronic low-grade inflammation in the development of insulin resistance (Lee & Lee, 2014; Straub, 2014). As previously mentioned, obesity-induced inflammation is caused by the infiltration of macrophages to the adipose tissue and the increased expression of pro-inflammatory cytokines such as TNFα (Ye, 2013). Acting through TNFα receptor 1 (TNFR1), TNFα inhibits IRS1 in the insulin signalling pathway, thereby rendering the cell less responsive to insulin by inhibiting GLUT4 translocation. This has been shown by Hotamisligil, et al. (1994), where TNFα inhibited insulin-stimulated tyrosine phosphorylation of IRS1 in skeletal muscle, while neutralization of TNFα restored insulin sensitivity to a level comparable to control animals. In addition to inhibiting IRS1, TNFα activates inflammatory pathways within the cell, including the IKKβ/NFκB pathway as well as the jun-N-terminal kinase 1 (JNK1) pathway (Ye, 2013). The activity of IKKβ and JNK1 inhibit insulin signalling by phosphorylating IRS1 at Ser^{307}, thereby preventing phosphorylation at tyrosine residues, which is required for insulin

sensitivity. TNFα also activates PPARγ, a nuclear receptor that drives lipid synthesis and fat storage in cells, further increasing insulin resistance (Zhang, et al., 2014).

Another mechanism by which obesity may lead to the development of insulin resistance is by increasing plasma FFAs. Free fatty acids enter the cell via the cluster of differentiation 36 (CD36) receptor and are metabolised, increasing long-chain fatty acid (LCFA) intermediates such as diacyl glycerol (DAG) and ceramides. These lipid intermediates bind and recruit protein kinase C theta (PKCθ) to the plasma membrane where it is activated and in turn activates IKKβ and JNK and proceeds to inhibit phosphorylation of $IRS1^{Ser307}$ (Szendroedi, et al., 2014).

1.5.1 Insulin resistance and cardiac dysfunction

Insulin resistance is a hallmark of T2DM, with T2DM being characterised by complete loss of pancreatic β-cell function. Both insulin resistance and T2DM are risk factors for the development of cardiac dysfunction through various pathways (Figure 1.4). Under normal physiological conditions the heart is metabolically flexible as it is able to utilize both fatty acids and glucose as a substrate/energy source (Jia, et al., 2017). However, in the case of myocardial insulin resistance GLUT4 is not translocated, while the translocation of CD36 is unaffected (Battiprolu, et al., 2013). This results in reduced glucose uptake into the heart with maintained fatty acid uptake, subsequently causing a shift in substrate preference to favour almost exclusive utilization of fatty acids (Schwenk, et al., 2008). Fatty acid metabolism in the heart is oxygen inefficient and renders the heart more susceptible to ischemic damage (Chowdhry, et al., 2007). Additionally, recent studies suggest that these metabolic changes initiate several molecular events in the heart that lead to morphological and mechanical changes, and ultimately cardiac dysfunction (Ghosh & Katare, 2018).

The shift in substrate preference and chronic hyperglycaemia is accompanied by increased ROS production in the mitochondria of the obese heart. This causes increased expression of pro-inflammatory cytokines, thereby contributing to the suppression of insulin signalling and activating apoptosis responses in the myocyte (Li, et al., 2012). During chronic hyperglycaemia, caused by insulin resistance, reducing sugars can bind to proteins or lipids to form advanced glycation end products (AGEs) (Zieman & Kass, 2004). This plays a role in the crosslinking of collagen fibres in the myocardium, promoting fibrosis (Aronson, 2003). Receptors of AGEs (RAGE) are also activated by oxidative stress, a result of the pro-inflammatory phenotype associated with obesity and diabetes, and in turn activates the NFκB

signalling pathway, which exacerbates insulin resistance and promotes fibrosis (Aragno, et al., 2006). Diabetes also causes the modification of Ca^{2+}/calmodulin dependent protein kinase 2 (CAMK2), which connects with sarco/endoplasmic reticulum Ca^{2+}-ATPase (SERCA) and is related to the pathophysiology of contractile dysfunction, though the exact mechanism is not known (Liu, et al., 2016).

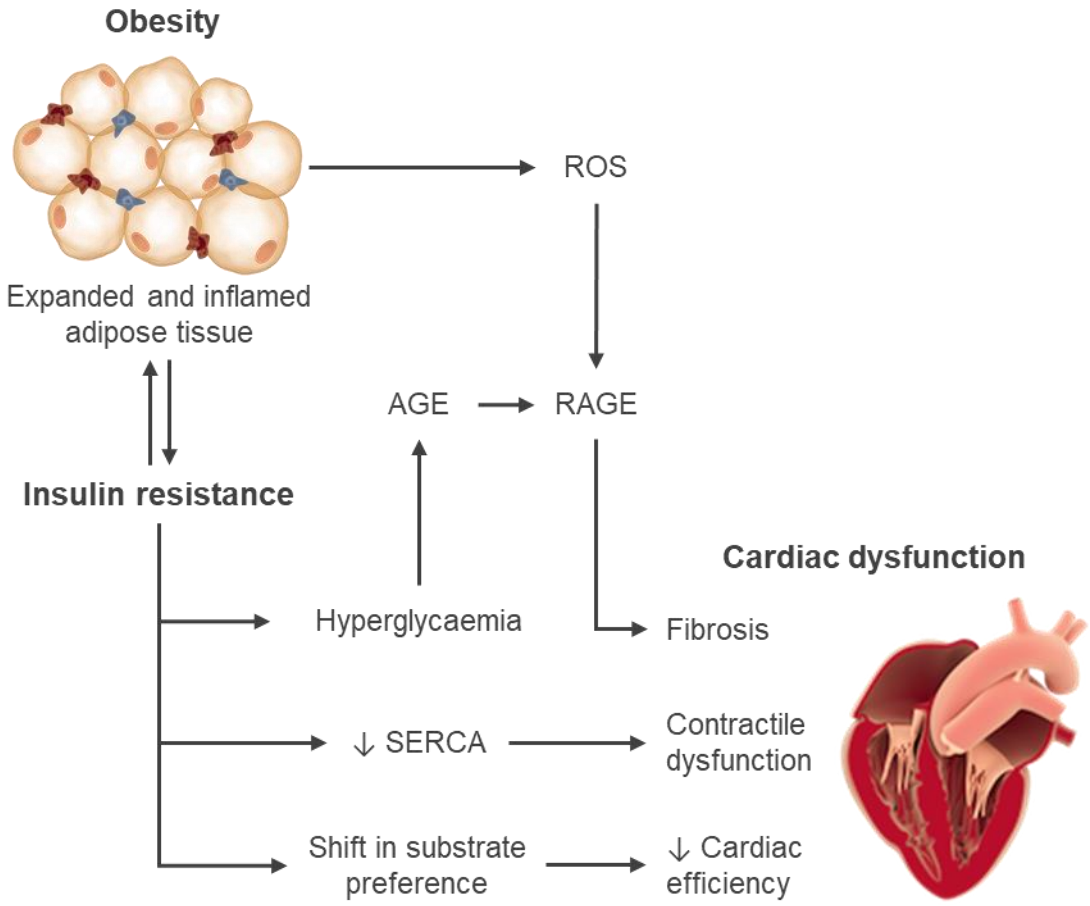

Figure 1.4: Insulin resistance leads to cardiac dysfunction. *Insulin resistance can lead to cardiac dysfunction by decreasing cardiac efficiency and by causing fibrosis and contractile dysfunction. Illustrations created using www.somersault1824.com.*

In addition to its manifold role in the development of cardiac dysfunction, insulin resistance is also known to occur in patients with NAFLD (Utzschneider & Kahn, 2006). Nevertheless, each condition can occur in the absence of the other, and each is known as an independent risk factor for the development of cardiometabolic aberrations (Mantovani, et al., 2015; Sirbu, et al., 2016). This raises the question of what exactly the mechanisms are by which the co-occurrence of insulin resistance and NAFLD leads to cardiac dysfunction.

1.6 NAFLD

Non-alcoholic fatty liver disease is the most common liver disease in the Western world (Ahmed, 2015) and is closely associated with obesity, with an estimated prevalence of 80-90% in obese patients. Several studies (Han & Lee, 2017; Ter Horst & Serlie, 2017) reported on NAFLD as the hepatic component of the metabolic syndrome, as intrahepatic lipid accumulation and inflammation has been identified as an independent risk factor for the development of CVD (Han & Lee, 2017). The disease itself develops in stages, starting with benign lipid accumulation and ranging to severe steatosis accompanied by inflammation and fibrosis (Figure 1.5).

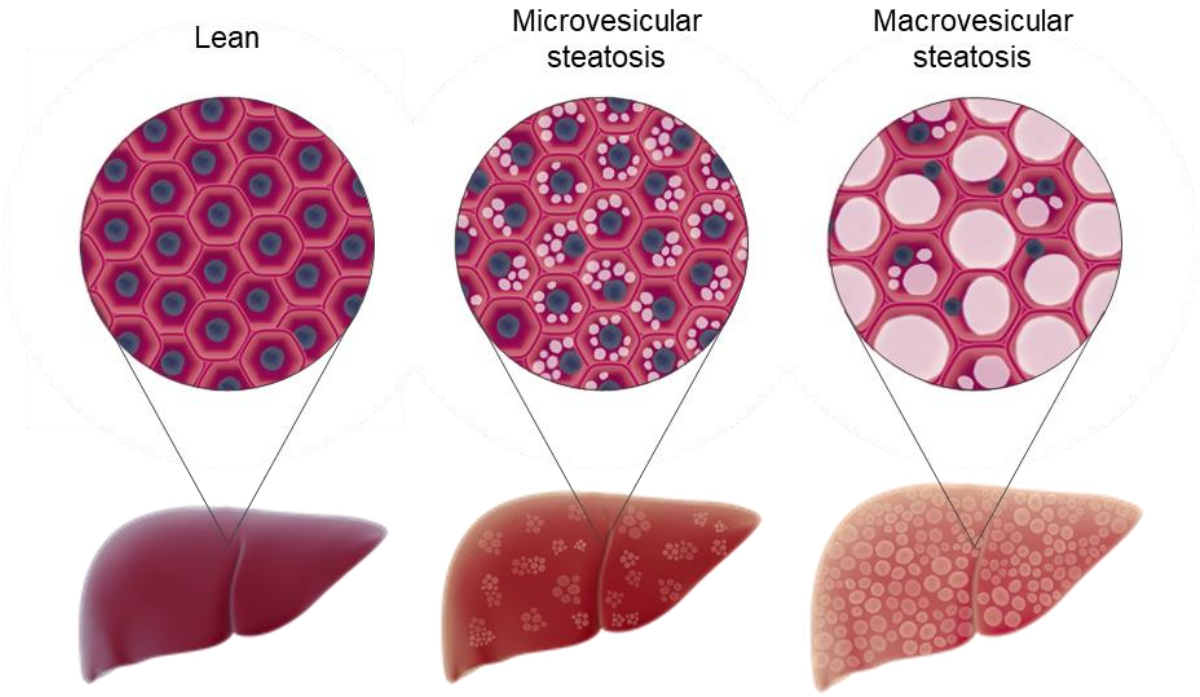

***Figure 1.5: Progression of NAFLD**. Intrahepatic lipid accumulation in non-alcoholic fatty liver disease (NAFLD) can progress from microvesicular changes to macrovesicular changes, the latter being accompanied by nuclear displacement and hepatocellular hypertrophy. Illustrations created using www.somersault1824.com.*

The earliest stage of NAFLD presents as simple steatosis, characterized by evidence of fat accumulation in more than 5% of the liver, beyond normal, healthy hepatic lipid content and in the absence of excessive alcohol consumption (Birkenfeld & Shulman, 2014). Approximately 37% of NAFLD cases undergo histopathological progression to non-alcoholic steatohepatitis (NASH), which can be identified when the excess lipid content is accompanied by inflammation and mild fibrosis. From there, up to 20% of cases progress to hepatic

cirrhosis, hepatocellular carcinoma, and end-stage liver failure (Bugianesi, et al., 2005; Liang, et al., 2014).

Hepatic lipid accumulation occurs due to an imbalance between lipid influx and lipid removal (Figure 1.6), leading to lipotoxicity and hepatic injury (Lonardo, et al., 2015). Several factors can contribute to this imbalance, including excessive FFA import and storage, increased *de novo* lipogenesis, impaired lipolysis by β-oxidation, and diminished export of FFA from liver (Trevaskis, et al., 2012; Yamada, et al., 2017)

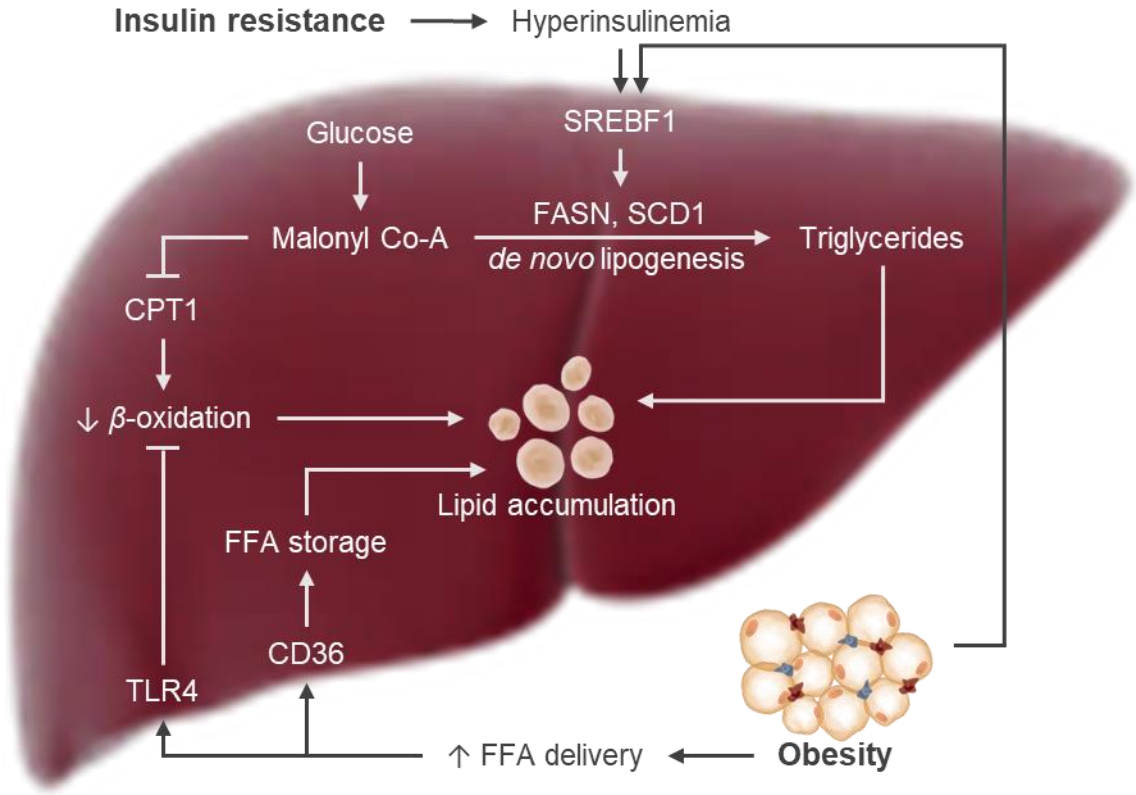

Figure 1.6: The two-fold causality of intrahepatic lipid accumulation*. Lipid accumulation in the liver can be caused by insulin resistance, leading to hyperinsulinaemia and subsequent activation of sterol regulatory element binding factor 1 (SREBF1), causing increased* de novo *lipogenesis and decreased fatty acid β-oxidation. Simultaneously, increased free fatty acid (FFA), spill-over from adipose tissue due to obesity, can be taken up into the liver via the cluster of differentiation 36 (CD36) receptor, where it accumulates as the rate of uptake is greater than the rate of disposal by β-oxidation. Illustrations created using www.somersault1824.com.*

In the obese state, hepatic insulin resistance may develop due to pro-inflammatory signalling from the adipose tissue. Hyperinsulinaemia due to insulin resistance acts via sterol-regulatory element-binding factor 1 (SREBF1) to produce excess lipogenic enzymes such as fatty acid synthase (FASN) and stearoyl-coenzyme A desaturase 1 (SCD1) (Sobel, et al., 2017). These

enzymes drive *de novo* lipogenesis by facilitating the conversion of glucose to triglycerides and can lead to lipid accumulation in the liver (Cohen, et al., 2011). This was shown by Repa, et al. (2014), who found that induction of SREBF1 stimulated lipogenesis and promoted hepatic hypertriglyceridaemia. Carnitine palmitoyl transferase 1 (CPT1) is an essential enzyme that transports fatty acids to the mitochondria for β-oxidation. However, Malonyl coenzyme A (Malonyl-CoA), an intermediate of triglyceride conversion, acts as an inhibitor of CPT1, reducing lipid clearance.

Obesity can also cause NAFLD independent of insulin resistance, as adipose tissue dysfunction results in FFA spill-over into circulation. These excess FFA are transported to the peripheral tissue such as the liver, where they are taken up via CD36 and stored within hepatocytes. Free fatty acids in circulation can also activate TLR4 in the liver and consequently inhibits AMPK signalling and β-oxidation (Viollet, et al., 2010), further disrupting the balance and promoting intrahepatic lipid accumulation.

1.6.1 NAFLD and cardiac dysfunction

As mentioned previously, NAFLD is also a known risk factor for cardiac dysfunction (Mantovani, et al., 2015) (Figure 1.7). Visceral adipose tissue and intrahepatic fat cause a systemic release of pathogenic mediators, such as C-reactive protein (CRP), IL6, TNFα, and other inflammatory cytokines (Mantovani, et al., 2015), exacerbating insulin resistance and conferring a 2- to 4-fold increased risk for the development of T2DM (Han & Lee, 2017). By enhancing the dysfunctional metabolic phenotype in such a way, NAFLD may contribute to cardiac dysfunction, as described under insulin resistance-induced cardiac dysfunction. Interestingly, an independent association has also been found between NAFLD and left ventricular diastolic dysfunction (LVDD) in type 2 diabetic patients, most probably additive to the myocardial defects already present in T2DM (Bonapace, et al., 2012). This is similar to findings by Karabay, et al. (2014), where patients with NAFLD showed evidence of subclinical myocardial dysfunction.

A positive relationship has been reported between the histological severity of NAFLD and certain features of CVD, including LVDD (Sookoian, et al., 2011). In the case of insulin resistance there is greater uptake of fatty acids into the cardiomyocyte, as described previously. In cases where myocardial lipid uptake exceeds FA oxidative metabolism, myocardial lipid accumulation can occur. The accumulation of lipid metabolism intermediates can then cause oxidative stress and apoptosis (Schulze, 2009). In the hyperlipidaemic state,

there is also increased activation of TGF-β (Hong, et al., 2016) which in turn activates connective tissue growth factor (CTGF) (Bonniaud_2004). In a study by Chen, et al. (2000), isolated human and rat cardiomyocytes were treated with TGF-β and showed consistently increased expression of CTGF. This was accompanied by increased expression of fibronectin, an indication of ECM remodelling, as well as inter-myofibril and perivascular fibrosis (Chen, et al., 2000).

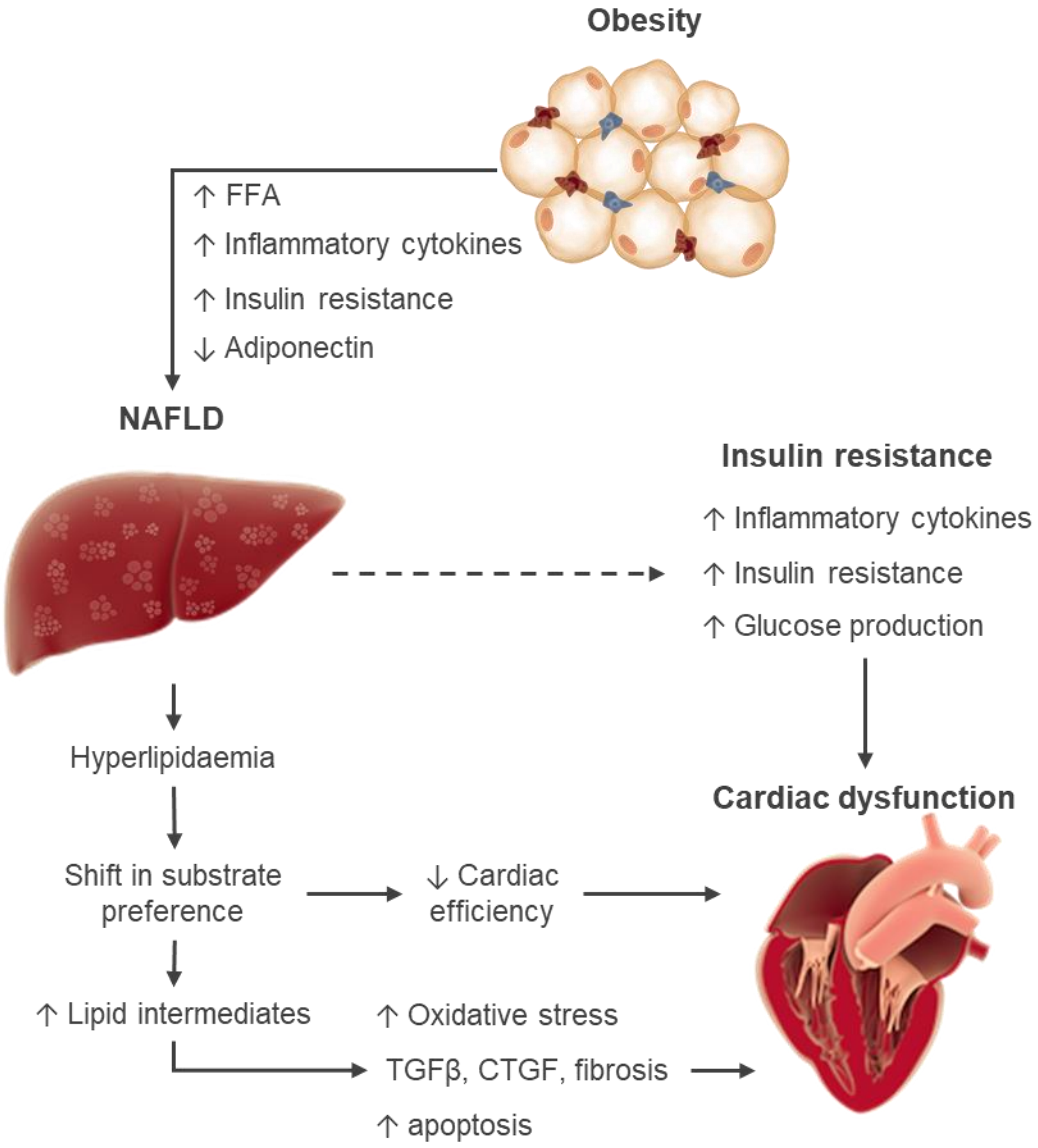

Figure 1.7: NAFLD causes Myocardial Dysfunction. *Non-alcoholic fatty liver disease (NAFLD) can lead to myocardial dysfunction via various pathways, including exacerbation of insulin resistance, dyslipidaemia, and oxidative stress. Illustrations created using www.somersault1824.com*

.

1.7 Connecting the underlying pathologies

Both insulin resistance and NAFLD have been identified as independent risk factors for cardiac dysfunction (Kumar, et al., 2016). Insulin resistance has been shown to play a role in myocardial dysfunction through various mechanisms, including hyperglycaemia, glucotoxicity, ROS, and inflammation, eventually causing cardiac damage and remodelling (Ghosh & Katare, 2018). Similarly, numerous studies suggest that NAFLD is not just a co-occurrence, but that it can contribute to the pathogenesis of cardiac dysfunction by causing lipotoxicity and contributing to the pathological phenotype (Mantovani, et al., 2015). At the same time, there is a close association between insulin resistance and NAFLD, with insulin resistance being well-known for causing NAFLD. However, whether hepatic fat accumulation can cause insulin resistance remains a topic of debate (Gruben, et al., 2014; Gastaldelli, 2017). Since a better understanding of the different diseases can allow for better treatment or prevention, it may prove useful to investigate the causal role of NAFLD in insulin resistance, and to delineate the order of onset leading up to the development of cardiac dysfunction.

1.7.1 Evidence that insulin resistance causes NAFLD

Insulin resistance is a known cause of hepatic lipid accumulation. Under physiological conditions, insulin inhibits hepatic gluconeogenesis and promotes hepatic lipogenesis. However, during insulin resistance inhibition of gluconeogenesis is halted, while lipogenesis remains activated, likely due to the activation of SREBF1 by hyperinsulinaemia, resulting in activation of lipogenic genes such as FASN and SCD1. This results in excess *de novo* lipogenesis and the development of NAFLD and has been reported in several studies, as discussed below and summarised in table 1.1.

In a study by Bugiuanesi, et al. (2005) the authors observed that NAFLD patients had marked peripheral insulin resistance and impaired lipid oxidation, leading to the conclusion that excess non-esterified fatty acids (NEFA) flux from the insulin resistant adipose tissue caused ectopic fat accumulation and the observed hepatic steatosis. This was also shown in a population-based longitudinal study where Zheng, et al. (2018) showed that insulin resistant individuals with increased circulating triglycerides and glucose had a significantly higher rate of incident NAFLD over the 9-year follow-up period.

Table 1.1: Summary of literature: insulin resistance as a cause of NAFLD

Model	Key findings	Reference
Human	Increased NEFA flux due to adipose tissue insulin resistance could cause NAFLD	(Bugianesi, et al., 2005)
Human	Patients with increased circulating triglycerides, glucose and insulin resistance had higher incident NAFLD on 9-year follow-up	(Zheng, et al., 2018)
Human	Alleviating insulin resistance with rosiglitazone treatment also improved NAFLD	(Neuschwander-tetri, et al., 2003)
Mouse (db/db)	Restoring the insulin signalling pathway could reverse NAFLD	(Xu, et al., 2018)

Table legend: db/db: leptin receptor-deficient, NEFA: non-esterified fatty acids, NAFLD, non-alcoholic fatty liver disease,

In support of insulin resistance as the cause of NAFLD, Neuschwander-tetri, et al. (2003) showed that improving insulin sensitivity with rosiglitazone also ameliorated NAFLD. Similarly, Xu, et al. (2018) showed that improvement of insulin sensitivity in a leptin receptor-deficient db/db (*Lepr*$^{db/db}$) mouse model by regulation of the IRS/PI3K/AKT signalling pathway could improve hepatic steatosis, showing the involvement of the insulin signalling pathway in the disease pathophysiology of NAFLD.

It is worth noting that most studies that investigated insulin resistance and NAFLD use obese humans or animal models. However, obesity is a known cause of insulin resistance, independent of the absence or presence of NAFLD possibly implicating obesity as a confounding factor when studying the causal role of NAFLD in insulin resistance (Pamir, et al., 2009; Schattenberg & Galle, 2010). Thus, to more clearly identify the effect of NAFLD on insulin resistance, without weight as a confounding factor, studies of “genetic” NAFLD may prove useful.

In a study where NAFLD was genetically induced by liver X receptor knock-out (LXR-KO), Grefhorst, et al. (2005) showed that increased activation of SREBF1 in the liver led to subsequent hepatic steatosis. However, this did not affect hepatic or peripheral insulin sensitivity. Similarly, a study by Koonen, et al. (2007) found that hepatic overexpression of the fatty acid transporter CD36 using adenoviral gene delivery (ad.CD36) caused fat accumulation in the livers of genetically modified mice but did not lead to the development of insulin resistance. Patatin-like phospholipase domain-containing protein 2 (*PNPLA2)* is a lipase that plays an important role in the hydrolysis of triglycerides. By creating a *PNPLA2* knock-out mouse model (*PNPLA2*-KO) Wu, et al. (2011) were able to study body-weight independent NAFLD. In this study, the authors observed that *PNPLA2*-KO mice developed marked hepatic steatosis, while insulin sensitivity remained comparable to that of controls. More recently, Franko, et al. (2018), showed that humans that carried a specific single nucleotide polymorphism (SNP) in the *PNPLA3* gene had fatty liver but maintained insulin sensitivity. In the same study it was observed that subjects that did not carry the SNP, but who had high liver fat, were insulin resistant. In further genetic studies, Amaro, et al. (2011) investigated subjects with familial hypobetalipoproteinaemia (FHBL), who had a defect in the export of triglycerides from the liver and subsequent intrahepatic lipid accumulation. In this study, FHBL patients had evident NAFLD, but maintained hepatic and peripheral insulin sensitivity. These studies are summarised in table 1.2 and provide evidence that NAFLD can develop independent of insulin resistance, and that the presence of NAFLD does not irrefutably lead to the development of insulin resistance.

Table 1.2: Summary of literature: evidence that NAFLD does not cause insulin resistance

Model	Key findings	Author
Mouse (ob/ob)	SREBF1-induced hepatic steatosis did not affect insulin sensitivity.	(Grefhorst, et al., 2005)
Mouse (Ad.CD36)	Hepatic overexpression of CD36 resulted in fat accumulation, but not insulin resistance.	(Koonen, et al., 2007)
Mouse (PNPLA-KO)	PNPLA-KO mice had marked steatosis, but maintained insulin sensitivity	(Wu, et al., 2011)
Human, FHBL	Steatosis is dissociated from insulin resistance in FHBL, which suggests that increased intrahepatic triglyceride content is a marker, not a cause, of metabolic dysfunction	(Amaro, et al., 2011)
Human, PNPLA3 SNP	SNP with high liver fat maintained insulin sensitivity while wild type subjects with high liver fat were insulin resistant	(Franko, et al., 2018)

Table legend: ob/ob: leptin-deficient, SREBF: Sterol regulatory element binding factor 1, CD36: cluster of differentiation 36, PNPLA: Patatin-like phospholipase domain-containing protein, FHBL: familial hypobetalipoproteinaemia, SNP: single nucleotide polymorphism

1.7.2 Evidence that NAFLD causes insulin resistance

While insulin resistance is frequently considered the cause of intrahepatic lipid accumulation (Sanyal, et al., 2001) evidence suggests that NAFLD can develop prior to and be a cause of insulin resistance (Yamada, et al., 2010; Singh, et al., 2015; Han & Lee, 2017). Excess triglycerides may be present in circulation independent of adipose tissue insulin resistance and are still taken up and stored as fat in the liver. Similarly, increased *de novo* lipogenesis may be attributed to the increase in uptake and conversion of glucose to fat. Interestingly, NAFLD in patients without insulin resistance is characterized by more severe liver damage, as evidenced by higher levels of aspartate transaminase (AST) and alanine transaminase (ALT) (Singh, et al., 2015). Thus, it may be that the lipid accumulation and inflammation associated with the later stages of NAFLD leads to insulin resistance and subsequent T2DM. Studies that provide evidence of the causal role of NAFLD in insulin resistance are discussed below and summarised in table 1.3.

The role of NAFLD-induced inflammation in the development of insulin resistance was displayed by Cai, et al. (2006), where hepatic lipid accumulation caused NFκB activation and downstream cytokine production, leading to both hepatic and systemic insulin resistance. Similarly, Korenblat, et al. (2008) observed that the progressive increase in hepatic triglyceride content is associated with the development of insulin resistance in the liver as well as skeletal muscle and adipose tissue in humans, and therefore state that NAFLD should be considered as a cause of insulin resistance. In a study on non-diabetic humans, Yamada, et al. (2009) showed that fatty liver is an independent risk factor for impaired fasting glucose and the later development of T2DM, independent of body weight. Additionally, Lomanco, et al. (2012) showed that the degree of insulin resistance increased proportionally with NAFLD severity and that insulin resistance was worse in obese patients with NAFLD compared to those without NAFLD, suggesting that insulin resistance is at least somehow affected by NAFLD.

Table 1.3: Summary of literature: evidence that NAFLD is a cause of insulin resistance

Model	Key findings	Author
Mouse IKKβ over-expression	Hepatic lipid accumulation caused inflammation and insulin resistance.	(Cai, et al., 2006)
Human	Increases in hepatic triglyceride content are associated with progressive development of insulin resistance.	(Korenblat, et al., 2009)
Human	Fatty liver is an independent risk factor for impaired fasting glucose	(Yamada, et al., 2010)
Human	Insulin resistance was worse in obese patients with NAFLD than obese patients without NAFLD	(Lomonaco, et al., 2012)

Table legend: IKKβ: Inhibitor of kappa B kinase beta, NAFLD, non-alcoholic fatty liver disease

1.8 *Lepr*$^{db/db}$ mice as a model organism to study NAFLD/IR

Murine models, due to their physiological similarity to humans and relative ease with which their condition can be manipulated, are widely used as a model organism in the research of metabolic diseases (Alquier & Poitout, 2018). Several murine models exist for the study of metabolic disorders, including those where obesity and diabetes are induced by feeding animals various combinations of a high-fat-high-sugar (HFHS) diet. Other models exist where the animal has been genetically manipulated to be predisposed to the development of obesity and diabetes; these include the leptin-deficient ob/ob (*Lepr*$^{ob/ob}$) mouse and the *Lepr*$^{db/db}$ mouse. The later model is popular in the study of obesity, dyslipidaemia, T2DM, NAFLD, and diabetic cardiomyopathy (Kobayashi, et al., 2000; Dludla, et al., 2017; Yin, et al., 2017; Guilbaud, et al., 2018). Due to the deficiency in leptin signalling, db/db mice become hyperphagic and develop obesity within four- to six-weeks when fed standard laboratory chow. Kobayashi et al. (2000) show that by six-weeks of age, these mice develop hyperlipidaemia that is comparable to that seen in obese humans, and that this is accompanied by hyperglycaemia and hyperinsulinaemia. Similarly, when comparing a db/db mouse model to two models of diet-induced obesity, Guilbaud et al. (2018) found that db/db mice became obese earlier than the diet-induced models, and also exhibited more severe hyperglycaemia and glucose intolerance. They thus conclude that the db/db model was more representative of human T2DM than a diet-induced model of obesity. While studying the development of NAFLD in db/db mice, Yin et al. (2017) found that this model had increased expression of SREBF1, FASN and SCD1 when compared to heterozygous leptin receptor-deficient lean control (*Lepr*$^{db/+}$) controls, corresponding with the human condition. Likewise, Dludla et al. (2017) have shown that db/db mice develop diabetes-related cardiac dysfunction around 16 weeks of age, characterised by hyperglycaemia, hyperlipidaemia, and cardiac muscle remodelling.

1.9 Conclusion

While findings with regards to the causal role of NAFLD in insulin resistance are apparently contradictory, Luukkonen, et al. (2016) suggests that the possible reason could be because of the different “origins” of NAFLD. They studied humans that were metabolically predisposed to NAFLD, due to diet and lifestyle, and compared them to humans who were genetically predisposed. Observations in this study showed that “metabolic” and “genetic” NAFLD had different pathologies in terms of the type of hepatic lipid content and the role that insulin

resistance played in the disease. In “genetic” NAFLD, it appears that an increase in lipid accumulation increases hepatic and systemic insulin resistance, while in “metabolic” NAFLD the combination of hyperinsulinaemia and hyperlipidaemia increases insulin resistance, which plays a causal role in the development of hepatic lipid accumulation (Gastaldelli, 2017).

With the rising burden of obesity-related heart failure, it is becoming increasingly important to understand disease pathophysiology to allow for early identification and treatment of risk factors associated with CVD. It is evident that there are many links between NAFLD and insulin resistance, and the development of cardiac dysfunction. Thus, a better understanding these pathways may be helpful in reducing the burden of disease (Bonapace, et al., 2012). When studying the progression of MetS and cardiac dysfunction, different models may give valuable insight into the various circumstances under which the disease develops, possibly paving the way for more individualized treatment and risk prediction.

Many review articles address the question of which came first, however much of the available research studies did not aim to investigate that specific relationship. Many studies indicate whether, but not “*when”*, subjects with insulin resistance also develop NAFLD. More experimental research is thus needed in this field. Specifically, longitudinal studies that track disease progression in different models. The purpose of the present study was to monitor mice that are known to develop both insulin resistance and NAFLD, and to establish when the onset of each event occurred. As both of these conditions are underlying causes of cardiac dysfunction, it also becomes imperative to monitor the state of the heart in such studies.

Aims of Investigation

Aim:

To investigate the order of onset of NAFLD and muscle insulin resistance, in a db/db mouse model, and the effect thereof on the development of cardiac dysfunction.

Objectives:

1. To determine the order of onset of NAFLD, insulin resistance and subsequent cardiac dysfunction in an obese db/db mouse model.
2. To investigate the gene regulatory network involved in NAFLD, insulin resistance and myocardial dysfunction.

Chapter 2: Methodology

2.1 Study design

Ethical clearance for the animal study was obtained from the South African Medical Research Council (SAMRC) Ethics Committee for Research on Animals (ECRA/05/15) and use of the tissues was approved by the University of Stellenbosch Research Ethics Committee for Animal Care and Use (Protocol #0301). Five-week old homozygous male leptin-receptor-deficient (*Lepr*$^{db/db}$) mice and their lean heterozygous littermates (*Lepr*$^{db/+}$) were acclimated for one week to the experimental environment at the Primate Unit and Delft Animal Centre (PUDAC) of the SAMRC. The animal facility is environmentally controlled, with a 12-hour light/dark cycle and a temperature range of 23 °C - 25 °C, with relative humidity ~50%. All animals were given free access to standard mouse chow (Afresh Vention, Cape Town, RSA) and tap water. At 6 weeks of age, animals were divided into either a control (*Lepr*$^{db/+}$) (n=32) or an experimental group (*Lepr*$^{db/db}$) (n=32), based on obesity phenotype. Animals in each group were then randomized and further sub-divided into 4 subgroups (7-, 10-, 13- and 15-weeks) with n=8 animals per group. Two animals were housed per cage grouping similar disease states together. Body weight, and fasting blood glucose levels were recorded weekly, while echocardiograph analysis was done for each time point 3 days prior to termination.

2.1.1 Fasting blood glucose and insulin

High fasting blood glucose and insulin levels are known to be associated with insulin resistance. For this reason, fasting blood glucose of both lean and obese animals was determined weekly (Dludla, et al., 2017). Briefly, animals were subjected to a 4-hour fast before blood was drawn by tail prick and analysed using a OneTouch Select® Glucose Meter (LifeScan Inc., California, USA). Insulin concentration in serum was determined using a Millipore, mouse insulin enzyme-linked immunosorbent assay (ELISA) kit (Merck, RSA). The homeostasis model assessment of insulin resistance (HOMA-IR) was calculated by multiplying the fasting glucose concentration by the fasting insulin concentration and dividing by the set coefficient 22.5 (HOMA-IR = [fasting blood glucose (mmo/L) * fasting insulin (mmol/L)] / 22.5).

2.1.2 Echocardiography

In vivo TDI echocardiographic analyses was used as a measure of left ventricular cardiac dysfunction. The procedure was carried out under anesthesia (1.0% - 2.5% isoflurane mixed with 0.5 L/min 100% O_2) and blinded to the genotype, at 7-, 10-, 11-, 13- and 15-weeks. Heart rates were maintained at 450 - 550 beats per minute. TDI echocardiograph analysis were performed using a Vevo 2100 high-resolution imaging system equipped with a 30 MHz transducer to measure left ventricular function. The % EF and fractional shortening were assessed as a measurement of systolic dysfunction.

2.1.3 Sample collection

At weekly intervals after the allotted time period, from 6- to 16-weeks of age, animals were fasted for 4 hrs before being euthanized by exsanguination. Blood was collected from the abdominal vena cava into SST Serum Separation Tubes. The following tissues were collected to investigate the respective objectives: liver (to ascertain the onset of NAFLD), skeletal muscle (from the quadriceps of the thigh, to verify insulin resistance), and heart (to confirm cardiac dysfunction).

2.1.4 Liver enzymes and lipogram

After collection, SST tubes containing serum were centrifuged at 4000 x g for 15 min at 4 °C, after which serum samples were sent to PathCare Medical Diagnostic Laboratories (Cape Town, South Africa) for analysis. Serum levels of the liver enzymes ALT and AST were measured as an indication of liver damage, which may result from hepatic steatosis. Similarly, lipograms for low density lipoprotein (LDL), total cholesterol, and triglycerides were determined as an indication of dyslipidaemia.

2.2 **Histology**

Histological analysis was performed on the liver in order to determine the onset and severity of hepatic lipid accumulation (steatosis). To ensure that the same area of the liver was sectioned, frozen liver tissues were sectioned sagittal to the lobe at 10 µm using a Leica Cryostat (Leica, Wetzlar, Germany) and transferred onto Superfrost® Microscope Slides (Thermo Fisher Scientific, Massachusetts, United States) and kept at -20 °C until staining.

2.2.1 Haematoxylin and Eosin stain

A haematoxylin and eosin (H&E) stain was performed to visualise general tissue morphology. Glass slides with liver sections were placed in a metal stain rack and equilibrated to room temperature, before being immersed 5 times in dH_2O. Slides were then submerged in filtered Mayer's Haematoxylin (Kimix Chemicals, Cape Town, South Africa) for 12 min, followed by a 10 min wash step in running tap water until the water ran clear, to facilitate staining of the nuclei. Thereafter, to stain cytoplasm and acidophilic structures, cells were counterstained with Eosin (Kimix Chemicals, Cape Town, South Africa) for 2 min before a final wash step in dH_2O until the water was clear. Sections were dehydrated by ascending slides 20 x in 95% alcohol, and then 100% alcohol before placing slides in a Columbia staining dish containing xylene for 1 min. Slides were removed from xylene and coverslips were mounted immediately using DPX mounting media (Sigma-Aldrich, Missouri, United States). Using the Nikon Eclipse Ti-S ProScan III microscope (Nikon, Tokyo, Japan), the portal areas of each section were identified by the proximity of a blood vessel. The central areas of the liver were also identified by the absence of portal blood vessels and images were captured of these areas at 400x magnification. Images where neither the portal vessel, nor the edge of the tissue was in the field were used for histological analysis.

2.2.2 Oil Red-O stain

To confirm the presence of lipid droplets in the liver, an Oil Red O (ORO) lipid stain was performed on the glass slides with liver sections. Briefly, sections were allowed to equilibrate to room temperature for 10 min before being immersed for 20 min in Oil Red-O working solution (prepared as in Appendix B4). Thereafter slides were removed and rinsed in running tap water for 5 min before being counterstained with 0.25% crystal violet solution for 1 min. Thereafter, slides were rinsed in running tap water for 5 min and allowed to air dry before mounting with buffered glycerol-jelly aqueous mounting media. Images were captured within 3 days using the Nikon Eclipse Ti-S inverted light microscope (Tokyo, Japan) at 400 x magnification.

2.3 Gene expression analysis

2.3.1 RNA extraction

2.3.1.1 Heart tissue

Ribonucleic acid (RNA) was extracted using Qiazol® reagent (Qiagen, Hilden, Germany) according to the manufacturer's instructions. Briefly, 50 mg of left ventricular tissue was cut and placed in a 2 mL Eppendorf tube (Eppendorf, Hamburg, Germany) containing a stainless-steel bead (Qiagen, Hilden, Germany) and 500 µL Qiazol reagent. Tissues were then homogenized using a Qiagen TissueLyser (Qiagen, Hilden, Germany) at 25 Hz for 1 min followed by incubation on ice for 1 min, a process repeated 4 times. The Eppendorf tubes containing the lysed tissues were then centrifuged at 15 000 x g for 10 min at 4 °C and the supernatant was transferred to a new 1.5 mL tube. Subsequently, 100 µL of chloroform (Sigma-Aldrich, Missouri, United States) was added to each tube, mixed intermittently for 3 min and centrifuged at 15 000 x g for 15 min at 4 °C. Thereafter, the upper aqueous phase was transferred to a new 1.5 mL Eppendorf tube (Eppendorf, Hamburg, Germany) without disturbing the white interphase. Precipitation of RNA was achieved by the addition of 250 µL isopropanol (Sigma-Aldrich, Missouri, United States) to the samples, which were mixed by inversion several times before overnight incubation at -20 °C. The following day, the RNA was pelleted by centrifugation at 15 000 x g for 30 min at 4 °C. The supernatant was discarded, and the pellet washed with 500 µL of 70% EtOH and centrifuged at 15 000 x g for 15 min at 4 °C. The wash step was repeated twice, and thereafter the supernatant was discarded and the pellet allowed to air dry for 30 min in a PCR hood. Thereafter, the RNA pellet was re-suspended in 50 µL nuclease-free water (Ambion, Texas, United States) and incubated at 55 °C for 10 min before the concentration was quantified using a NanoDrop® One Spectrophotometer (Thermo Fisher Scientific, Massachusetts, United States) as described in section 2.3.2, after which the RNA was stored at -80 °C until further use.

2.3.1.2 Liver tissue

Ribonucleic acid was extracted from liver using the RNeasy Mini Kit (Qiagen, Hilden, Germany) according to the manufacturer's instructions. Briefly, 30 mg of tissue was cut from the right anterior of the liver and placed in a 2 mL Eppendorf tube (Eppendorf, Hamburg, Germany) containing a stainless-steel bead (Qiagen, Hilden, Germany) and 600 µL RLT buffer. Tissues were then homogenized using a Qiagen TissueLyser (Qiagen, Hilden, Germany) at 25 Hz for 1 min followed by incubation on ice for 1 min, a process repeated 4 times. The Eppendorf tubes containing the lysed tissues were then centrifuged at 15 000 x g for 3 min at 4 °C, after which the supernatant was transferred to a new tube and the pellet was discarded. One volume of 70% EtOH was added to each tube and mixed by pipetting. The

samples were then transferred to an RNeasy spin column, and centrifuged at 15 000 x g for 15 sec, after which the flow-through was discarded. Subsequently, 700 µL RW1 buffer was added to the RNeasy spin column, before the spin column was centrifuged at 15 000 x g for 15 sec and the flow-through was discarded. Next, 500 µL RPE buffer was added to the spin column, centrifuged at 15 000 x g for 15 sec and the flow-through was discarded. This step was repeated twice, after which the spin column was placed in a new 2 mL collection tube and centrifuged at 15 000 x g for 1 min to completely dry the membrane. The RNeasy spin column was placed in a new 1.5 mL Eppendorf tube (Eppendorf, Hamburg, Germany) and 50 µL nuclease-free water was added directly to the spin column membrane. The column was allowed to stand for 1 min before being centrifuged at 15 000 x g for 1 min to elute the RNA, which was subsequently quantified.

2.3.2 RNA quantification

Ribonucleic acid was quantified using a NanoDrop® One Spectrophotometer (Thermo Fisher Scientific, Massachusetts, United States). The NanoDrop® was initialized and blanked by pipetting 1 µL of nuclease free water onto the pedestal. Thereafter, 1 µL of each sample was added to the pedestal and absorbance was read in triplicate. The average of the three readings were used to determine the concentration, while the ratio of 260 nm to 280 nm was used to evaluate the purity of the RNA, and the 260 to 230 ratio was used to check for DNA contamination. Ratios between 1.8 and 2 were considered acceptable. After quantification, RNA was stored at -80 °C until further use.

2.3.3 DNAse treatment of RNA

To remove DNA contaminants, RNA samples were treated using the Turbo DNA-free™ kit (Ambion, Texas, United States) following the manufacturer's instructions. Briefly, 1 µL of DNAse and 5 µL of DNAse buffer were added to 20 µg of RNA and the reaction volume was made up to 50 µL with nuclease-free water (Ambion, Texas, United States). Samples were mixed and incubated for 30 min at 37 °C, after which an additional 1 µL DNAse was added, followed by a further 30 min incubation at 37 °C. DNAse activity was halted by the addition of 10 µL DNase inactivation reagent, followed by a 5 min incubation at room temperature, with mixing. The samples were then centrifuged at 10 000 x g for 1.5 min and the supernatant was transferred to a new 0.5 mL Eppendorf tube (Eppendorf, Hamburg, Germany). RNA concentrations were determined using a NanoDrop® One Spectrophotometer (Thermo Fisher Scientific, Massachusetts, United States) (Section 2.3.2).

2.3.4 Determination of RNA integrity

Ribonucleic acid integrity was determined using the Agilent 2100 Bioanalyzer and Agilent 6000 Nano kit (Agilent Technologies, California, United States) according to the manufacturer's instructions. Briefly, bioanalyzer electrodes were decontaminated before use by placing them in 350 µL RNaseZAP™ (Invitrogen by Thermo Fisher Scientific, Massachusetts, United States) for 1 min, followed by nuclease-free water for 10 sec. Once decontaminated, the lid of the bioanalyzer was left open for 10 sec to allow the electrodes to dry. To prepare the gel-dye mix, reagents were equilibrated to room temperature for 30 min, after which new filtered gel aliquots were prepared: 550 µL RNA gel matrix was filtered in the centrifuge at 1 500 x g for 10 min at room temperature and 65 µL aliquots were made. RNA 6000 Nano dye concentrate was vortexed and spun down, and 1 µL added to a 65 µL aliquot of gel matrix. The solution was vortexed and centrifuged at 13 000 x g for 10 min at room temperature.

Figure 2: Representative image of the Agilent 6000 Nano Chip.

The RNA 6000 Nano chip (Figure 2) was prepared by placing it on the chip priming station and adding 9 µL of gel-dye mix into well marked with a circled **G**. The plunger was adjusted to 1 mL, after which the chip priming station was closed, and the plunger pressed down until it was held by the clip. After 30 sec the clip was released, and the plunger was allowed to decompress for a further 30 sec before opening the priming station. Ribonucleic acid samples and RNA ladder were placed in a heating block for 2 min at 70 °C for denaturation. Thereafter, 9 µL of gel-dye mix was added to each of the two wells marked G, and 5 µL of RNA 6000 Nano marker was added to each of the sample and ladder wells. Subsequently, 1 µL of sample or ladder was loaded into the respective wells. The chip was vortexed at 542 x g for 30 sec, placed in the electrode chamber of the bioanalyzer and run within 5 min. The integrity of the

RNA samples was determined using 2100 Expert Software (Agilent Technologies, Santa Clara, California, USA) with a RIN value of ≥ 6.00 being considered acceptable

2.3.5 Synthesis of complimentary DNA

The synthesis of complimentary DNA (cDNA) from RNA was performed using the High Capacity cDNA Reverse Transcription Kit (Applied Biosystems, California, United States) according to the manufacturer's instructions. Briefly, 1 µg of RNA was aliquoted into a 0.2 mL PCR tube (Axygen, California, USA) and made up to 10 µl with nuclease free water. All samples were prepared in duplicate for RT-Plus and RT-Minus reactions. Two master mix solutions were prepared containing high quality deoxynucleotide triphosphates (dNTPs), reaction buffer, random primers, RNase inhibitor and nuclease-free water. One master mix was labelled RT-Minus and served as a negative control, while the other was labelled RT-Plus and contained reverse transcriptase. The cDNA synthesis reaction was then prepared by adding 10 µL of either RT-Plus or RT-Minus master mix to the respective duplicates of each sample (Table 2.1). The tubes were vortexed and spun down before being placed in an Applied Biosystems 2720 Thermal Cycler (Applied Biosystems, California, United States). The Thermal Cycler conditions were set for 10 min at 25 °C, 120 min at 37 °C, and 5 sec at 85 °C, after which the temperature was rapidly lowered to 4 °C. Samples were stored at 4 °C until further use.

Table 2.1: Reaction mixture used for cDNA synthesis

Reagent	RT-Plus Volume/Reaction (µL)	RT-Minus Volume/Reaction (µL)	Final concentration
1 µg RNA	10	10	10% w/v
10x RT buffer	2	2	1X
25x dNTP mix	0.8	0.8	1X
10x Random primers	2	2	1X
RNase inhibitor	1	1	-
Nuclease-free water	3.2	4.2	-
Reverse transcriptase	1	-	-
Total volume	20	20	

2.3.6 Test for genomic DNA

To test for genomic DNA (gDNA) contamination, cDNA was amplified using *β-Actin* (*ActB*) exon spanning primers. A reaction mix was prepared containing *ActB* forward and reverse primers, PowerUp™ SYBR® Green Master Mix (Applied Biosystems, California, United States) and nuclease-free water to a final volume of 25 µL (Table 2.2).

Table 2.2: Master mix used for the detection of genomic DNA contamination.

Reagent	Volume/Reaction (µL)	Final concentration
PowerUp™ SYBR® Green Master Mix	12.5	1X
ACTB Forward primer (10 µM) 5'-GGGCCCGGACTCATCGTACT-3'	1	400nM
ACTB Reverse primer (10 µM) 5'-GCCTCACTGTCCACCTTCCA-3'	1	400nM
Nuclease free water	9.5	-
cDNA	1	-
Total volume	25	

A MicroAmp™ Optical 96-well Reaction Plate (Applied Biosystems, California, United States) was prepared by adding 1 µL of either RT-Plus or RT-Minus cDNA to each well, after which 24 µL of SYBR green reaction mix was added. The plate was sealed with MicroAmp™ Optical Adhesive Film (Thermo Fisher Scientific, Massachusetts, United States), placed on a plate shaker at 500 rpm for 10 min and briefly centrifuged at 3000 x g for 1 min before the plate was placed in the Applied Biosystems 7500 Sequence Detection System (Applied Biosystems, California, United States) for quantitative PCR analysis. The cDNA was amplified using the cycling conditions described in Table 2.3.

Table 2.3: Cycling conditions used to test cDNA for genomic DNA contamination.

Step	Temperature (°C)	Time	Cycles
Activation and denaturation	50	2 min	1
	95	10 min	
Fluorescence data collection	95	15 sec	40
	60	1 min	
Dissociation curve	95	15 sec	1
	60	1 min	
	95	15 sec	

The quantity of cDNA for each reaction was determined from the default threshold cycle (Ct) and baseline obtained during the exponential phase. To determine if gDNA contamination could influence quantification, Ct values of the RT-Plus samples were subtracted from the Ct values of the corresponding RT-Minus samples. If the difference in Ct values were equal to or greater than 10 between the corresponding RT-Minus and RT-Plus strand, the presence of contamination was considered to be negligible.

2.3.7 Quantitative Real-Time Polymerase Chain Reaction (qRT-PCR) analysis

Quantitative Real-Time gene expression analysis was performed using TaqMan® gene expression probe assays (Johnson, et al., 2016) (Table 2.4) (Thermo Fisher Scientific, Massachusetts, United States).

Table 2.4: TaqMan® probe assays used in qRT-PCR analysis

Function	Symbol	Gene	Probe assay
		Housekeeping	
	ACTB	Beta actin	Mm02619580_g1
	B2M	Beta 2 microglobulin	Mm00437762_M1
	HPRT1	Hypoxanthine phosphoribosyl transferase 1	Mm03024075_m1
		Liver	
Cholesterol synthesis	*APOB*	Apolipoprotein B	Mm01545150_m1
	HMGCR	3-Hydroxy-3-Methylglutaryl-CoA Reductase	Mm01282499_m1
Lipid synthesis	*SREBF1*	Sterol regulatory element binding factor 1	Mm00550338_m1
	FASN	Fatty Acid Synthase	Mm00662319_m1
	SCD1	Stearoyl-coenzyme A desaturase 1	Mm00448918_m1
Lipid metabolism	*PPARα*		
	CPT1A	Carnitine palmitoyl transferase 1-a	Mm01231183_m1
		Heart	
Oxidative stress	*NOX4*	NADPH oxidase 4	Mm00479246_m1
Inflammation	*NFκB*	Nuclear factor κ B	Mm00495541_m1
Apoptosis	*CASP3*	Caspase 3	Mm01195085_m1
Fibrosis	*CTGF*	Connective tissue growth factor	Mm01192933_m1
	NPPA	Natriuretic peptide precursor A	Mm01255747_g1
Energy homeostasis	*PRKAA2*	Protein kinase, AMP-activated, alpha 2 catalytic subunit	Mm01264789_m1

A standard curve was prepared from a 10-fold serial dilution of pooled cDNA(100, 10, 1, 0.1,0.01, 0.001, 0.0001). cDNA from unknown samples to be tested, was prepared by diluting 1:5 in nuclease free water. A PCR master mix was prepared by combining 5 µL of 2 x TaqMan® Universal PCR Master Mix (Thermo Fisher Scientific, Massachusetts, United States), 3.5 µL nuclease-free water, and 0.5 µL TaqMan® gene expression assay per reaction (Table 2.5). Plates were prepared by adding 1 µL of sample to a MicroAmp™ Optical 96-well Reaction Plate (Applied Biosystems, California, United States) in duplicate, after which 9 µL PCR master mix was added to each well. The plate was sealed, placed on a plate shaker and mixed at 500 rpm for 10 min and thereafter centrifuged at 3000 x g for 1 min. The plate was then placed in an ABI 7500 Sequence Detection System Instrument (Applied Biosystems, California, United States) to conduct the qRT-PCR reactions using the PCR cycling conditions as described in Table 2.3. The quantity, mean, and standard deviation values were calculated by the ABI Standard Quantification software and data was subsequently used to calculate the relative expression values. β-Actin (*ACT-B*) and Hypoxanthine phosphoribosyl transferase 1 (*HPRT1*) were used as endogenous housekeeping genes. Gene quantities were normalised by dividing the mean quantity of target genes by the mean quantity of the housekeeping genes *ACT-B* and *HPRT1* and obtaining a mean of the two values.

Table 2.5: Reaction mixture used to conduct qRT-PCR

Reagent	Volume/Reaction (µL)
Taqman universal PCR master mix	5
Nuclease-free water	3.5
Probe assay	0.5
cDNA	1
Total Volume	10

2.4 **Protein expression by Western blot**

2.4.1 Protein extraction

To further investigate peripheral insulin resistance, protein was extracted from skeletal muscle samples and expression of proteins involved in the insulin signalling pathway was determined. Approximately 100 mg of tissue was placed in a 2 mL Eppendorf tube (Eppendorf, Hamburg, Germany) and rinsed in cold phosphate buffered saline (PBS) (Lonza, Verviers, Belgium), after which the rinse was discarded and 500 µL cold Lysis Buffer and a stainless-steel bead was added to the tube. Tissues were then homogenized using a Qiagen TissueLyser (Qiagen, Hilden, Germany) at 25 Hz for 1 min followed by incubation on ice for 1 min, a process repeated for 4 times. The tubes containing the lysed tissues were then centrifuged at 15 000 x g for 10 min at 4 °C, after which the supernatant was transferred to a new 1.5 mL Eppendorf tube (Eppendorf, Hamburg, Germany) and stored at -80 °C until further use.

2.4.2 Protein concentration determination

Protein concentrations were determined using the reducing agent compatible and detergent compatible (RC DC) protein assay kit (Bio-Rad, California, United States) according to manufacturer's instructions. Sample dilutions (1:20) were prepared by adding 5 µL lysate to 95 µL nanopore water. To prepare reagent A' solution, 20 µL DC reagent S was added to 1 mL DC reagent A. Subsequently, 5 µL of bovine serum albumin (BSA) standards (Bio-Rad, California, United States) [0.125, 0.25, 0.5, 1, 1.5, and 2 mg/ml] and diluted samples was added to a clear 96-well plate. Thereafter, 25 µL of reagent A' and 200 µL of reagent B were added to each well containing standards and samples. The plate was mixed on a plate shaker at 500 rpm for 10 sec and incubated for an additional 10 min at room temperature before measuring absorbance at 630 nm using a SpectraMax i3 plate reader (Molecular Devices, California, United States) and Gen 6 software (Molecular Devices, California, United States). A standard curve with linear equation ($y = mx + c$) was generated using absorbance values of BSA standards to calculate the concentration of each sample based on its mean absorbance value. The concentration of the sample was then determined by multiplying the obtained concentration by the dilution factor.

2.4.3 Protein gel electrophoresis

Sample buffer was prepared by adding 50 µL β-mercaptoethanol (Fluka, Bucharest, Romania) to 950 µL 2 x Laemmli Sample Buffer (Bio-Rad, California, United States). Between 30-50 µg protein lysates were mixed with sample buffer in a 1:1 ratio and denatured by heating for 5

min at 95 °C, and snap-cooled by placing on ice immediately. Criterion™ TGX™ 12% Precast Midi Gels (Bio-Rad, California, United States) were placed in a gel electrophoresis tank which was then filled with 1x Tris/Glycine/SDS running buffer (Bio-Rad, California, United States). Subsequently, 5 µL Precision Plus Protein™ Western C™ marker (Bio-Rad, California, United States), and 30-50 µg protein sample was loaded onto the gel and electrophoresis was initiated using the PowerPac HC (Bio-Rad, California, United States) at 150 V for 70 min.

2.4.4 Western blot analysis

2.4.4.1 Transfer to Nitrocellulose membrane

Following gel electrophoresis, separated proteins were transferred to a nitrocellulose (NC) membrane using Trans-Blot® Turbo™ Midi NC transfer packs (Bio-Rad, California, United States). The transfer sandwich was assembled in the transfer cassette of a Trans-Blot® Turbo™ (Bio-Rad, California, United States) and run for 10 min at 25 V and 2.5 A.

2.4.4.2 Ponceau S stain

Once the transfer was complete, the membrane was removed and marked with a pencil before submerging in Ponceau S stain (Sigma-Aldrich, Missouri, United States) and placing on an orbital shaker for 10 min. Thereafter the membrane was rinsed gently in dH_2O until the background was clear and complete protein transfer could be confirmed by the presence of red stained bands on the membrane. The stain was then reversed by washing the membrane in 1 x Tris-buffered saline with 0.1% Tween 20 (TBS-T) for 5 min (prepared as in Appendix B2).

2.4.4.3 Membrane labelling

The NC membrane containing separated proteins was blocked in 5% (w/v) Skim Milk Powder (Sigma-Aldrich, Missouri, United States) in TBS-T for 120 min at room temperature on an orbital shaker. Subsequently the membrane was rinsed thrice for 5 min in TBS-T, before being incubated in primary antibody in TBS-T overnight at 4 °C on an orbital shaker. The respective antibodies as well as the dilutions used are indicated in table 2.6. The following day, the membrane was rinsed thrice for 5 min in TBS-T, before incubating in StrepTactin® HRP Conjugate (Bio-Rad, California, United States) as well as horseradish peroxidase (HRP) conjugated secondary antibody specific to the host species of the primary antibody, in 2.5% (w/v) Skim Milk Powder (Sigma-Aldrich, Missouri, United States) in TBS-T for 90 min. Subsequently, the membrane was rinsed thrice for 5 min in TBS-T, before proceeding to chemiluminescent detection. Clarity Western Enhanced Chemiluminescence (ECL) substrate

(Bio-Rad, California, United States) was prepared by mixing part A and part B in a 1:1 ratio before and immersing the membrane therein. The membrane was incubated for 5 min, avoiding direct light exposure, before imaging on the Bio-Rad ChemiDoc MP System (Bio-Rad, California, United States). Protein bands were quantified using Image Lab™ Software (Bio-Rad, California, United States) and all proteins were normalized to a housekeeping gene, β-Actin, which served as the loading control (Johnson, et al., 2016).

Table 2.6: Antibodies and dilutions used for Western blot analysis

Antibody	Dilution	Catalogue number	Company
pPI3K	1:500	4228	Cell Signalling
Pi3K	1:500	5569	Cell Signalling
pAKT	1:500	9271	Cell Signalling
AKT	1:500	9272	Cell Signalling
pAMPK	1:500	2535	Cell Signalling
AMPK	1:500	2532	Cell Signalling
GLUT4	1:500	2213	Cell Signalling
CPT1A	1:1000	Ab53532	Abcam
B-actin	1:1000	47778	Santa Cruz

2.4.4.4 Stripping of membranes

Membranes were stripped by incubating the nitrocellulose membrane for 5 min, in Restore PLUS™ Western Blot Stripping Buffer (Thermo Fisher Scientific, Massachusetts, United States). Buffer was discarded, and nitrocellulose membrane was washed in TBST thrice for 10 min on an orbital shaker. Membranes were rinsed in TBS-T before continuing with blocking and probing as described in section 2.4.4.3.

2.5 **Statistical analysis**

Data are expressed as the mean ± standard error of the mean (SEM). Statistical analysis was performed using GraphPad Prism (Version 7.00, California, USA). Groups of data were compared with a two-way analysis of variance (ANOVA) followed by Dunnet's Multiple Comparison tests. The unpaired, two-tailed student t-test was used when only two groups were compared. Values of $p<0.05$ were regarded as statistically significant.

Chapter 3: Results

3.1 Morphometric Data

Six- to fifteen-week-old *Lepr*$^{db/db}$ mice and their lean *Lepr*$^{db/+}$ controls were fed a standard mouse chow diet for 10 weeks. Body weights and fasting blood glucoses were recorded weekly. By 6 weeks of age, the body weights of db/db mice were significantly higher compared to their age-matched lean controls (31.75 g ± 0.71 vs. 20.50 g ± 0.55, $p < 0.001$) and this remained significantly higher throughout (Fig 3.1 A). At 8 weeks of age, four-hour fasting blood glucose levels of db/db mice were elevated by 65% compared to db/+ controls (13.27 mmol/L ± 3.60 vs. 8.04 mmol/L ± 2.14, $p < 0.05$). At 9 weeks of age, fasting blood glucose levels in db/db mice increased further and remained above 20 mmol/L for the remainder of the experimental time points whereas blood glucose for the db/+ control remained consistently low (Fig 3.1 B). Calculated HOMA-IR was slightly elevated in db/db mice when compared to db/+ controls (0.48 ± 0.06 vs. 0.20 ± 0.03) at 7 weeks and was significantly increased in db/db mice at 15 weeks (1.46 ± 0.50 vs 0.1 ± 0.02, $p < 0.001$) (Fig 3.1 C).

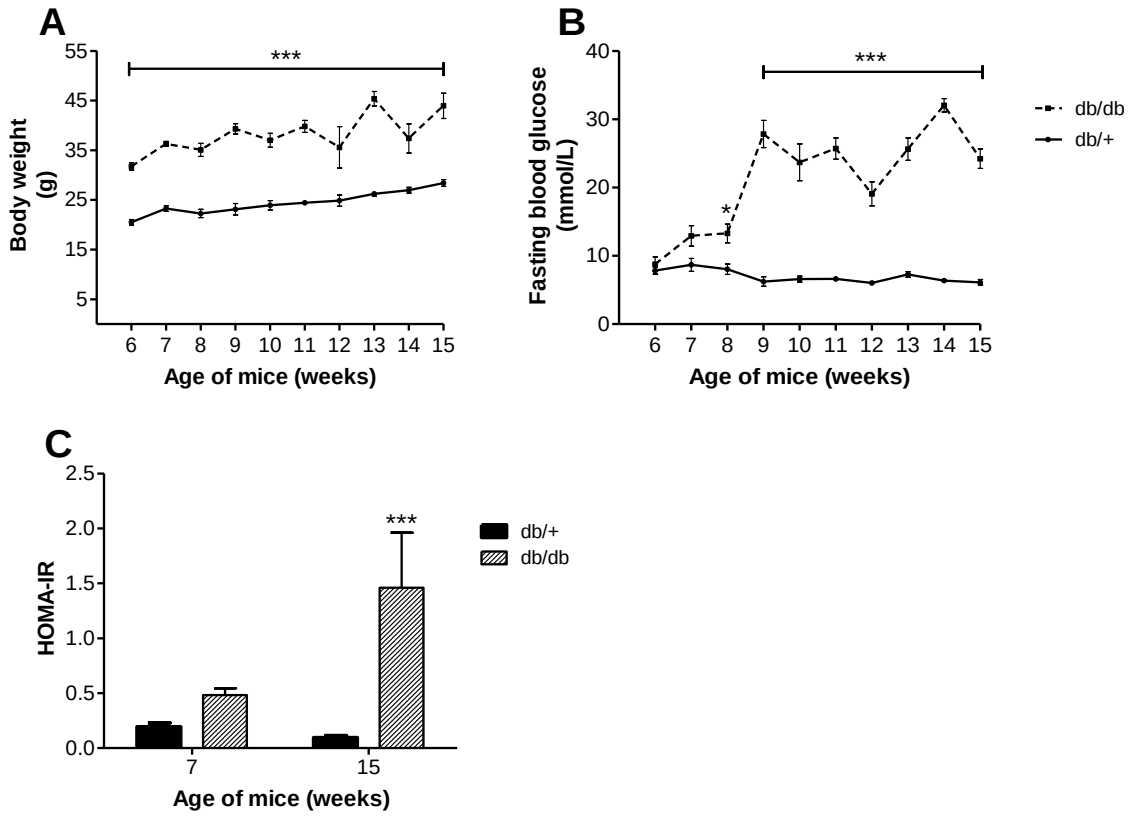

Figure 3.1: Body weights, fasting blood glucose levels and HOMA-IR. *Body weights (A), four-hour fasting blood glucose levels (B) and HOMA-IR index (C) of leptin receptor deficient mice ($Lepr^{db/db}$) and heterozygous lean controls ($Lepr^{db/+}$) from 6 to 15 weeks of age were significantly increased compared to the db/+ control. Results are presented as mean ± SEM of 8 animals per group. Data were analysed using two-way analysis of variance (ANOVA) followed by Dunnet's Multiple Comparison tests. * p ≤ 0.05, ***p ≤ 0.001 db/db versus age-matched db/+ control.*

3.2 Echocardiography

In the obese state, structural and functional modifications to the myocardium results in cardiac hypertrophy and contractile dysfunction, affecting ejection capacity. To investigate this pathology, TDI echocardiography was used to determine % EF in db/db compared to db/+ controls. At 13 weeks of age db/db mice displayed a significantly reduced % EF when compared to db/+ controls (51.40 ± 2.50 vs. 61 ± 4.53, $p < 0.05$) (Figure 3.2).

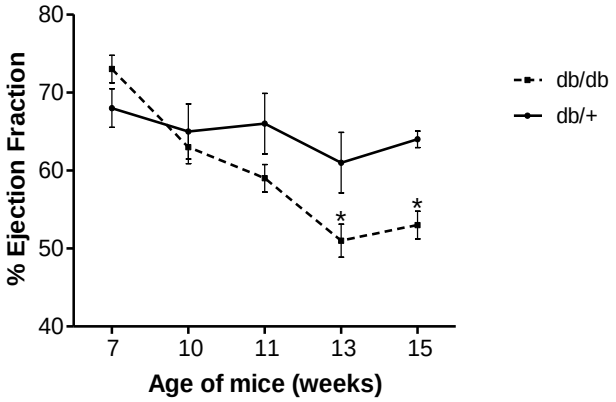

Figure 3.2: Echocardiography. *Percentage ejection fraction of leptin receptor deficient mice ($Lepr^{db/db}$) and heterozygous lean controls ($Lepr^{db/+}$) from 7 to 15 weeks of age as determined by tissue doppler echocardiography. Results are presented as mean ± SEM of 6 animals per group Data were analysed using two-way analysis of variance (ANOVA) followed by Dunnet's Multiple Comparison tests. * $p \leq 0.05$ versus age-matched control.*

3.3 **Lipogram**

As an indication of dyslipidaemia and a measure of metabolic risk, lipid profiles were performed in db/db mice and their heterozygous db/+ controls. At 7 weeks, triglyceride levels were significantly elevated in db/db mice when compared to the lean db/+ controls (2.43 mmol/L ± 0.11 vs. to 0.84 mmol/L ± 0.08, $p < 0.001$), and levels remained elevated throughout the experimental timeframe (Fig 3.3 A). Similarly, serum LDL levels were significantly elevated at 7 weeks in the db/db group when compared to the db/+ controls (0.55 mmol/L ± 0.03 vs. 0.30 mmol/L ± 0.004, $p < 0.01$) and remained elevated at 13 and 15 weeks, though not significant at 10 weeks (0.38 mmol/L ± 0.05 vs. 0.30 mmol/L ± 0.01) (Fig 3.3 B). Furthermore, at 7 weeks total cholesterol levels of db/db mice were significantly raised when compared to db/+ controls (3.90 mmol/L ± 0.14 vs. 1.90 mmol/L ± 0.04, $p < 0.001$) and remained elevated throughout the study (Fig 3.3 C).

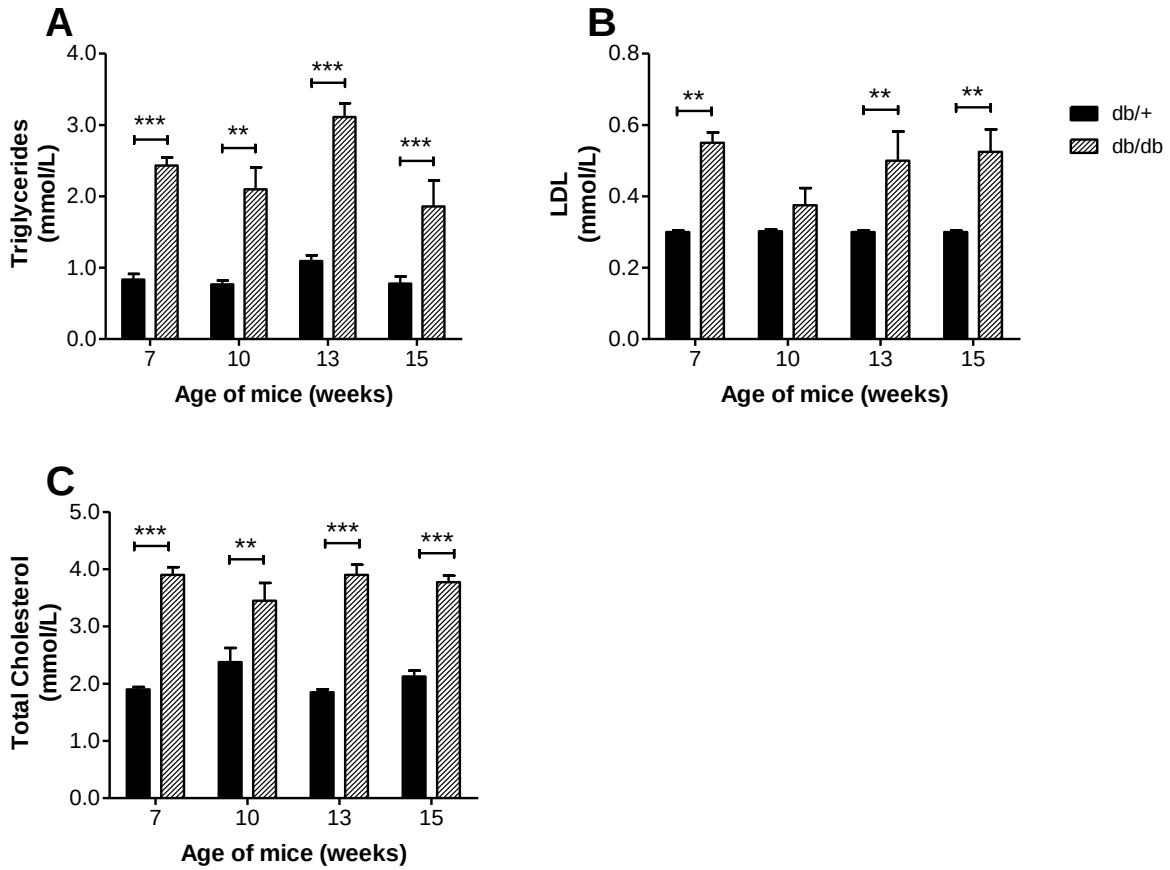

Figure 3.3: Serum lipid levels. *Triglycerides (A), low-density lipoprotein (LDL) (B), and total cholesterol (C) as determined by serum lipogram was increased leptin receptor deficient mice ($Lepr^{db/db}$) when compared to heterozygous lean controls ($Lepr^{db/+}$) from 7 to 15 weeks of age. Results are presented as mean ± SEM of 8 animals per group Data were analysed using two-way analysis of variance (ANOVA) followed by Dunnet's Multiple Comparison tests. ** p ≤ 0.01, ***p ≤ 0.001 versus age-matched control.*

3.4 Liver Enzymes

Aspartate Transaminase and ALT are known markers of liver toxicity. There was a significant increase in AST at 13 weeks in the db/db group when compared to db/+ controls (128.75 IU/L ± 29.48 vs. 50.75 IU/L ± 0.85, $p < 0.01$) (Fig 3.4 A). Similarly, at 7 weeks, ALT levels were significantly higher in the db/db group when compared to db/+ controls (110.33 IU/L ± 13.32 vs. 46.50 IU/L ± 11.30, $p < 0.05$) (Fig 3.4 B). While AST and ALT can be used as a measure of liver damage, the ratio of AST/ALT can give an indication of the type of liver damage, with a high ratio, around 2, associated with alcoholic liver disease, and a ratio lower than 1 associated with non-alcoholic hepatic lipid accumulation (Sorbi, et al., 1999). The ratio of AST/ALT in db/db mice was less than 1 at 7 weeks (0.76 ± 0.07) and remained below 1 throughout (Fig 3.4 C), indicating the presence of hepatic steatosis.

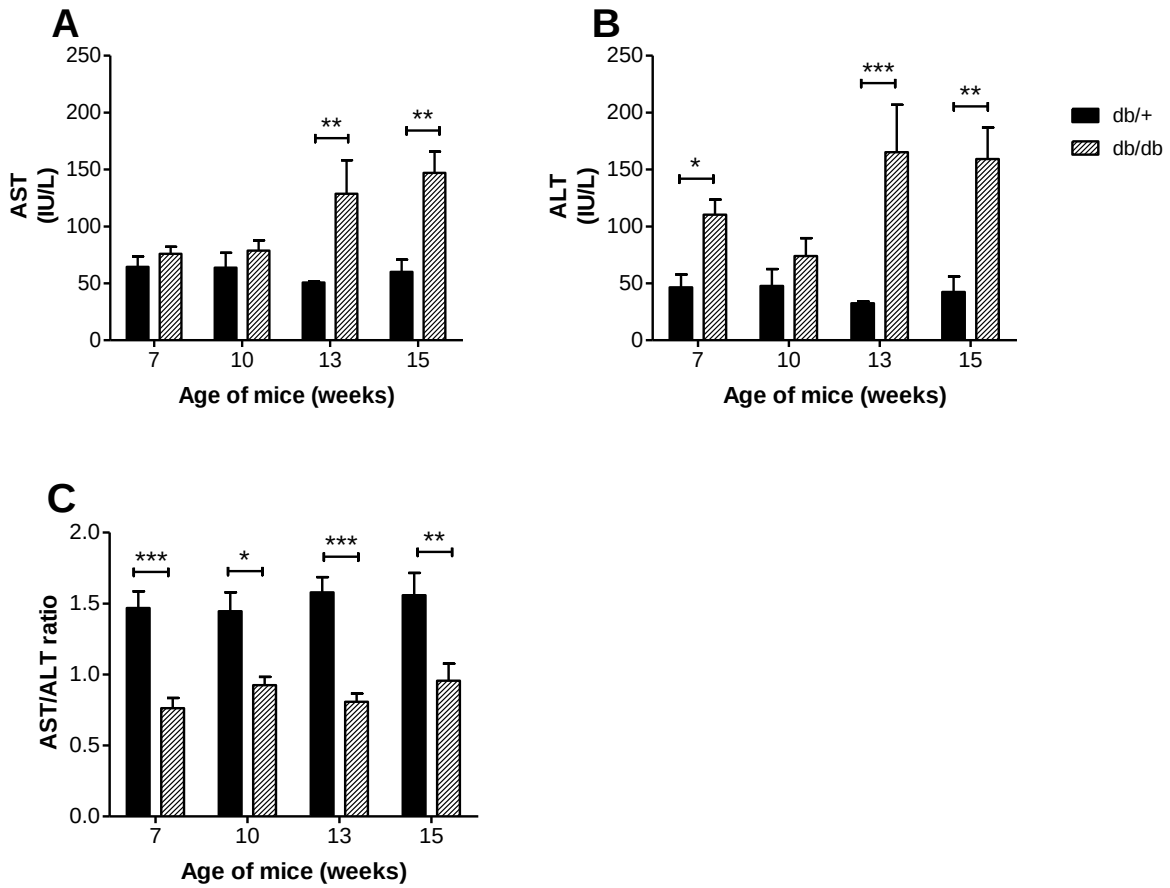

Figure 3.4: Aspartate Transaminase and Alanine Transaminase levels in serum. *Levels of Aspartate Transaminase (AST) (A), Alanine Transaminase (ALT) (B), and AST/ALT ratio (C) in serum of leptin receptor deficient mice ($Lepr^{db/db}$) remained altered when compared to heterozygous lean controls ($Lepr^{db/+}$) from 7 to 15 weeks of age. Results are presented as mean ± SEM, * $p \leq 0.05$, ** $p \leq 0.01$. Data were analysed using two-way analysis of variance (ANOVA) followed by Dunnet's Multiple Comparison tests. ***$p \leq 0.001$ db/db versus age-matched db/+ control.*

3.5 Haematoxylin and Eosin stain of liver sections

While liver enzymes can be used as a marker of liver damage, histological analysis remains the gold standard for confirming the onset of NAFLD. Upon H&E-staining and histological analysis of paraffin-embedded liver sections, our results indicated that simple steatosis was present at 7 weeks of age and that the severity of hepatic lipid accumulation increased with age. Microvesicular steatosis was identified at 7 weeks by the accumulation of multiple, small lipid droplets in hepatocytes, as indicated by white arrows (Fig 3.5 B). At 10 weeks microvesicular steatosis persisted, with an increased number of hepatocytes displaying lipid accumulation. By 13 weeks of age, intracellular lipid accumulation in the db/db group (Fig 3.5 F) led to hypertrophy with the nucleus of some cells displaced to the side of the cell. This phenomenon worsened by 15 weeks of age (Fig 3.5 H), where the steatosis appeared to be progressing towards macrovesicular steatosis, where the lipid droplets within the cell merge into one and the nucleus is eventually disintegrated.

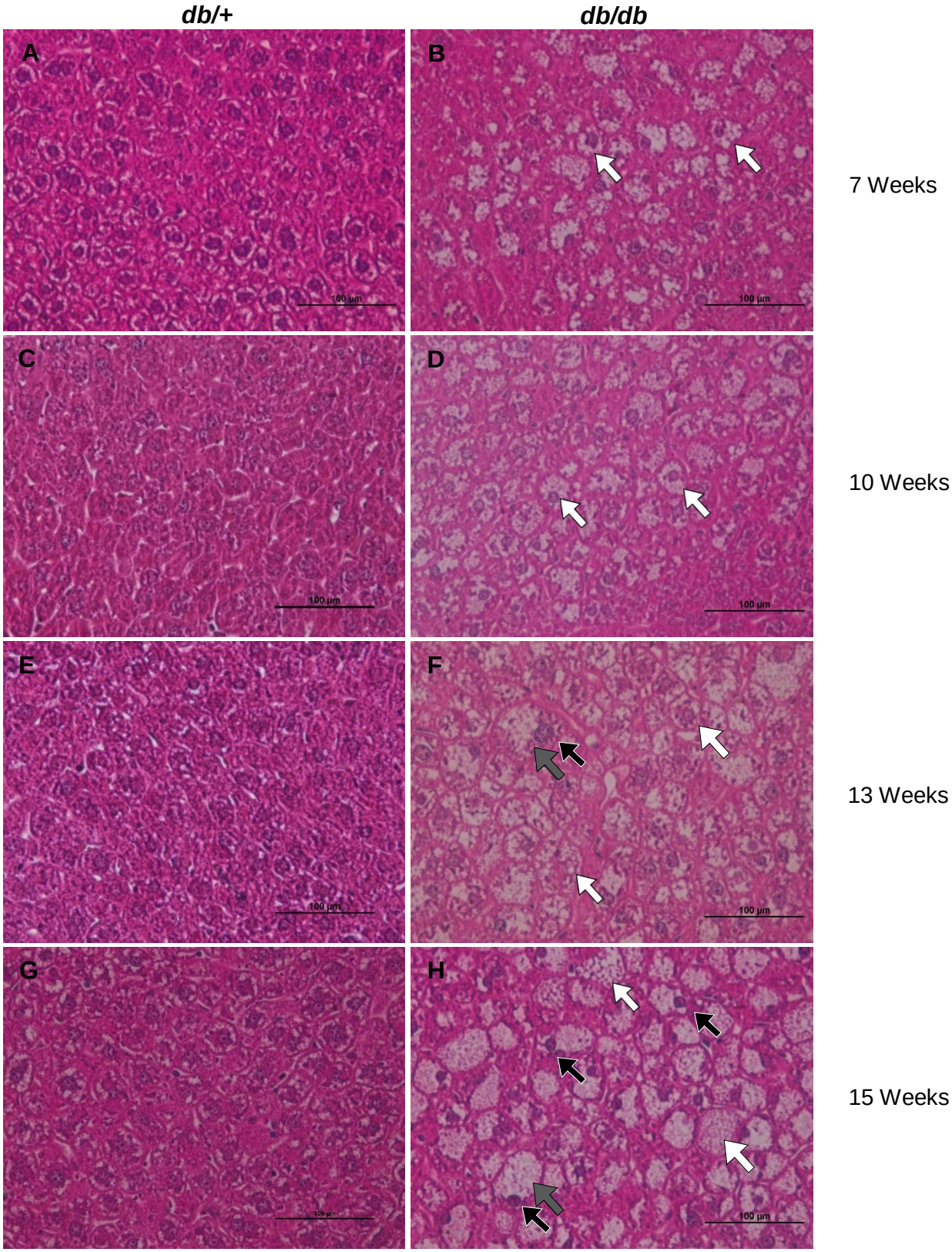

Figure 3.5: Haematoxylin and Eosin stain of liver sections. *Photomicrographs of paraffin-embedded liver sections of heterozygous controls ($Lepr^{db/+}$) retained normal morphology (A, C, E, G), while leptin receptor deficient mice ($Lepr^{db/db}$) (B, D, F, H) displayed microvesicular steatosis from 7 to 10 weeks, which progressed towards macrovesicular steatosis at 15 weeks of age with displacement of the nucleus to the side of the cell. Scale bar = 100 µm, white arrow = microvesicular steatosis, grey arrow = hypertrophy, black arrow = nuclear displacement*

3.6 Gene and protein expression analysis

3.6.1 Liver gene expression

3.6.1.1 De novo lipogenesis

To further investigate hepatic lipid accumulation, genes involved in lipid metabolism and *de novo* lipid synthesis were investigated. The mRNA expression of the transcriptional regulator *SREBF1*, involved in fatty acid biosynthesis, was not significantly altered in db/db mice when compared to age-matched db/+ controls at any of the time points (Fig 3.6 A). Interestingly, the expression of mRNA for *FASN*, the enzyme that catalyses fatty acid synthesis, was significantly increased at 7 weeks in db/db mice when compared to db/+ controls (1.16 ± 0.18 vs. 0.25 ± 0.05, $p < 0.01$) and remained elevated throughout (Fig 3.6 B). Similarly, the expression of mRNA for SCD1, an enzyme involved in the synthesis of monounsaturated fatty acids, was also significantly increased by 7 weeks in db/db mice when compared to db/+ controls (1.03 ± 0.08 vs. 0.20 ± 0.05, $p < 0.001$) and remained elevated throughout (Fig 3.6 C). Augmented *HMGCR*, a rate-controlling enzyme in cholesterol biosynthesis, is known to cause an increase in LDL clearance, of which ApoB is the main protein constituent. In this study mRNA expression of *HMGCR*, was significantly increased at 7 weeks in the db/db group when compared to db/+ controls (1.29 ± 0.09 vs 0.71 ± 0.13, $p < 0.001$) and remained elevated at 13 and 15 weeks. Expression was also increased at 10 weeks, though not significantly (Fig 3.6 D). Interestingly, there was no significant change in *APOB* mRNA expression at any of the time points (Fig 3.6 E).

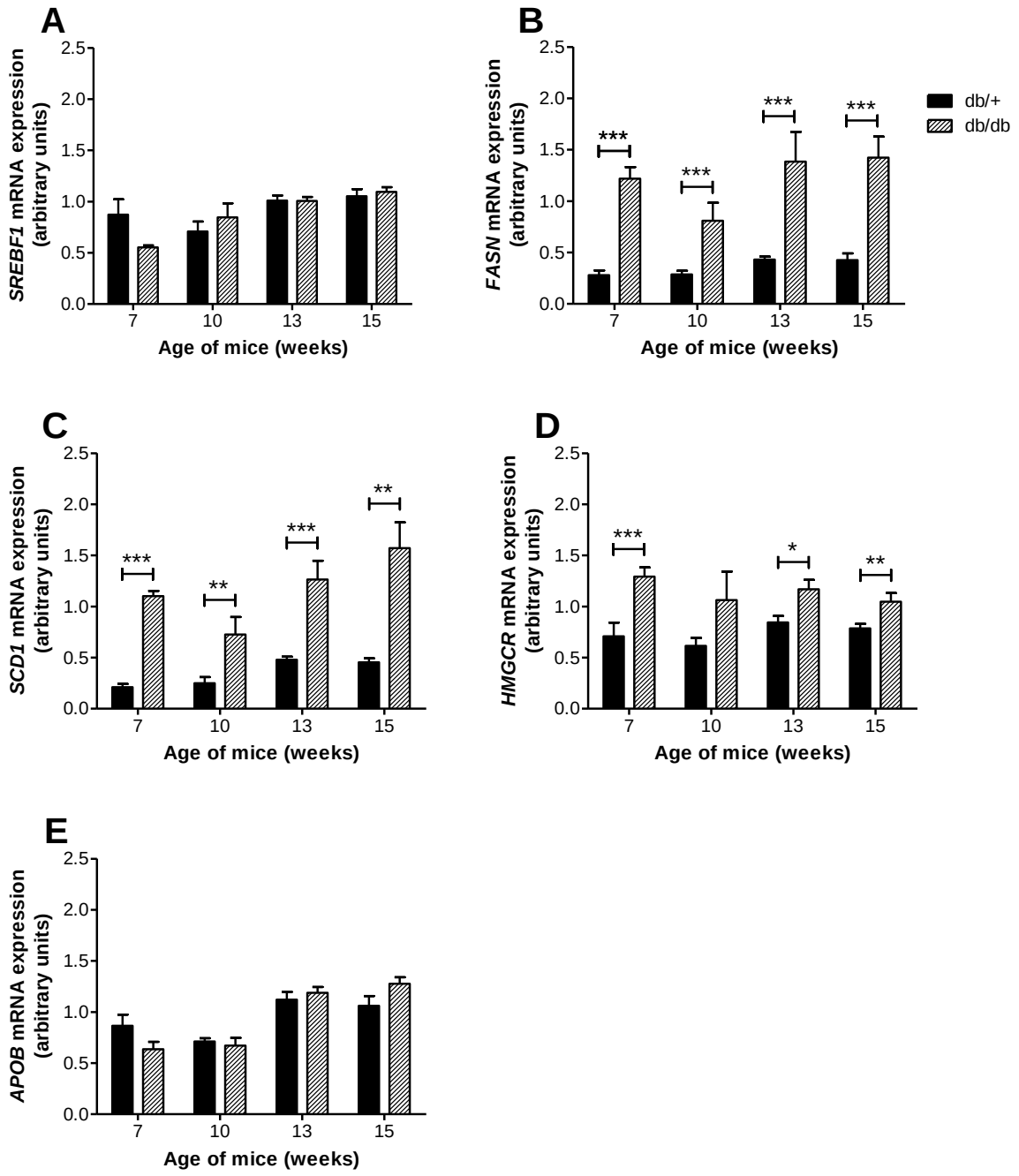

Figure 3.6: Expression of lipogenic genes in liver. *Expression of lipogenic genes in livers of leptin receptor deficient mice ($Lepr^{db/db}$) and heterozygous lean controls ($Lepr^{db/+}$) from 7 to 15 weeks of age. Results are normalized to ACTB and HPRT1, and presented as mean ± SEM of 8 animals per group. Data were analysed using an unpaired, two-tailed student t-test. * $p \leq 0.05$, ** $p \leq 0.01$, *** $p \leq 0.001$ versus age-matched control.*

3.6.1.2 Hepatic fatty acid oxidation

Long-chain fatty acids, a known inducer of *CPT1* modulate fatty acid β-oxidation through the activation of *PPARα*. In this study the expression of *PPARα* was slightly decreased in db/db mice at 7 weeks, though not significantly, and increased at 15 weeks (1.53 ± 0.13 vs. 1.12 ± 0.10 $p < 0.01$) (Fig 3.7 A). *CPT1* was significantly decreased in db/db mice compared to controls (0.63 ± 0.03 vs. 0.99 ± 0.09, $p < 0.01$) at 7 weeks of age, but not at any of the other time points (Fig 3.7 B).

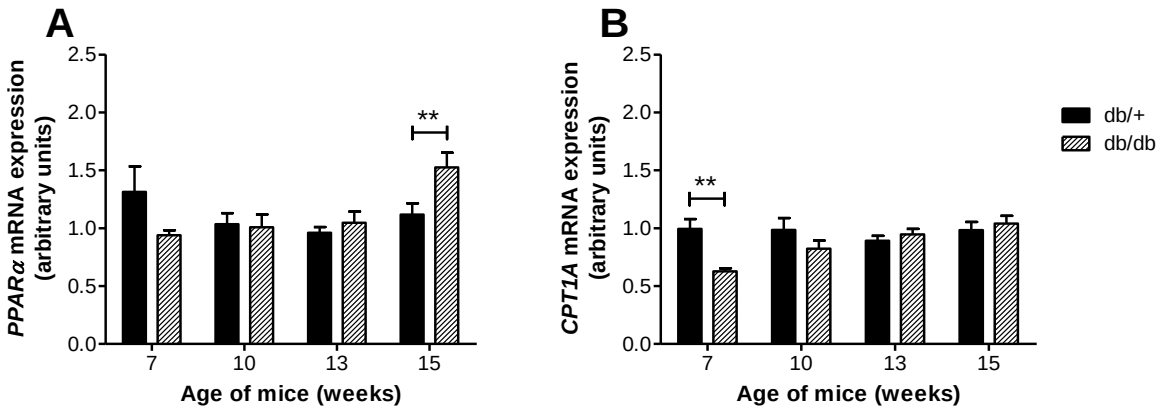

Figure 3.7: Expression of lipolytic genes in liver. *Expression of genes involved in fatty acid β-oxidation in livers of leptin receptor deficient mice ($Lepr^{db/db}$) and heterozygous lean controls ($Lepr^{db/+}$) from 7 to 15 weeks of age. Results are normalized to ACTB and HPRT1, and presented as mean ± SEM of 8 animals per group. Data were analysed using an unpaired, two-tailed student t-test. * $p \leq 0.05$, ** $p \leq 0.01$, *** $p \leq 0.001$ versus age-matched control.*

3.6.2 Cardiac gene expression

In the heart, increased oxidative stress, inflammation and fibrosis leads to the activation of pro-apoptotic pathways and ultimately contractile dysfunction. Gene expression of *NOX4*, a major source of oxidative stress, was significantly increased in db/db mice compared to db/+ controls at 10 and 15 weeks of age (1.23 ± 0.30 vs. 0.77 ± 0.09, $p < 0.05$) (Fig 3.8 A). Expression of *NFκB* mRNA, a transcription factor involved in inflammation and cell survival, was significantly increased in the db/db group when compared to db/+ controls (1.68 ± 0.09 vs. 0.69 ± 0.04, $p < 0.001$) at 10 weeks of age and remained elevated throughout (Fig 3.8 B). Connective tissue growth factor (*CTGF*), a protein involved in fibrosis, also showed significantly increased mRNA expression in the obese db/db group when compared to db/+ controls (2.08 ± 0.39 vs. 0.98 ± 0.27, $p < 0.001$) at 15 weeks of age (Fig 3.8 C). Caspase 3 (*CASP3*), a known determinant of apoptosis was significantly increased in db/db mice when compared to db/+ controls (1.42 ± 0.10 vs. 1.06 ± 0.06, $p < 0.05$) at 10 weeks of age and remained elevated throughout the study (Fig 3.8 D).

Expression of NPPA mRNA, encoding for Atrial Natriuretic Peptide (ANP), a protein involved in cardiac metabolic homeostasis as well as the prevention of maladaptive cardiac hypertrophy, was not significantly different between the db/db mice and db/+ controls at any of the time points (Fig 3.8 E). Similarly, AMPK, an enzyme involved in maintaining cellular energy homeostasis, was not significantly different between the db/db mice and db/+ controls at any of the time points (Fig 3.8 F).

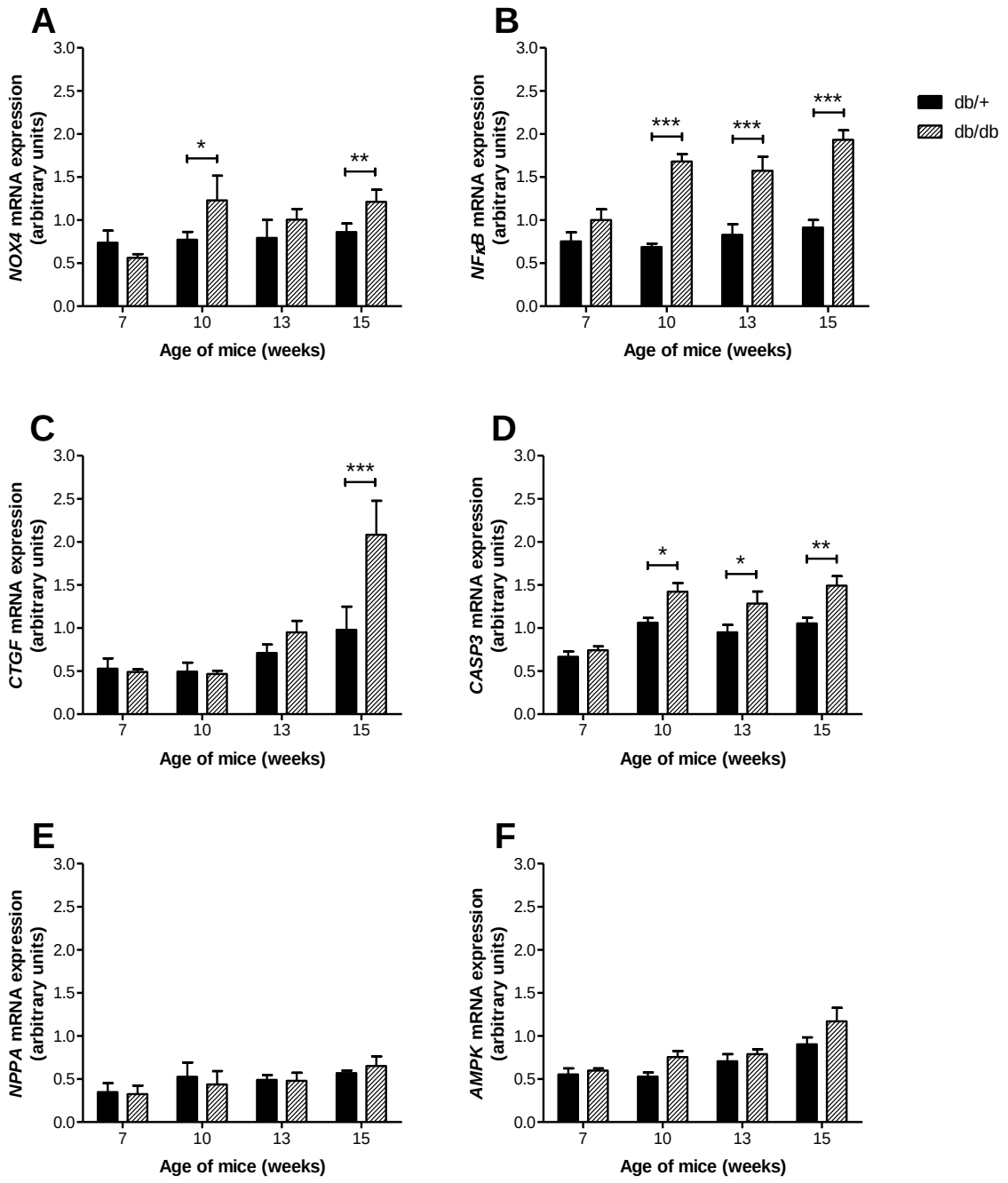

Figure 3.8: mRNA expression in heart tissue. *Expression of mRNA in hearts of leptin receptor deficient mice (Lepr$^{db/db}$) and heterozygous lean controls (Lepr$^{db/+}$) from 7 to 15 weeks of age. Results are normalized to ACTB and B2M, and presented as mean ± SEM of 8 animals per group. Data were analysed using an unpaired, two-tailed student t-test. * $p \leq 0.05$, ** $p \leq 0.01$, *** $p \leq 0.001$ versus age-matched control.*

3.6.3 Protein Expression by Western Blot

Insulin resistance is characterised not only by altered circulating insulin levels, but also by impaired glucose uptake in peripheral tissues (Wilcox, 2005). Insulin signalling can be activated either by the insulin-dependent pathway (IRS/PI3K/AKT) or the insulin-independent pathway (AMPK) that results in the translocation of GLUT4 to the cell membrane. Thus, to investigate glucose uptake into peripheral tissue, the activation of proteins in this pathway was quantified. There was a decrease in the p/tPI3K ratio in db/db mice at 10 weeks (0.17 ± 0.03 vs 0.10 ± 0.01, $p < 0.01$) (Fig 3.9 A). This was accompanied by a similar decrease in the p/tAKT ratio in db/db mice at 10 weeks (0.23 ± 0.06 vs 0.12 ± 0.03, $p < 0.05$) (Fig 3.9 B). There was no change in the p/t AMPK ratio (Fig 3.9 C). Expression of GLUT4 in the cytosolic fraction of skeletal muscle was increased at 13 and 15 weeks of age when compared to db/+ controls, though this difference was not statistically significant (Fig 3.9 D). Carnitine Palmitoyltransferase-1 (CPT1) is a mitochondrial membrane protein involved in the transport of fatty acids into the mitochondria for beta oxidation. CPT1 is inhibited by malonyl-CoA and it's downregulation promotes lipid accumulation and subsequent exacerbation of insulin resistance. Protein expression of CPT1 decreased with age and was significantly lower in the db/db group than in db/+ controls (0.03 ± 0.004 vs. 0.08 ± 0.22, $p < 0.05$) at 15 weeks of age (Fig 3.9 E).

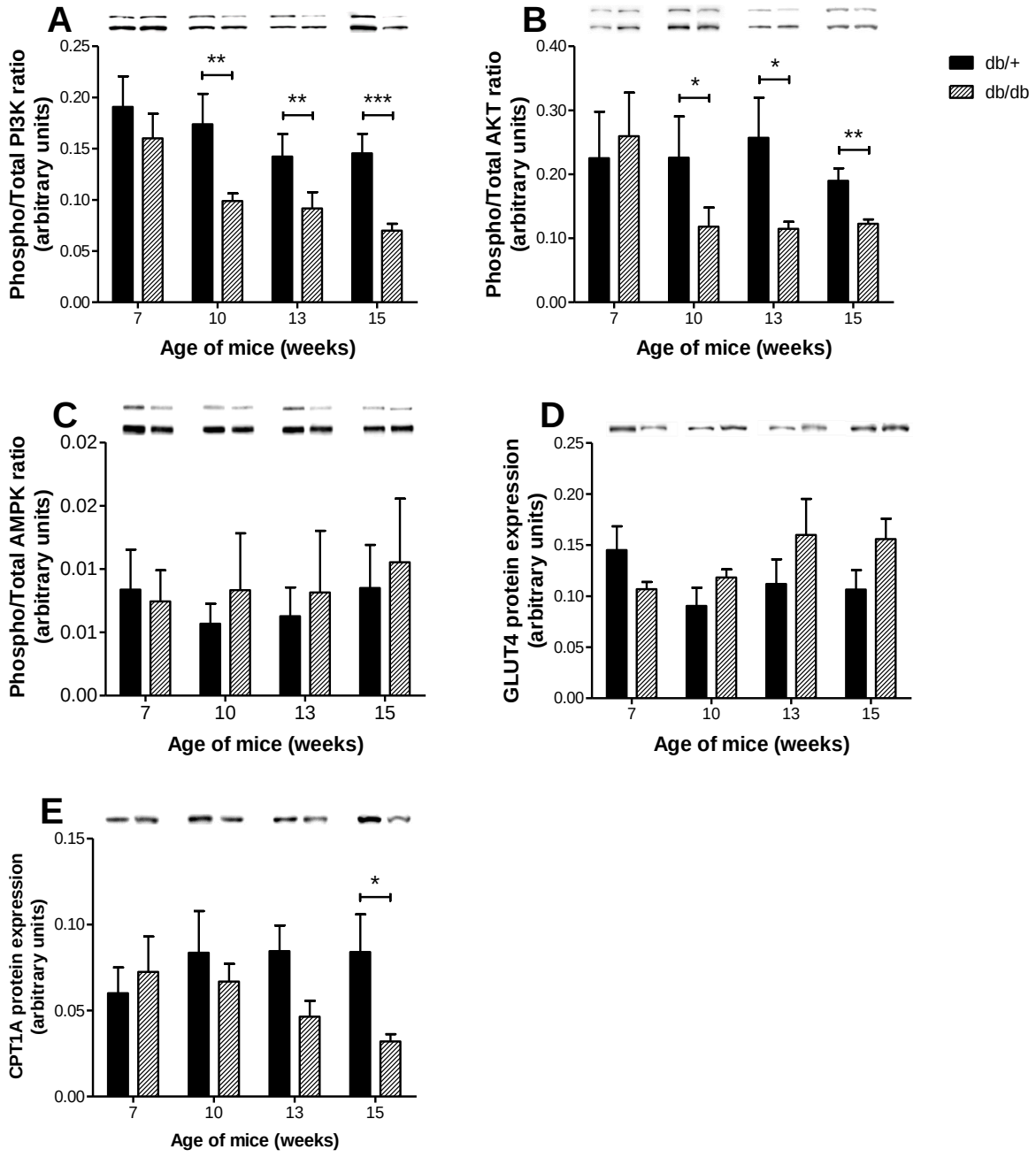

Figure 3.9: Protein expression in skeletal muscle. *Ratio of phosphorylated to total protein expression of PI3K (p/tPI3K) (A), p/t AKT (B), p/tAMPK (C), and CPT1 (D) in skeletal muscle lysates of leptin receptor deficient mice (Lepr$^{db/db}$) and heterozygous lean controls (Lepr$^{db/+}$) from 7 to 15 weeks of age, normalised to β-actin as a loading control. Results are presented as mean ± SEM of 6 animals per group, Data were analysed using an unpaired, two-tailed student t-test. ** p ≤ 0.01 versus age-matched control.*

Chapter 4: Discussion

4.1 Obesity

Obesity constitutes a major health concern, as it is associated with the development of dyslipidaemia, NAFLD, insulin resistance, and subsequent cardiac dysfunction (Kopelman, 2000; Mantovani, et al., 2015; Fruh, 2017). In the obese state, increased lipolysis is a major source of augmented FFA that is invariably associated with increased fatty acid accumulation in patients with NAFLD as well as insulin resistance (Turner, et al., 2014; Feng, et al., 2017). It has been reported that 80 - 90% of obese individuals also have NAFLD (Gaggini, et al., 2013), ensuing in the putative belief that NAFLD is the hepatic manifestation of metabolic syndrome (Ter Horst & Serlie, 2017; Han & Lee, 2017). Furthermore, the prevalence of NAFLD in the general population is between 25% and 30%, while amongst T2DM patients it is up to 70% (Gaggini, et al., 2013), suggesting that an interplay exists between NAFLD and insulin resistance. However, whether obesity-induced NAFLD initiates peripheral insulin resistance, or whether peripheral insulin resistance precedes the onset of NAFLD remains to be explored (Gruben, et al., 2014).

As health costs related to metabolic syndrome and cardiovascular disease continue to rise, it becomes increasingly important to understand the related disease pathology. Understanding the mechanism that links NAFLD and insulin resistance to cardiac dysfunction may assist in the identification of therapeutic targets to combat the disease pathology. More so, it may allow for the identification and screening of prognostic markers, which may in turn allow for early interventions to prevent the onset of disease entirely.

In this study, a leptin receptor-deficient db/db mouse model was employed to investigate the disease state. The afore mentioned is a well-established and translatable model for the development of T2DM and cardiac dysfunction, in which db/db mice become grossly obese, hyperglycaemic and hyperlipidaemic as early as 6 weeks of age, while displaying left ventricular dysfunction at 12 weeks of age (Kobayashi, et al., 2000; Hall, et al., 2014; Wang, et al., 2014; Dludla, et al., 2017). Our study confirms previous findings, showing that db/db mice displayed raised body weight at 6 weeks of age, accompanied by the classical trio of hypertriglyceridemia, hypercholesterolaemia, and augmented LDL, characteristic of metabolic syndrome (Hur, et al., 2015).

Another element of metabolic syndrome includes chronically elevated levels of blood glucose and insulin. Blood glucose is naturally increased post-prandially and decreases as insulin action facilitates glucose clearance. In a fasted state blood glucose levels are maintained through a balance between gluconeogenesis in the liver and glucose uptake by other tissues (Röder, et al., 2016). However, in the case of insulin resistance, glucose uptake is not facilitated, resulting in the build-up of glucose in the blood, persisting even in the fasted state (Abdul-Ghani, et al., 2006). Fasting blood glucose levels can thus be used as an indication of possible insulin resistance. Similarly, HOMA-IR is a known method to assess β-cell function and insulin resistance from fasting blood glucose level and C-peptide concentrations. As HOMA-IR calculation uses both the fasting blood glucose and fasting blood insulin, it gives an indication of the ability of insulin to stimulate glucose clearance. High levels of fasting blood glucose concurrent with high levels of insulin would thus give a high HOMA score and indicate reduced insulin sensitivity (Matthews, et al., 1985).

Studies such as those done by Dong, et al. (2015) and Lim, et al. (2016) show that both fasting blood glucose and HOMA-IR are significantly increased in db/db mice as insulin resistance develops. This supports findings in the current study, where fasting blood glucose levels were slightly elevated in db/db mice by 7 weeks of age, though not significantly. At the same time, HOMA-IR was slightly raised but remained below 1, indicating maintained insulin sensitivity. Fasting blood glucose levels were significantly elevated by 8 weeks of age and increased dramatically by 9 weeks of age, correlating with changes in muscle insulin signalling at 10 weeks and possibly indicating the onset of insulin resistance.

4.2 The onset of hepatic lipotoxicity

In addition to studies investigating T2DM, db/db mice are frequently used as a murine model in the examination of NAFLD, as these mice display mild to severe steatosis with associated increased aminotransferases (Trak-Smayra, et al., 2011; Liu, et al., 2016). The aminotransferases AST and ALT are early markers of hepatocellular damage and are used as predictive measures to evaluate an individual at risk for developing NAFLD (Bi, et al., 2014). Furthermore, hepatic steatosis due to increased alcohol consumption is frequently linked with an AST/ALT ratio > 2, while an AST/ALT ratio < 1 has a strong association with NAFLD (Sorbi, et al., 1999; Botros & Sikaris, 2013). A study by Trak-Smayra (2011) found that db/db mice with histologically confirmed NAFLD had significantly increased AST and ALT levels, while a decrease in NAFLD by a herbal medicine was also accompanied by decreases in the levels of these enzymes. In our study, we found that db/db mice displayed increased ALT and AST from 7 weeks and 13 weeks, respectively. This was accompanied by an AST/ALT ratio of < 1

from 7 weeks onwards, which indicated lipid accumulation and correlated with histological and lipogram findings.

While AST and ALT are a widely used to screen for NAFLD, some individuals may present with normal levels of liver enzymes throughout the disease progression (Mofrad, et al., 2003) and therefore histological analysis remains the gold standard for the conclusive diagnosis of NAFLD (Kleiner & Makhlouf, 2017). Initially, NAFLD presents histologically as simple steatosis in the form of individual, small lipid droplets within the hepatocyte. This can later progress to NASH, where lipid accumulation advances into macrovesicular changes and is accompanied by apoptosis, inflammation, and fibrosis (Birkenfeld & Shulman, 2014; Liang, et al., 2014; Kleiner & Makhlouf, 2017). In a model characterisation by Trak-Smayra (2011), findings showed that db/db mice almost invariably displayed microvesicular steatosis at 13 weeks of age, while Kondo, et al. (2013) showed that db/db mice have macrovesicular steatosis and NASH at 24 weeks of age. Data presented in this study confirm this phenomenon, where obese mice presented with evidence of simple steatosis in the form of microvesicular steatosis by the age of 7 weeks. Furthermore, the histological severity of NAFLD increased with age, where by 10 weeks there was an increase in lipid accumulation, while at 13 weeks hepatocytes were hypertrophic with the nucleus displaced to the periphery of the cell.

NAFLD is considered as the hepatic manifestation of MetS and this has been associated with activation of a cascade of metabolic pathways that cause the biosynthesis of saturated fatty acids. This is due to enhanced expression of *de novo* lipogenic genes such as *FASN* and *SCD1*, which are under the transcriptional control of *SREBF1* (Li, et al., 2018). The formation of monounsaturated fatty acids is catalysed by *SCD1*, while *FASN* is a rate-limiting enzyme involved in this process. Ge, et al. (2016) reported that an increase in hepatic triglycerides occur as a result of an increase in LCFA synthetic enzymes and not due to increased hepatic LCFA uptake. Furthermore, it has been reported that inhibition of *FASN* in db/db mice, reduced the development of steatosis when compared to untreated db/db mice (Kong, et al., 2016), while inhibition of SCD1 reduced hepatic triglycerides and steatosis (Iida, et al., 2018). Additionally, FASN, SCD1 and HMGCR gene and protein expression was increased in the livers of db/db mice and accompanied liver steatosis, the severity of which was ameliorated by a herbal compound that targeted these enzymes (Lim, et al., 2016; Su, et al., 2016). This was confirmed in the present study where we showed that mice displaying increased hepatic expression of *SCD1*, *FASN* and *HMGCR* also presented with an augmented steatotic phenotype. Interestingly, no changes in *SREBF1* were observed. This is contrary to findings by Knebel, et al. (2012), which indicated *SREBF1* as a central regulator of lipid metabolism in

NAFLD. However, while mRNA can give an indication of gene expression, there are other post-translational factors that may play a role in protein activity. In the case of SREBF1, protein cleavage is regulated in the endoplasmic reticulum (ER) (Yan, et al., 2007). Especially in the hyperlipidaemic state, chronically increased FFA can induce ER stress and promote SREBF1 activity (Angeles & Hudkins, 2016). This post-translational regulation may thus explain why no changes in gene expression were observed by us, and why the downstream transcriptional targets were still up-regulated despite this observation.

Furthermore, augmented hepatic expression of *PPARα* and *CPT1* has been associated with increased β-oxidation in the liver, which resulted in a decrease in triglycerides, aminotransferases and liver steatosis (Chen, et al., 2008; Jia, et al., 2016). In the current study, we found that *CPT1* expression was decreased in db/db mice at 7 weeks, possibly contributing to hepatic lipid accumulation. This corresponds with similar findings by Wortham, et al. (2014), where a decrease in *CPT1* expression in db/db mice was accompanied by hepatic steatosis. In the present study, *PPARα* expression was increased in the db/db mice by 15 weeks of age, though there was no increase in *CPT1* expression. We propose that the observed increase in *PPARα* expression could indicate that *CPT1* expression and subsequent β-oxidation might have been up-regulated at a later time point. This may be due to the activation of an adaptive mechanism to combat lipid accumulation, as observed in a study by Trak-Smayra, et al. (2011). Additionally, in a study performed by Teng, et al. (2018) the authors showed that *CPT1* expression was increased in db/db mice at 20 weeks of age.

4.3 The onset of muscle insulin resistance

To further elucidate the causal role, we investigated peripheral insulin resistance in skeletal muscle. In the obese state, dyslipidaemia causes chronic low-grade inflammation, accompanied by increased release of FFA in the blood and peripheral tissue (Lomonaco, et al., 2012). Augmented FFA uptake results in the generation of excess ceramide and DAG, which in turn activates PKCθ (Szendroedi, et al., 2014). Increased PKCθ activation promotes the phosphorylation of IRS^{Ser307}, preventing the phosphorylation of IRS^{Tyr612} in response to insulin binding to the insulin receptor (Ragheb, et al., 2009). This reduces the capacity of the $pPI3K^{Tyr688}$/$pAKT^{Ser473}$ complex to inhibit glycogen synthesis while increasing GLUT4 expression and transport to the plasma membrane (Paz, et al., 1999; Brewer, et al., 2014). Sharma, et al. (2015), showed that decreased phosphorylation of IRS, PI3K and AKT in skeletal muscle of 12-week old db/db mice resulted in the inhibition of GLUT4 translocation/activity. This is further supported in a study by Zheng, et al. (2015) in which

observations included decreased p/t ACC, AKT and GSK3β in skeletal muscle of db/db mice at 16 weeks of age.

This correlated with our findings, which showed a decrease in the phosphorylation of PI3K as well as AKT at 10 weeks of age, with a concomitant increase in the amount of GLUT4 in the cytosolic fraction of skeletal muscle at 10 and 15 weeks, respectively. This increased subcellular cytosolic fraction of GLUT4 suggest an impaired translocation of GLUT4 to the plasma membrane, due to increased insulin resistance. In support of this, Samad, et al. (2017) found that GLUT4 translocation to the plasma membrane was significantly reduced in insulin resistant db/db mice when compared to insulin-sensitive controls.

Glucose uptake can also be activated via the insulin-independent AMPK pathway. AMPK is activated in response to cellular energy levels (Hardie, et al., 2016) and promotes GLUT4 translocation independent of the IRS/AKT pathway (Manna & Jain, 2015). This was displayed in a study by Duan, (2017), which showed that activation of AMPK by a herbal extract in db/db mice led to increased expression of GLUT4 and significant improvement of hyperglycaemia. However, data obtained in our study showed no alterations in AMPK activation, indicating that glucose uptake did not occur via this pathway. This corresponds with findings by Kang, et al. (2017) which also found that there was no significant difference in AMPK phosphorylation between db/db mice and lean controls.

Fatty acid oxidation and glucose oxidation are major fuel sources in muscle and heart tissue. To meet the energy demand of the cell, depending on the disease state of the organism and substrate availability, there will be inter-regulation between fatty acids and glucose as the preferred substrate, a phenomenon termed the Randle cycle (Randle, 1998). It has been indicated that the preferred substrate choice may contribute to the development of insulin resistance (Zhang, et al., 2010). Most studies are in support of the concept that β-oxidation is increased in insulin-resistant muscle tissue from obese animals, due to the unavailability of glucose and excess availability of FFA. In the present study, due to the decrease in glucose uptake in the muscle of db/db mice, it might be expected that there would be a subsequent increase in fatty acid β-oxidation to compensate for energy needs.
However, in our study we observed a decrease in CPT1 protein expression in db/db mice at 15 weeks, which infers that beta oxidation was decreased. This may be caused by an increase in lipogenesis and subsequent inhibition of lipolysis. Lipogenesis is activated when excess FFA, overflow from the adipose tissue, are metabolised into triacyl glycerol (TAG) for storage.

Malonyl-CoA, an intermediate of TAG synthesis, inhibits CPT1 and subsequently β-oxidation. As CPT1 is a mitochondrial protein, differences between the disease states may have been more evident if mitochondrial fractions instead of whole-cell lysates were used.

Muscle insulin resistance can be attributed to an increase in FFA flux and fatty acid β-oxidation, as the intracellular accumulation of lipid intermediates can inhibit insulin signalling (Takeuchi, et al., 2018). However, therapies aimed at decreasing β-oxidation may not be effective in the prevention of insulin resistance, as defects in mitochondrial substrate oxidation are related to lipid build-up, which can cause an inflammatory response and subsequent insulin resistance (Goodpaster & Wolf, 2004). The most effective treatment to alleviate lipid-induced insulin resistance would thus likely be to simply reduce the availability of FFA by dietary intervention.

4.4 The onset of cardiac dysfunction

Diabetes and NAFLD are known risk factors for the development of cardiac dysfunction. Chronic hyperglycaemia and hyperlipidaemia cause glucolipotoxicity, with deleterious consequences to the myocardium. Glucolipotoxicity modulates key signal transduction genes in processes that regulate bioenergetics, oxidative stress, inflammation, fibrosis, and apoptosis, compromising cardiac structure and function.

A key enzyme in the electron transport chain, NOX transfers electrons from NADPH. The NOX4 isoform is found specifically in cardiac myocytes and is a potent inducer of oxidative stress. Kuroda, et al. (2010) found that *NOX4* knock-out mice presented with attenuated cardiac hypertrophy, fibrosis and apoptosis, while *NOX4* over-expression was a major source of mitochondrial oxidative stress. This correlated with our results, which showed an increase in *NOX4* expression in db/db mice by 10 weeks of age, concurrent with hyperglycaemia and hyperlipidaemia

The above was accompanied by cardiac inflammation, as seen in db/db mice at 10 weeks of age by an increase in *NFκB* expression, one of the major transcription factors associated with pro-inflammatory signalling (Zhao, et al., 2015). This is supported by a study done by Madonna, et al. (2013), which showed that 12-week-old obese, diabetic db/db mice had increased *NFκB* expression in the heart. Chronic NFκB activation in the heart has been associated with inflammation, ER stress response, fibrosis and cell death (Gordon, et al.,

2011). Conversely, inhibition of NFκB by Resveratrol attenuated cardiac oxidative stress and diabetic complications (Bagul, et al., 2015).

Oxidative stress and inflammation affect fibroblast activation and ECM deposition in tissues such as the myocardium (Ayoub, et al., 2017). As a potent mediator of ECM deposition and subsequent fibrosis, CTGF is found to be increased in the tissues, including the heart, of diabetic models. Rawal, et al. (2017) found that CTGF has increased in the hearts of diabetic humans as well as db/db mice, and that it was associated with fibrotic remodelling. This correlates with findings in the current study, which showed a definite increase in *CTGF* expression in the hearts of 15-week old db/db mice. Chen, et al. (2018) also showed that inhibition of CTGF reduces collagen deposition and myocardial fibrosis and improves cardiac dysfunction. This may imply that an increase in CTGF expression and subsequent fibrosis causes a decrease in the contractility of the myocardium, leading to the decline in cardiac function and %EF.

Inflammation, ROS, fibrosis, and dysregulation of leptin lead to cardiomyocyte apoptosis by lipotoxic pathways. Trivedi 2008 shows that cleaved casp3, pro-casp3 and apoptotic bodies are increased in the hearts of 8 - 12-week old db/db mice and that this phenomenon increased with age. In the current study *CASP3* expression was significantly increased in db/db mice at 10 weeks of age, corresponding with inflammation and ROS signaling. It is interesting to note that *CASP3* expression was increased prior to the increase in *CTGF* expression, as fibrosis is a strong driver of apoptosis. Possible explanations for this is that *CASP3* expression was increased by factors other than fibrosis, such as ROS/inflammation, or that ROS/inflammation initiated activation of TGFβ, which is known to play a role in cardiac dysfunction (Khalil, et al., 2017).

The alterations in gene expression observed in the present study was accompanied by a significant reduction in % EF in db/db mice by 13 weeks of age, confirming a decline in the functioning of the heart. This correlates with findings by Faita, (2018) in a model characterisation study, which also showed that db/db mice had reduced % EF and cardiac function at 13 weeks of age.

ANP (NPPA) helps prevent hypertrophy by controlling cardiac remodelling. In NPPA knock-out mice, marked cardiac hypertrophy was observed, despite dietary and pharmacological treatment (Feng, et al., 2003). Similarly, Wang, et al. (2017) found that there was a significant increase in ANP protein expression in db/db mice compared to wild-type mice, and that this

was correlated with cardiac hypertrophy. Our findings, however, showed that there was no alteration in *NPPA* gene expression. This may be because proANP is localised mainly in the cardiac atrium and released in response to stress. It is thus possible that there was not yet atrial stress at this stage of the disease progression. This is supported by Zois, et al. (2017) who found no changes in cardiac ANP expression in insulin resistant human males.

Chapter 5: Conclusion

In summary, results obtained showed that db/db mice were obese and dyslipidaemic by 7 weeks of age. At this time, obese mice also presented with simple steatosis in the liver, accompanied by increased expression of lipogenic genes and liver enzymes indicative of hepatic lipotoxicity. Fasting blood glucose, HOMA-IR and protein expression confirmed that insulin resistance was not yet present at the onset of NAFLD. Gene expression and echocardiography indicated the onset of cardiac dysfunction between 10 and 13 weeks of age, following the development of NAFLD and insulin resistance (Figure 5).

Though several studies have shown that peripheral insulin resistance precedes the onset of hepatic steatosis, this study reported that hepatic lipid accumulation and lipotoxicity preceded the onset of peripheral insulin resistance that leads to cardiac abnormalities. We further speculate that, in the current "genetic" db/db mouse model, NAFLD might be the main driver of insulin resistance and subsequent cardiac dysfunction.

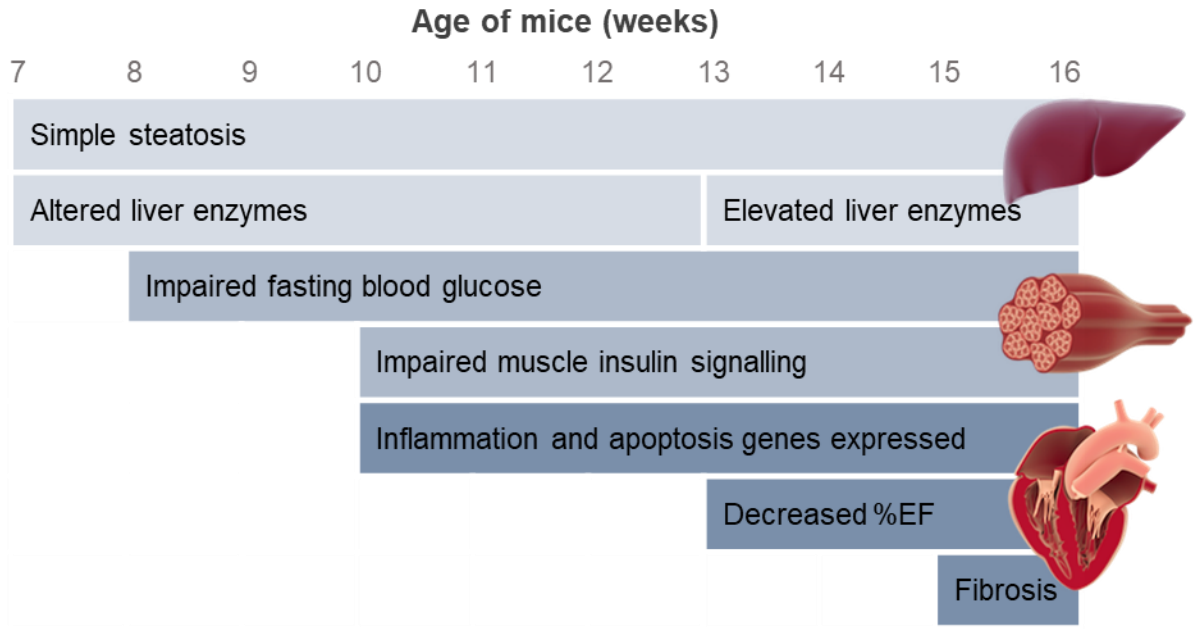

***Figure 5: Summary of findings in the present study**. In a leptin receptor-deficient (Lepr$^{db/db}$) mouse model, hepatic steatosis and lipotoxicity was present at 7 weeks of age, preceding the onset of peripheral insulin resistance at 10 weeks and cardiac dysfunction at 13 weeks. Illustrations created using www.somersault1824.com.*

In conclusion, the prevalence and financial burden of lifestyle-associated diseases emphasizes the importance of finding treatment or preventative therapies for these conditions. It is evident that there is much interplay between the components of the metabolic syndrome, and these connections provide an important avenue for research in order to better understand the disease pathology. Contradictory evidence still exists regarding the order of onset of NAFLD and insulin resistance, as well as the role that NAFLD plays in the development of insulin resistance. However, the current study provides strong evidence that NAFLD plays a casual role in the development of peripheral insulin resistance, and subsequent time dependant onset of cardiac dysfunction.

We hypothesize that there is a difference between the pathophysiology of the “genetic” and “metabolic” causes of NAFLD. Where, in a genetically modified model such as the db/db mouse model used in this study, insulin resistance appears to be a consequence of NAFLD, whereas in a high-fat-high-sugar diet, insulin resistance is more likely to precede and contribute to the development of NAFLD. Furthermore, it is likely that the relationship between insulin resistance and NAFLD is a vicious cycle: insulin resistance can cause or exacerbate existing hepatic lipid accumulation, which can then aggravate hepatic and peripheral insulin resistance. We thus propose that it is important to investigate genetic and metabolic NAFLD independently, and that this may allow for a more individualized approach to be taken in the development of effective screening tests or therapeutics.

Chapter 6: Limitations and Future Outlook

The model used in this study may be considered a limitation, as it is more representative of “genetic” NAFLD and may not be translatable to the “metabolic” development of the disease. The alterations in leptin signalling may have had an underlying effect of disease progression that may not be present in all cases. To address this, future studies should employ and compare both a genetic model as well as a HFHS diet-induced model, where the genetic (db/db model) are fed both ar standard chow, or a HFHS diet.

While the mouse model used is time- and cost-effective, the small body size severely limits the amount of tissue and serum that can be collected. This caused limitations in the present study, as a sufficient amount of serum to quantify insulin levels could only be collected at some of the time points. Similarly, collected heart tissue was only large enough to extract RNA, and protein expression analysis could not be performed. In future, a larger murine model could be employed, such as a HFHS diet fed Wistar rat and Zucker fatty rats. To more clearly identify the onset of insulin resistance, future research should include glucose tolerance tests on experimental animals, as well as collection of pancreatic and adipose tissue to investigate the onset of insulin resistance in different sites in the body. Skeletal muscle protein lysates should also be separated into cytosolic and membrane fractions to see GLUT4 translocation, and mitochondria could be isolated to more accurately quantify CPT1 and other mitochondrial proteins.

While gene expression profiling by mRNA can give some information, it is also important to validate findings with protein expression. In future studies, protein activity should be analysed using protein assays, to support gene expression findings. Specifically, in the case of SREBF1, where no changes in gene expression were observed, but there was still activation of its downstream targets. To support findings of hepatic lipid accumulation and NAFLD, and to draw a comparison between the db/db and db/+ groups, the hepatic triglyceride content of each animal will be quantified in future.

References

Abdul-Ghani, M. A., Tripathy, D. & DeFronzo, R. A., 2006. Contributions of β-cell dysfunction and insulin resistance to the pathogenesis of impaired glucose tolerance and impaired fasting glucose. *Diabetes Care,* 29(5), pp. 1130-1139.

Ahmed, M., 2015. Non-alcoholic fatty liver disease in 2015. *World Journal of Hepatology,* 7(11), pp. 1450-1459.

Alquier, T. & Poitout, V., 2018. Considerations and guidelines for mouse metabolic phenotyping in diabetes research. *Diabetologia,* Volume 61, pp. 526-538.

Amaro, A. et al., 2011. Dissociation between Intrahepatic Triglyceride Content and Insulin Resistance in Familial Hypobetalipoproteinemia. *Gastroenterology,* 139(1), pp. 149-153.

Angeles, T. S. & Hudkins, R. L., 2016. Recent advances in targeting the fatty acid biosynthetic pathway using fatty acid synthase inhibitors. *Expert Opinion on Drug Discovery,* 11(12), pp. 1187-1199.

Aragno, M. et al., 2006. Oxidative stress-dependent impairment of cardiac-specific transcription factors in experimental diabetes. *Endocrinology,* 147(12), pp. 5967-5974.

Aronson, D., 2003. Cross-linking of glycated collagen in the pathogenesis of arterial and myocardial stiffening of aging and diabetes. *Journal of Hypertension,* 21(1), pp. 3-12.

Ayoub, K. F. et al., 2017. Immunity, Inflammation, and Oxidative Stress in Heart Failure: Emerging Molecular Targets. *Cardiovascular Drugs and Therapy,* 31(5), pp. 593-608.

Bagul, P. K., Deepthi, N., Sultana, R. & Banerjee, S. K., 2015. Resveratrol ameliorates cardiac oxidative stress in diabetes through deacetylation of NFkB-p65 and histone 3. *Journal of Nutritional Biochemistry,* 26(11), pp. 1298-1307.

Bai, Y. & Sun, Q., 2015. Macrophage recruitment in obese adipose tissue. *Obesity Reviews,* 16(2), pp. 127-136.

Battiprolu, P. K. et al., 2013. Diabetic cardiomyopathy and metabolic remodeling of the heart. *Life Sciences,* 92(11), pp. 609-615.

Birkenfeld, A. L. & Shulman, G. I., 2014. Non Alcoholic Fatty Liver Disease, Hepatic Insulin Resistance and Type 2 Diabetes. *Hepatology,* 59(2), pp. 713-723.

Bi, W. R. et al., 2014. Large-scale analysis of factors influencing nonalcoholic fatty liver disease and its relationship with liver enzymes. *Genetics and molecular research,* 13(3), pp. 5880-5891.

Bonapace, S. et al., 2012. Nonalcoholic fatty liver disease is associated with left ventricular diastolic dysfunction in patients with type 2 diabetes. *Diabetes Care,* 35(2), pp. 389-395.

Borghetti, G. et al., 2018. Diabetic Cardiomyopathy: Current and Future Therapies. Beyond Glycemic Control. *Frontiers in Physiology,* 9(1514), pp. 1-15.

Botros, M. & Sikaris, K. A., 2013. The De Ritis Ratio : The Test of Time. *Clin Biochem Rev,* 34(1), pp. 117-130.

Brewer, P. D. et al., 2014. Insulin-regulated Glut4 translocation: Membrane protein trafficking with six distinctive steps. *Journal of Biological Chemistry,* 289(25), pp. 17280-17298.

Bugianesi, E. et al., 2005. Insulin resistance in non-diabetic patients with non-alcoholic fatty liver disease: Sites and mechanisms. *Diabetologia,* 48(4), pp. 634-642.

Cai, D. et al., 2006. Local and systemic insulin resistance resulting from hepatic activation of IKK-β and NF-κB. *Nat Med,* 11(2), pp. 183-190.

Chen, L. et al., 2018. miR-30a attenuates cardiac fibrosis in rats with myocardial infarction by inhibiting CTGF. *Experimental and Therapeutic Medicine,* 15(5), pp. 4318-4324.

Chen, M. M. et al., 2000. CTGF expression is induced by TGF-β in cardiac fibroblasts and cardiac myocytes: A potential role in heart fibrosis. *Journal of Molecular and Cellular Cardiology,* 32(10), pp. 1805-1819.

Chen, X. et al., 2008. Improvement of dyslipidemia, insulin sensitivity, and energy balance by a peroxisome proliferator-activated receptor α agonist. *Metabolism: Clinical and Experimental,* 57(11), pp. 1516-1525.

Chowdhry, M. F., Vohra, H. A. & Galiñanes, M., 2007. Diabetes increases apoptosis and necrosis in both ischemic and nonischemic human myocardium: Role of caspases and poly-adenosine diphosphate-ribose polymerase. *Journal of Thoracic and Cardiovascular Surgery,* 134(1), pp. 124-131.

Cohen, J. C., Horton, J. D. & Hobbs, H. H., 2011. Human Fatty Liver Disease: Old Questions and New Insights. *Science,* 332(6037), pp. 1519-1523.

Dludla, P. V. et al., 2017. Age-dependent development of left ventricular wall thickness in type 2 diabetic (db/db) mice is associated with elevated low-density lipoprotein and triglyceride serum levels. *Heart and Vessels,* 32(8), pp. 1025-1031.

Dong, Y. et al., 2015. Activation of the liver X receptor by agonist TO901317 improves hepatic insulin resistance via suppressing reactive oxygen species and JNK pathway. *PLoS ONE,* 10(4), pp. 1-20.

Duan, B. et al., 2017. Antidiabetic Effect of Tibetan Medicine Tang-Kang-Fu-San in db / db Mice via Activation of PI3K / Akt and AMPK Pathways. *Front. Pharmacol,* 8(535), pp. 1-11.

Faita, F. et al., 2018. Ultrasonographic Characterization of the db/db Mouse: An Animal Model of Metabolic Abnormalities. *Journal of diabetes research,* Volume 2018, pp. 1-9.

Feng, J. A. et al., 2003. Pressure-independent enhancement of cardiac hypertrophy in atrial natriuretic peptide-deficient mice.. *Clin Exp Pharmacol Physiol.,* 30(6), pp. 343-349.

Feng, R. et al., 2017. Free fatty acids profile among lean, overweight and obese non-alcoholic fatty liver disease patients: A case - Control study. *Lipids in Health and Disease,* 16(1), pp. 1-9.

Finkelstein, E. et al., 2012. Obesity and Severe Obesity Forecasts Through 2030. *Am J Prev Med,* 42(6), pp. 563-570.

Fonseca, V. A., 2003. Management of diabetes mellitus and insulin resistance in patients with cardiovascular disease. *Am J Cardiol,* Volume 92, pp. 50-60.

Fotbolcu, H. et al., 2010. Impairment of the left ventricular systolic and diastolic function in patients with non-alcoholic fatty liver disease. *Cardiol J,* 17(5), pp. 457-463.

Franko, A. et al., 2018. Dissociation of fatty liver and insulin resistance in I148M PNPLA3 carriers: Differences in diacylglycerol (DAG) FA18:1 lipid species as a possible explanation. *Nutrients,* 10(9), pp. 1-12.

Fruh, S., 2017. Obesity: Risk factors, complications, and strategies for sustainable long-term weight management. *Journal of the American Association of Nurse Practitioners,* 29(1), pp. 3-14.

Gaggini, M. et al., 2013. Non-alcoholic fatty liver disease (NAFLD) and its connection with insulin resistance, dyslipidemia, atherosclerosis and coronary heart disease. *Nutrients,* 5(5), pp. 1544-1560.

Gastaldelli, A., 2017. Insulin resistance and reduced metabolic flexibility: cause or consequence of NAFLD?. *Clinical Science,* 131(22), pp. 2701-2704.

Ge, J. F., Walewski, J. L., Anglade, D. & Berk, P. D., 2016. Regulation of hepatocellular fatty acid uptake in mouse models of fatty liver disease with and without functional leptin signaling: roles of NFkB and SREBP-1C and the effects of Spexin. *Seminars in Liver Disease,* 36(4), pp. 360-372.

Ghosh, N. & Katare, R., 2018. Molecular mechanism of diabetic cardiomyopathy and modulation of microRNA function by synthetic oligonucleotides. *Cardiovascular Diabetology,* 17(43), pp. 1-25.

Goland, S. et al., 2006. Cardiac abnormalities as a new manifestation of nonalcoholic fatty liver disease: echocardiographic and tissue Doppler imaging assessment.. *Journal of clinical gastroenterology,* 40(10), pp. 949-955.

Goodpaster, B. H. & Wolf, D., 2004. Skeletal muscle lipid accumulation in obesity, insulin resistance, and type 2 diabetes. *Pediatric Diabetes,* 5(4), pp. 219-226.

Gordon, J. W., Shaw, J. A. & Kirshenbaum, L. A., 2011. Multiple facets of NF-κB in the heart: To be or not to NF-κB. *Circulation Research,* 108(9), pp. 1122-1132.

Grefhorst, A. et al., 2005. Differential effects of pharmacological liver X receptor activation on hepatic and peripheral insulin sensitivity in lean and ob/ob mice. *American Journal of Physiology-Endocrinology and Metabolism,* 289(5), pp. E829-E838.

Gruben, N., Shiri-Sverdlov, R., Koonen, D. P. & Hofker, M. H., 2014. Nonalcoholic fatty liver disease: A main driver of insulin resistance or a dangerous liaison?. *Biochimica et Biophysica Acta - Molecular Basis of Disease,* 1842(11), pp. 2329-2343.

Guilbaud, A. et al., 2018. The LepR db / db mice model for studying glycation in the context of diabetes. *Diabetes Metab Res Rev,* 2019(e310), pp. 1-10.

Gurka, M. J., Filipp, S. L., Pearson, T. A. & DeBoer, M. D., 2018. Assessing Baseline and Temporal Changes in Cardiometabolic Risk Using Metabolic Syndrome Severity and Common Risk Scores. *Journal of the American Heart Association,* 7(16), pp. 1-9.

Hall, M. E., Maready, M. W., Hall, J. E. & Stec, D. E., 2014. Rescue of cardiac leptin receptors in db/db mice prevents myocardial triglyceride accumulation. *Endocrinology and Metabolism,* 307(3), pp. 316-325.

Han, E. & Lee, Y., 2017. Non-Alcoholic Fatty Liver Disease: The Emerging Burden in Cardiometabolic and Renal Diseases. *Diabetes Metab J,* 41(1), pp. 430-437.

Hardie, D. G., Schaffer, B. E. & Brunet, A., 2016. AMPK: an energy-sensing pathway with multiple inputs and outputs. *Trends Cell Biol,* 26(3), pp. 190-201.

Hong, S. H., Kang, M., Lee, K. S. & Yu, K., 2016. High fat diet-induced TGF-β/Gbb signaling provokes insulin resistance through the tribbles expression. *Scientific Reports,* 6(1), pp. 1-10.

Hotamisligil, G. S. et al., 1994. Reduced tyrosine kinase activity of the insulin receptor in obesity-diabetes . Central role of tumor necrosis factor-alpha . Find the latest version : Reduced Tyrosine Kinase Activity of the Insulin Receptor in Obesity-Diabetes Central Role of Tumor Necro. *J Clin Invest,* 94(4), pp. 1543-1549.

Hur, J. et al., 2015. The metabolic syndrome and microvascular complications in a murine model of type 2 diabetes. *Diabetes,* 64(9), pp. 3294-3304.

Iida, T. et al., 2018. Discovery of potent liver-selective stearoyl-CoA desaturase-1 (SCD1) inhibitors, thiazole-4-acetic acid derivatives, for the treatment of diabetes, hepatic steatosis, and obesity. *European Journal of Medicinal Chemistry,* 158(1), pp. 832-852.

Jia, G., Whaley-connell, A. & Whaley-connell, J. R., 2017. Diabetic cardiomyopathy : a hyperglycaemia- and insulin-resistance-induced heart disease. *Diabetologia,* pp. 1-8.

Jia, Y. et al., 2016. Astaxanthin reduces hepatic lipid accumulations in high-fat-fed C57BL/6J mice via activation of peroxisome proliferator-activated receptor (PPAR) alpha and

inhibition of PPAR gamma and Akt. *Journal of Nutritional Biochemistry,* 28(1), pp. 9-18.

Johnson, R. et al., 2016. Aspalathin , a dihydrochalcone C -glucoside , protects H9c2 cardiomyocytes against high glucose induced shifts in substrate preference and apoptosis. *Mol Nutr Food Res,* 60(4), pp. 922-934.

Kang, O. H. et al., 2017. Anti-diabetic effect of black ginseng extract by augmentation of AMPK protein activity and upregulation of GLUT2 and GLUT4 expression in db/db mice. *BMC Complementary and Alternative Medicine,* 17(1), pp. 1-11.

Karabay, C. Y. et al., 2014. Impaired left ventricular mechanics in nonalcoholic fatty liver disease: a speckle-tracking echocardiography study.. *European journal of gastroenterology & hepatology,* 26(3), pp. 325-331.

Khalil, H. et al., 2017. Fibroblast-specific TGF-β-Smad2/3 signaling underlies cardiac fibrosis. *Journal of Clinical Investigation,* 127(10), pp. 3770-3783.

Kim, J. Y., Bacha, F., Tfayli, H. & Michaliszyn, S. F., 2018. Adipose Tissue Insulin Resistance in Youth on the Spectrum From Normal Weight to Obese and From Normal Glucose Tolerance to Impaired Glucose Tolerance to Type 2 Diabetes. *Diabetes Care,* pp. 1-8.

Kleiner, D. E. & Makhlouf, H. R., 2017. Histology of NAFLD and NASH in adults and children. *Clin Liver Dis,* 20(2), pp. 293-312.

Knebel, B. et al., 2012. Liver-Specific Expression of Transcriptionally Active SREBP-1c Is Associated with Fatty Liver and Increased Visceral Fat Mass. *PLoS ONE,* 7(2), pp. 1-15.

Kobayashi, K. et al., 2000. The db/db mouse, a model for diabetic dyslipidemia: Molecular characterization and effects of western diet feeding. *Metabolism,* 49(1), pp. 22-31.

Kondo, Y. et al., 2013. Leprdb/dbMice with Senescence Marker Protein-30 Knockout (Leprdb/dbSmp30Y/-) Exhibit Increases in Small Dense-LDL and Severe Fatty Liver Despite Being Fed a Standard Diet. *PLoS ONE,* 8(6), pp. 1-11.

Kong, Q. et al., 2016. Tangshen formula attenuates hepatic steatosis by inhibiting hepatic lipogenesis and augmenting fatty acid oxidation in db/db mice. *International Journal of Molecular Medicine,* 38(6), pp. 1715-1726.

Koonen, D. P. Y. et al., 2007. Increased hepatic CD36 expression contributes to dyslipidemia associated with diet-induced obesity. *Diabetes,* 56(12), pp. 2863-2871.

Kopelman, P. G., 2000. Obesity as a medical problem. *Nature,* 404(6), pp. 635-643.

Korenblat, K. M., Fabbrini, E., Mohammed, B. S. & Klein, S., 2009. Liver, Muscle and Adipose Tissue Insulin Action is Directly Related to Intrahepatic Triglyceride Content in Obese Subjects. *Gastroenterology,* 134(5), pp. 1369-1375.

Kumar, M. S. et al., 2016. Cardiovascular Autonomic Dysfunction in Patients of Nonalcoholic Fatty Liver Disease. *International Journal of Hepatology,* Volume 2016, pp. 1-8.

Kuroda, J. et al., 2010. NADPH oxidase 4 (Nox4) is a major source of oxidative stress in the failing heart. *Proceedings of the National Academy of Sciences,* 107(35), pp. 15565-15570.

Landrier, J. F., Marcotorchino, J. & Tourniaire, F., 2012. Lipophilic micronutrients and adipose tissue biology. *Nutrients,* 4(11), pp. 1622-1649.

Lebovitz, H. E., 2001. Insulin resistance: Definition and consequences. *Experimental and Clinical Endocrinology and Diabetes,* 109(2), pp. 135-148.

Lee , B. C. & Lee, J., 2014. Cellular and molecular players in adipose tissue inflammation in the development of obesity-induced insulin resistance. *Biochimica et Biophysica Acta - Molecular Basis of Disease,* 1842(3), pp. 446-462.

Leong, D. P. et al., 2017. Reducing the Global Burden of Cardiovascular Disease, Part 2. *Circulation Research,* 121(1), pp. 695-710.

Lessard, J. et al., 2014. Low abdominal subcutaneous preadipocyte adipogenesis is associated with visceral obesity, visceral adipocyte hypertrophy, and a dysmetabolic state. *Landes Bioscience,* 3(3), pp. 197-205.

Liang, W. et al., 2014. Establishment of a general NAFLD scoring system for rodent models and comparison to human liver pathology. *PLoS ONE,* 9(12), pp. 1-17.

Lim, E. et al., 2016. Xylobiose, an alternative sweetener, ameliorates diabetes-related metabolic changes by regulating hepatic lipogenesis and miR-122a/33a in db/db Mice. *Nutrients,* 8(12), pp. 1-18.

Li, N. et al., 2018. Brg1 regulates pro-lipogenic transcription by modulating SREBP activity in. *Molecular Basis of Disease,* 1864(2018), pp. 2881-2889.

Liu, Q. et al., 2016. 1-Deoxynojirimycin alleviates liver injury and improves hepatic glucose Metabolism in db/db mice. *Molecules,* 21(3), pp. 1-12.

Li, Z. L. et al., 2012. Progression from obesity to metabolic syndrome is associated with altered myocardial autophagy and apoptosis. *Arteriosclerosis, thrombosis, and vascular biology,* 32(5), pp. 1132-1141.

Lomonaco, R. et al., 2012. Effect of adipose tissue insulin resistance on metabolic parameters and liver histology in obese patients with nonalcoholic fatty liver disease. *Hepatology,* 55(5), pp. 1389-1397.

Lonardo, A. et al., 2015. Epidemiological modifiers of non-alcoholic fatty liver disease: focus on high-risk groups. *Dig Liver Dis,* 47(1), p. 997–1006.

Loncarevic, B., Trifunovic, D., Soldatovic, I. & Vujisic-Tesic, B., 2016. Silent diabetic cardiomyopathy in everyday practice: A clinical and echocardiographic study. *BMC Cardiovascular Disorders,* 16(1), pp. 1-11.

Luo, D. et al., 2017. Natural product celastrol suppressed macrophage M1 polarization against inflammation in diet-induced obese mice via regulating Nrf2/HO-1, MAP kinase and NF-κB pathways. *Aging,* 9(10), pp. 2068-2081.

Luukkonen, P. K. et al., 2016. Hepatic ceramides dissociate steatosis and insulin resistance in patients with non-alcoholic fatty liver disease. *Journal of Hepatology,* 64(5), pp. 1167-1175.

Madonna, R., Wu, H., Shelat, H. & Geng, Y. J., 2013. CD1d-associated expression of NF-κB and cardiac dysfunction in diabetic and obese mice. *International Journal of Immunopathology and Pharmacology,* 26(1), pp. 59-73.

Mandviwala, T., Khalid, U. & Deswal, A., 2016. Obesity and Cardiovascular Disease: a Risk Factor or a Risk Marker?. *Current Atherosclerosis Reports,* 18(21), pp. 1-10.

Manna, P. & Jain, S. K., 2015. Obesity, Oxidative Stress, Adipose Tissue Dysfunction, and the Associated Health Risks: Causes and Therapeutic Strategies. *Metabolic Syndrome and Related Disorders,* 13(10), pp. 423-444.

Mantovani, A. et al., 2015. Nonalcoholic fatty liver disease is independently associated with early left ventricular diastolic dysfunction in patients with type 2 diabetes. *PLoS ONE,* 10(8), pp. 1-13.

Matthews, D. R. et al., 1985. Homeostasis model assessment: insulin resistance and β-cell function from fasting plasma glucose and insulin concentrations in man. *Diabetologia,* 28(7), pp. 412-419.

Michaud, A. et al., 2016. Abdominal adipocyte populations in women with visceral obesity. *European Journal of Endocrinology,* 174(2), pp. 227-239.

Mofrad, P. et al., 2003. Clinical and histologic spectrum of nonalcoholic fatty liver disease associated with normal ALT values. *Hepatology,* 37(6), pp. 1286-1292.

Neuschwander-tetri, B. A., Brunt, E. M., Wehmeier, K. R. & Bacon, B. R., 2003. Improved Nonalcoholic Steatohepatitis After 48 Weeks of Treatment With the PPAR-y Ligand Rosiglitazone. *Clinical Trials,* 38(4), pp. 1008-1017.

Pamir, N. et al., 2009. Receptors for tumor necrosis factor-alpha play a protective role against obesity and alter adipose tissue macrophae status. *Endocrinology,* Volume 150, pp. 4124-4134.

Paschos, P. & Paletas, K., 2009. Non alcoholic fatty liver disease and metabolic syndrome. *Hippocratia,* 13(1), pp. 9-19.

Paz, K. et al., 1999. Phosphorylation of insulin receptor substrate-1 (IRS-1) by protein kinase B positively regulates IRS-1 function. *Journal of Biological Chemistry,* 274(40), pp. 28816-28822.

Ragheb, R. et al., 2009. Free fatty acid-induced muscle insulin resistance and glucose uptake dysfunction: Evidence for PKC activation and oxidative stress-activated signaling pathways. *Biochemical and Biophysical Research Communications,* 389(2), pp. 211-216.

Randle, P. J., 1998. Regulatory interactions between lipids and carbohydrates: the glucose fatty acid cycle after 35 years. *Diabetes Metab Rev,* 14(1), pp. 263-283.

Rask-Madsen, C. & Kahn, C. R., 2012. Tissue-specific insulin signaling, metabolic syndrome and cardiovascular disease. *Arterioscler Thromb Vasc Biol,* 32(9), pp. 2052-2059.

Rawal, S. et al., 2017. Downregulation of miR-15a/b accelerates fibrotic remod elling in the type- 2 diabetic human and mouse heart. *Clinical Science,* pp. 1-19.

Reaven, G. M., 2011. The metabolic syndrome: Time to get off the merry-go-round?. *Journal of Internal Medicine,* 269(2), pp. 127-136.

Repa, J. J. et al., Regulation of mouse sterol regulatory element-binding protein-1c gene (SREBP-1c) by oxysterol receptors, LXRalpha and LXRbeta. *Genes Dev,* 2000(14), pp. 2819–2830.

Röder, P. V., Wu, B., Liu, Y. & Han, W., 2016. Pancreatic regulation of glucose homeostasis. *Experimental & molecular medicine,* 48(1), pp. 1-19.

Rubler, S. et al., 1972. New type of cardiomyopathy associated with diabetic glomerulosclerosis. *The American Journal of Cardiology,* 30(6), pp. 595-602.

Samad, M. B. et al., 2017. [6]-Gingerol, from Zingiber officinale, potentiates GLP-1 mediated glucose- stimulated insulin secretion pathway in pancreatic β-cells and increases RAB8/ RAB10-regulated membrane presentation of GLUT4 transporters in skeletal muscle to improve hyperglyce. *BMC Complementary and Alternative Medicine,* 17(1), pp. 1-13.

Samuel, V. T., Petersen, K. F. & Shulman, G. I., 2010. Lipid-induced insulin resistance: unravelling the mechanism. *Lancet,* 375(9733), pp. 2267-2277.

Sanyal, A. J. et al., 2001. Nonalcoholic steatohepatitis: Association of insulin resistance and mitochondrial abnormalities. *Gastroenterology,* 120(5), pp. 1183-1192.

Schattenberg, J. M. & Galle, P. R., 2010. Animal models of non-alcoholic steatohepatitis: Of mice and man. *Digestive Diseases,* 28(1), pp. 247-254.

Schulze, P. C., 2009. Myocardial lipid accumulation and lipotoxicity in heart failure. *J Lipid Res,* 50(11), pp. 2137-2138.

Schwenk, R. W., Luiken, J. F., Bonen, A. & Glatz, J. F., 2008. Regulation of sarcolemmal glucose and fatty acid transporters in cardiac disease. *Cardiovascular Research,* 79(2), pp. 249-258.

Sharma, B. R., Kim, H. J. & Rhyu, D. Y., 2015. Caulerpa lentillifera extract ameliorates insulin resistance and regulates glucose metabolism in C57BL/KsJ-db/db mice via PI3K/AKT signaling pathway in myocytes. *Journal of Translational Medicine,* 13(1), pp. 1-10.

Singh, S. P. et al., 2015. Nonalcoholic fatty liver disease (NAFLD) without insulin resistance: Is it different?. *Clinics and Research in Hepatology and Gastroenterology,* 39(4), pp. 482-488.

Sirbu, O. et al., 2016. Non-alcoholic fatty liver disease-From the cardiologist perspective.. *Anatolian journal of cardiology,* 16(7), pp. 534-541.

Sobel, J. A. et al., 2017. Transcriptional regulatory logic of the diurnal cycle in the mouse liver. *PLoS Biology,* 15(4), pp. 1-33.

Sookoian, S. et al., 2011. Liver transcriptional profile of atherosclerosis-related genes in human nonalcoholic fatty liver disease. *Atherosclerosis,* 218(2), pp. 378-385.

Sorbi, D., Boynton, J. & Lindor, K. D., 1999. The ratio of aspartate aminotransferase to alanine aminotransferase: Potential value in differentiating nonalcoholic steatohepatitis from alcoholic liver disease. *American Journal of Gastroenterology,* 94(4), pp. 1018-1022.

Stevanovic, A. & Dekleva, M., 2018. The importance of subclinical left ventricular dysfunction and blood pressure pattern in asymptomatic type-2 diabetic patients: the diagnostic and prognostic significance of Tissue Doppler parameters, left ventricular global longitudinal strain, and night. *Journal of Diabetes and its Complications,* 32(1), pp. 41-47.

Straub, R., 2014. Insulin resistance, selfish brain, and selfish immune system: An evolutionarily positively selected program used in chronic inflammatory diseases. *Arthritis Research and Therapy,* 16(54), pp. 1-15.

Su, M. L., He, Y., Li, Q. S. & Zhu, B. H., 2016. Efficacy of acetylshikonin in preventing obesity and hepatic steatosis in db/db mice. *Molecules,* 21(8), pp. 1-14.

Szendroedi, J. et al., 2014. Role of diacylglycerol activation of PKCθ in lipid-induced muscle insulin resistance in humans. *Proceedings of the National Academy of Sciences,* 111(26), pp. 9597-9602.

Takeuchi, M. et al., 2018. Higher Fasting and Postprandial Free Fatty Acid Levels Are Associated With Higher Muscle Insulin Resistance and Lower Insulin Secretion in Young Non-Obese Women.. *Journal of clinical medicine research,* 10(11), pp. 822-829.

Teng, Y. et al., 2018. Dietary supplement of large yellow tea ameliorates metabolic syndrome and attenuates hepatic steatosis in db/db mice. *Nutrients,* 10(1), pp. 1-17.

Ter Horst, K. W. & Serlie, M. J., 2017. Fructose consumption, lipogenesis, and non-alcoholic fatty liver disease. *Nutrients,* 9(9), pp. 1-20.

Trak-Smayra, V. et al., 2011. Pathology of the liver in obese and diabetic ob/ob and db/db mice fed a standard or high-calorie diet. *International Journal of Experimental Pathology,* 92(6), pp. 413-421.

Trevaskis, J. L. et al., 2012. Glucagon-like peptide-1 receptor agonism improves metabolic, biochemical, and histopathological indices of nonalcoholic steatohepatitis in mice. *AJP: Gastrointestinal and Liver Physiology,* 302(8), pp. 762-772.

Trivedi, P., Yang, R. & Barouch, L. A., 2008. Decreased p110α catalytic activity accompanies increased myocyte apoptosis and cardiac hypertrophy in leptin deficient ob/ob mice. *Cell Cycle,* 7(5), pp. 506-565.

Turnbull, P. C. et al., 2016. Increases in skeletal muscle ATGL and its inhibitor G0S2 following 8 weeks of endurance training in metabolically different rat skeletal muscles. *American Journal of Physiology-Regulatory, Integrative and Comparative Physiology,* 310(2), p. 125.

Turner, N., Cooney, G. J., Kraegen, E. W. & Bruce, C. R., 2014. Fatty acid metabolism, energy expenditure and insulin resistance in muscle. *Journal of Endocrinology,* 220(2), pp. 61-79.

Utzschneider, K. M. & Kahn, S. E., 2006. The Role of Insulin Resistance in Nonalcoholic Fatty Liver Disease. *The Journal of Clinical Endocrinology & Metabolism,* 91(12), pp. 4753-4761.

Viollet, B. et al., 2010. AMPK inhibition in health and disease. *Critical Reviews in Biochemistry and Molecular Biology,* 45(4), pp. 276-295.

Wang, B., Chandrasekera, P. C. & Pippin, J. J., 2014. Leptin- and Leptin Receptor-Deficient Rodent Models: Relevance for Human Type 2 Diabetes. *Current Diabetes Reviews,* 10(2), pp. 131-145.

Wang, S. et al., 2017. Zinc prevents the development of diabetic cardiomyopathy in db/db mice. *International Journal of Molecular Sciences,* 18(3), pp. 1-14.

Wilcox, G., 2005. Insulin and insulin resistance. *The Clinical biochemist. Reviews / Australian Association of Clinical Biochemists,* 26(2), pp. 19-39.

Wortham, M. et al., 2014. The Transition from Fatty Liver to NASH Associates with SAMe Depletion in db/db Mice Fed a Methionine Choline-Deficient Diet. *Dig Dis Sci,* 53(10), pp. 2761-2774.

Wu, J. W. et al., 2011. Deficiency of liver adipose triglyceride lipase in mice causes progressive hepatic steatosis. *Hepatology,* 54(1), pp. 122-132.

Xu, J. et al., 2018. Hypoglycemic and hypolipidemic effects of total saponins from Stauntonia chinensis in diabetic db/db mice.. *Journal of cellular and molecular medicine,* 2018(22), pp. 6026-6038.

Yamada, S. et al., 2017. Cholic Acid Enhances Visceral Adiposity, Atherosclerosis and Nonalcoholic Fatty Liver Disease in Microminipigs. *Journal of Atherosclerosis and Thrombosis,* 24(1), pp. 1-17.

Yamada, T. et al., 2010. Fatty liver predicts impaired fasting glucose and type 2 diabetes mellitus in Japanese undergoing a health checkup. *Journal of Gastroenterology and Hepatology (Australia),* 25(2), pp. 352-356.

Yan, D. et al., 2007. Oxysterol binding protein induces upregulation of SREBP-1c and enhances hepatic lipogenesis. *Arteriosclerosis, Thrombosis, and Vascular Biology,* 27(5), pp. 1108-1114.

Yano, H. et al., 2018. PHD3 regulates glucose metabolism by suppressing stress-induced signalling and optimising gluconeogenesis and insulin signalling in hepatocytes. *Scientific Reports,* 8(1), pp. 1-16.

Ye, J., 2013. Mechanisms of insulin resistance in obesity. *Front Med,* 7(1), pp. 14-24.

Yin, Y. et al., 2017. Luteolin improves non-alcoholic fatty liver disease in db / db mice by inhibition of liver X receptor activation to down-regulate expression of sterol regulatory element binding protein 1c. *Biochemical and Biophysical Research Communications,* 482(4), pp. 720-726.

Zhang, L. et al., 2010. Role of fatty acid uptake and fatty acid β-oxidation in mediating insulin resistance in heart and skeletal muscle. *Biochimica et Biophysica Acta - Molecular and Cell Biology of Lipids,* 1801(1), pp. 1-22.

Zhang, Y. et al., 2014. TNF-α promotes early atherosclerosis by increasing transcytosis of LDL across endothelial cells: Crosstalk between NF-κB and PPAR-γ. *Journal of Molecular and Cellular Cardiology,* 72(2014), pp. 85-94.

Zhao, L. et al., 2015. Inflammation-induced microvascular insulin resistance is an early event in diet-induced obesity. *Clinical Science,* 129(12), pp. 1025-1036.

Zheng, R., Du, Z., Wang, M. & Mao, Y., 2018. A longitudinal epidemiological study on the triglyceride and glucose index and the incident nonalcoholic fatty liver disease. *Lipids in Health and Disease,* 17(262), pp. 1-9.

Zheng, T. et al., 2015. Salidroside ameliorates insulin resistance through activation of a mitochondria-associated AMPK/PI3K/Akt/GSK3β pathway. *British Journal of Pharmacology,* 172(13), pp. 3284-3301.

Zieman, S. J. & Kass, D. A., 2004. Advanced glycation endproduct crosslinking in the cardiovascular system: Potential therapeutic target for cardiovascular disease. *Drugs,* 64(5), pp. 459-470.

Zois, N. E. et al., 2017. Effect of Pancreatic Hormones on pro-Atrial Natriuretic Peptide in Humans. *EBioMedicine,* 17(1), pp. 88-94.

Appendix A: List of reagents, consumables and equipment

Table A1: Reagents and consumables

Reagent/consumable	Catalogue number	Company
0.2 mL PCR Tubes	32102051	Axygen, Union City, California, USA
0.5 mL Eppendorf safe-lock tubes	0030 123.301	Eppendorf, Hamburg, Germany
1.5 mL Eppendorf safe-lock tubes	0030 123.328	Eppendorf, Hamburg, Germany
2 mL Eppendorf safe-lock tubes	0030 123. 344	Eppendorf, Hamburg, Germany
15 mL centrifuge tubes	602072	NEST Biotechnology, Jiangsu China Wuxi
50 mL centrifuge tubes	601001	NEST Biotechnology, Jiangsu China Wuxi
96-well plate	CI59018	Sigma-Aldrich, Missouri, United States
β-mercaptoethanol	63880	Fluka, Bucharest, Romania
Chloroform	136112-00-0	Sigma-Aldrich, Missouri, United States
Criterion™ TGX™ 12% Precast Midi Gels	5671043	Bio-Rad, California, United States
Crystal violet		Kimix Chemicals, Cape Town, South Africa
DPX mounting media	6522	Sigma-Aldrich, Missouri, United States
Eosin		Kimix Chemicals, Cape Town, South Africa
Ethanol	2875	Sigma-Aldrich, Missouri, United States
OneTouch Select®, Glucose Meter		LifeScan Inc., California, United States
Isopropanol	I9516	Sigma-Aldrich, Missouri, United States
Lysis Buffer		
Laemmli Sample buffer	161-0737	Bio-Rad, California, United States
Methanol	1070182511	Merck, New Jersey, United States
MicroAmp™ Optical Adhesive Film	43-119-71	Thermo Fisher Scientific, Massachusetts, United States
MicroAmp™ Optical PCR 96-well clear plates	N8010560	Applied Biosystems, California, United States
Myer's Haematoxylin		Kimix Chemicals, Cape Town, South Africa
NaCl	53014	Sigma-Aldrich, Missouri, United States
Nuclease-free water	Am9937	Ambion, Texas, United States
Oil Red-O		Kimix Chemicals, Cape Town, South Africa
OneTouch Select®, Glucose Meter		LifeScan Inc., California, United States

PBS	BE17513F	Lonza, Verviers, Belgium
Ponceau S	P23295	Sigma-Aldrich, Missouri, United States
PowerUpTM SYBR® Green Master Mix	A25742	Thermo Fisher Scientific, Massachusetts, United States
Precision Plus Protein™ Western C™ marker	1610385	Bio-Rad, California, United States
Qiazol	79306	Qiagen, Hilden, Germany
Restore PLUS™ Western Blot stripping buffer	46430	Thermo Fisher Scientific, Massachusetts, United States
RNaseZAP™	AM9780	Invitrogen by Thermo Fisher Scientific, Massachusetts, United States
Skim Milk Powder	70166	Sigma-Aldrich, Missouri, United States
StrepTactin® HRP Conjugate	1610381	Bio-Rad, California, United States
Superfrost® Microscope Slides	1255014	Thermo Fisher Scientific, Massachusetts, United States
TaqMan® Probe Assays	4331182	Thermo Fisher Scientific, Massachusetts, United States
TaqMan® Universal PCR Master Mix	4304437	Thermo Fisher Scientific, Massachusetts, United States
TGX Tris/Glycine/SDS running buffer	1610772	Bio-Rad, California, United States
Trans-Blot® Turbo™ Midi NC transfer packs	BBRD1704159	Bio-Rad, California, United States
Tris-base	93352	Sigma-Aldrich, Missouri, United States
Tween 20	58980C	Sigma-Aldrich, Missouri, United States
Xylene		Kimix Chemicals, Cape Town, South Africa

A2: Kits

Kit	Catalogue number	Company
Agilent 6000 Nano kit	1511	Agilent Technologies Inc.
Bio-Rad RC DC protein kit	500-0201	Bio-Rad, California, United States
BSA standards	5000007	Bio-Rad, California, United States
Clarity™ Western ECL substrate	1705060	Bio-Rad, California, United States
High capacity cDNA kit	PN 4375575	Applied Biosystems, California, United States
Insulin ELISA		Merck
RNeasy® mini kit	74106	Qiagen, Hilden, Germany
Turbo DNA-Free™ kit	AM1907	Ambion, Texas, United States

A4: Equipment

Equipment	Product Number	Supplier
2100 Expert Software		Agilent Technologies, Santa Clara, California, USA
2720 Thermal Cycler	4413750	Applied Biosystem, California, United States
ABI 7500 Real Time PCR system	4351104	Applied Biosystem, Foster City, California, United States
Agilent Bioanalyser	G2946-90004	Agilent Technologies,Santa Clara, California
Benchtop Centrifuge	SL16R	Thermo Fisher Scientific, Massachusetts, United States
ChemiDoc™ MP Imaging System	734BR0212	Bio-Rad, California, United States
GraphPad Prism 7		GraphPad Software, La Jolla, California, USA
Heating Block	S62927099	Labnet
ImageLab Software		Bio-Rad, California, United States
Leica Cryostat	CM1860	Leica, Wetzlar, Germany
NanoDrop® One Spectrophotometer	269309102	Thermo Fisher Scientific, Massachusetts, United States
Nikon Eclipse Ti inverted microscope	Ti inverted	Nikon, Tokyo, Japan
Orbital Shaker		Torrey Pines Scientific
pH Meter	702038	Lasec, Cape Town, South Africa
PowerPac™ HC	165-8025	Bio-Rad, California, United States
Softmax Pro6 Software		Molecular Devices, Sunnydale, California, United States
SpectraMax® i3 plate reader		Molecular Devices, Sunnydale, California, United States
Stainless Steel Beads	69989	Qiagen, Hilden, Germany
TissueLyser	85300	Qiagen, Hilden, Germany
Trans-Blot® TurboTM	1704070	Bio-Rad, California, United States

Appendix B: Preparation of reagents

B1: 10 x Tris-buffered saline (TBS) stock solution

The 10x TBS stock solution was prepared by dissolving 48.44 g Trizma-Base and 160.12 g NaCl in 1.8 L dH_2O. The pH was adjusted to 7.6 by gradually adding concentrated HCl, and the volume was topped up to 2 L with dH_2O. Stored at 4 °C.

B2: 1 x TBS-T working solution

The 1 x TBS-T working solution was prepared by adding 200 mL of 10 x TBS stock solution to 1800 mL dH_2O and 2 mL Tween 20. Stored at 4 °C.

B3: Transfer buffer

Transfer buffer was prepared by combining 200 mL 5 x transfer buffer (Bio-Rad, California, United States), 200 mL absolute ethanol and 600 mL dH_2O. Stored at room temperature.

B4: Oil Red-O (ORO) stain

Oil Red-O (ORO) stock solution was prepared by dissolving 0.9 g Oil Red O in 180 mL isopropanol and Dextrin stock solution was prepared by dissolving 1.2g Dextrin in 120 mL distilled water. Oil Red O working solution was prepared fresh before use by adding 30ml Oil Red stock to 20 mL Dextrin stock. The working solution was filtered before use.

B5: Crystal Violet

Crystal Violet working solution was prepared by diluting 25 mL 0.5% Crystal Violet in 25 mL distilled water.

Appendix C: Ethical Approval

SOUTH AFRICAN MEDICAL RESEARCH COUNCIL

ETHICS COMMITTEE FOR RESEARCH ON ANIMALS (ECRA)

PO Box 19001, Tygerberg, 7505, Cape Town, South Africa;
off Hindle Road, Brentwood Park, Driftsands
Tel: +27 (0)21 955 1900, Fax: +27 (0)21 955 1330
E-mail: gielana.fourie@mrc.ac.za
http://www.sahealthinfo.org/Modules/ethics.htm

4 December 2015

Dr R Johnson
BRIP
MEDICAL RESEARCH COUNCIL

Dear [redacted]

YOUR APPLICATION TO THE ECRA : REF. 05/15 "Identification of sub-clinical biomarkers that predict the risk of developing diabetic cardiomyopathy using H9c2 rat cell line and C57BLKS/J (Lepr^{de}) mice model".

Your revised application has been reviewed by round robin and it was approved.

You will be responsible for 6 monthly interim reports and ECRA will remind you thereof. Please inform the ECRA Committee if you encounter any difficulties during your study or need an extension if the approved timeline is not enough for the completion of the study.

Attached herewith please find your Certificate of Approval.

Kind regards.

[redacted]

Chairperson : ECRA Committee

Animal Ethics Approval Certificate

Decision of the Animal Ethics Committee for the use of living vertebrates for research, diagnostic procedures and product development

APPROVAL PERIOD: 1 Jun3 2016 - 31December 2018

PROJECT NUMBER:	05/15			
PROJECT TITLE:	**"Identification of sub-clinical biomarkers that predict the risk of developing diabetic cardiomyopathy using H9c2 rat cell line and C57BLKS/J (Lepr^{db}) mice model"**			
PROJECT LEADER:	Dr Rabia Johnson			
DIVISION:	Biomedical Research and Innovation Platform (BRIP), SAMRC			
CATEGORY:	Diabetic			
SPECIES OF ANIMAL:	Mice: K..CgDoc (m) + /C57BLKS/J (Lepr^{db})	Males 17-40gr	6 – 16 weeks old	
NUMBER OF ANIMALS:	*In vivo* 176			
NOT APPROVED:	n/a			
APPROVED:	4 December 2015			

PLEASE NOTE: Should the number or species of animal(s) required, or the experimental procedure(s) change, please submit a revised animal ethics clearance form to the animal ethics committee for approval before commencing with the experiment

[redacted]

DATE: **4 December 2015**

CHAIRPERSON ANIMAL ETHICS COMMITTEE

UNIVERSITEIT
STELLENBOSCH
UNIVERSITY

Animal Tissue Use Approval

Date: 19 October 2017

PI Name: Ms Anel Boshoff

Protocol #: 0301

Title: Understanding the liver to protect the heart

Dear Anel Boshoff

The 0301 , was reviewed on 17 October 2017 by the Research Ethics Committee: Animal Care and Use via committee review procedures and was approved. Please note that this clearance is valid for a period of five years. A new application must be submitted when the source of the material changes.

Applicants are reminded that they are expected to comply with accepted standards for the use of animals in research and teaching as reflected in the South African National Standards 10386: 2008. The SANS 10386: 2008 document is available on the Division for Research Developments website www.sun.ac.za/research.

As provided for in the Veterinary and Para-Veterinary Professions Act, 1982. It is the principal investigator's responsibility to ensure that all study participants are registered with or have been authorised by the South African Veterinary Council (SAVC) to perform the procedures on animals, or will be performing the procedures under the direct and continuous supervision of a SAVC-registered veterinary professional or SAVC-registered para-veterinary professional, who are acting within the scope of practice for their profession.

Please remember to use your protocol number, 0301 on any documents or correspondence with the REC: ACU concerning your research protocol.

Please note that the REC: ACU has the prerogative and authority to ask further questions, seek additional information, require further modifications or monitor the conduct of your research.

Any event not consistent with routine expected outcomes that results in any unexpected animal welfare issue (death, disease, or prolonged distress) or human health risks (zoonotic disease or exposure, injuries) must be reported to the committee, by creating an Adverse Event submission within the system.

We wish you the best as you conduct your research.

If you have any questions or need further help, please contact the REC: ACU secretariat at [redacted]

Sincerely,

[redacted]

REC: ACU Secretariat

Research Ethics Committee: Animal Care and Use

Appendix D: Turnitin report

Turnitin Originality Report

Processed on: 30-Nov-2018 00:42 SAST
ID: 1047070850
Word Count: 16023
Submitted: 2

Draft 2 By Anel Willamien Boshoff

Similarity Index 25%

Similarity by Source
Internet Sources: 16%
Publications: 17%
Student Papers: 9%

4% match (student papers from 01-Dec-2016)
Submitted to University of Zululand on 2016-12-01

1% match (publications)
"Abstract Book 2008", Diabetologia, 09/2007

1% match (Internet from 23-Nov-2017)
http://scholar.sun.ac.za/bitstream/handle/10019.1/100390/jack_investigation_2016.pdf?isAllowed=y&sequence=1

1% match (Internet from 22-May-2012)
http://uspace.uzulu.ac.za/bitstream/handle/10530/618/AN%20IN%20VITRO%20STUDY%20OF%20THE%20EFFECTS%20OF%20FREE%20FATTY%20ACIDS.pdf?sequence=1

< 1% match (publications)
Hepatic De Novo Lipogenesis and Regulation of Metabolism, 2016.

< 1% match (publications)
"Abstracts of 52nd EASD Annual Meeting", Diabetologia, 2016

< 1% match (Internet from 15-May-2018)
https://pure.uva.nl/ws/files/24088470/155109_Costes_thesis_met_cover.pdf

< 1% match (publications)
"Abstracts", Diabetologia, 08/2005

< 1% match (publications)
Keshari, K. R., D. M. Wilson, V. Sai, R. Bok, K.-Y. Jen, P. Larson, M. Van Criekinge, J. Kurhanewicz, and Z. J. Wang. "Non-invasive in vivo imaging of diabetes-induced renal oxidative stress and response to therapy using hyperpolarized 13C dehydroascorbate magnetic resonance", Diabetes, 2014.

< 1% match (publications)
J. M. Nielsen, "Blockage of receptor for advanced glycation end products prevents development of cardiac dysfunction in db/db type 2 diabetic mice", European Journal of Heart Failure, 07/01/2009

< 1% match (Internet from 17-Feb-2017)
http://www.mdpi.com/1420-3049/22/2/219/pdf-vor

< 1% match (Internet from 14-Feb-2018)
http://www.journalofparasitology.org/doi/full/10.1645/GE-307R

Appendix E: Submitted research article

Article

Hepatic steatosis: a cause or consequence of muscle insulin resistance and subsequent cardiac dysfunction in a leptin receptor-deficient db/db mice model

*#Rabia Johnson[1,2], #Anel Boshoff[1,2], Barbara Huisamen[1,2], Sandrine Lecour[3], Martin Cour[3], Johan Louw[1,4] and Christo Muller[1,2,4]

1 Biomedical Research and Innovation Platform (BRIP), South African Medical Research Council (SAMRC), South Africa; rabia.johnson@mrc.ac.za; Christo.Muller@mrc.ac.za, Johan.Louw@mrc.ac.za
2 Division of Medical Physiology, Faculty of Health Sciences, Stellenbosch University, Tygerberg, South Africa; rabia.johnson@mrc.ac.za, Anel.Boshoff@mrc.ac.za, Christo.Muller@mrc.ac.za, bh3@sun.ac.za.
3 Hatter Institute for Cardiovascular Research in Africa (HICRA), University of Cape Town, South Africa; martin.cour@chu-lyon.fr, Sandrine.Lecour@uct.ac.za,
4 Department of Biochemistry and Microbiology, University of Zululand, KwaDlangezwa 3886, South Africa; Christo.Muller@mrc.ac.za, johan.Louw@mrc.ac.za.

#Equal contribution
* Correspondence:

Received: date; Accepted: date; Published: date

Article was submitted to IJMS

Abstract: The global obesity epidemic has been associated with various metabolic disorders, including insulin resistance (IR) and non-alcoholic fatty liver disease (NAFLD). Insulin resistance, a hallmark of NAFLD, is an established risk factor for type 2 diabetes (T2D) and cardiac dysfunction. While various factors that contribute to cardiac dysfunction have been identified, it is not evident whether NAFLD is a cause or consequence of muscle IR that drives changes in cardiac structure. Thus, to better understand the pathophysiology of NAFLD, this study sought to characterize the order of onset of NAFLD and muscle IR in the development of diabetes-induced cardiac dysfunction. Six- to sixteen-week-old male Leptin receptor deficient ($Lepr^{db/db}$) mice and their lean littermate controls ($Lepr^{db/+}$) were monitored weekly to measure fasting blood glucose, body weight, and heart function. Serum was collected weekly to measure lipogram and liver enzymes. Liver tissues were stained with haematoxylin and eosin to determine onset of hepatic steatosis, while gene and protein expression analysis were performed on liver, muscle and heart tissue to determine the molecular basis and onset of NAFLD, muscle IR and cardiac dysfunction. Data obtained showed that $Lepr^{db/db}$ mice were overweight and dyslipidaemic, with increased fasting blood glucose by 7 weeks of age. Histological analysis and protein expression of lipogenic genes confirmed the presence of mild hepatic steatosis, which increased in severity as the animal aged. Interestingly, muscle insulin resistance was not present at the onset of NAFLD. However, from 10 weeks onwards, a decrease in muscle phosphorylated PI3K/AKT signalling was observed and this was concomitant to an increased in cytosolic GLUT4 protein expression. Gene expression analysis confirmed an increase in oxidative stress, inflammation, and apoptosis in the heart of $Lepr^{db/db}$ mice by 10 weeks with a reduction in ejection fraction observed by 13 weeks. In summary, our data suggest that, contrary to the general believe, hepatic steatosis preceded and likely contributes to the development of IR and subsequent

cardiac dysfunction in a Lepr$^{db/db}$ mice model. However, we speculate that the observed effect could be dependent on the "metabolic model" under study as well as "genetics" and thus require further investigation.

Keywords: Alanine aminotransferase, Aspartate aminotransferase, Cardiovascular dysfunction, Hepatic steatosis, Muscle insulin resistance, Nonalcoholic fatty liver disease (NAFLD), Triglycerides

---

1. Introduction

Cardiovascular diseases remain the leading cause of global deaths, with 17.9 million individuals dying of heart disease in 2016 [1]. High blood pressure, increased triglycerides, low-density lipoproteins (LDL), cholesterol and smoking are key risk factors associated with cardiac dysfunction, while conditions such as binge drinking, poor diet, and physical inactivity, are modifiable risk factors known to aggravate the epidemic, placing individuals at increased risk for heart failure.

The pathophysiology associated with cardiovascular dysfunction is mainly linked to diabesity-induced glucolipotoxicity. According to the World Health Organization (WHO), it is estimated that 39% of adults worldwide are overweight and obese (BMI ≥ 25). In South Africa this number is doubled with 61% of South Africans being overweight and obese, with obesity strongly linked to *de novo* lipogenesis [2,3]. In the obese state impaired lipid metabolism leads to excessive fat accumulation in hepatocytes, which is a prime cause of nonalcoholic fatty liver disease (NAFLD). NAFLD is a feature of metabolic syndrome and main driver of insulin resistance (IR), and as such, both conditions are linked to visceral adiposity and dyslipidemia. This has been confirmed in, numerous dietary intervention studies, reporting on IR and excessive serum fatty acids as pivotal drivers in the development of NAFLD [4-6]. More importantly, NAFLD and IR have become common diseases that affect western societies and remain key in the development and onset of type 2 diabetes mellitus (T2DM). With the mentioned diseases aggravating metabolic syndrome Hence, it is important to delineate the role NAFLD plays in the development of IR in order to improve or better current therapeutics.

To date, conflicting evidence exists regarding the order of onset, making it difficult to develop effective therapies. While most studies support the notion that IR causes hepatic steatosis [7-9], very few support IR being a consequence of NAFLD [10,11]. It has been well documented that insulin has a dual effect on the liver through its control of *de novo* lipogenesis and gluconeogenesis. During systemic insulin resistance, the ability of insulin to blunt free fatty acid (FFA) released from the adipocytes is no longer effective. This results in an excessive influx of serum triglycerides into the hepatocytes, causing the onset of simple steatosis [12]. This increased lipid overflow stimulates *de novo* lipogenesis and gluconeogenesis, whilst inhibiting pathways associated with beta (β)-oxidation, which further exacerbates oxidative stress while promoting inflammation, fibrosis and subsequent microvesicular steatosis [10,13,14]. On a molecular basis, excessive *de novo* lipogenesis is said to activate sterol regulatory element binding protein 1c (SREBP-1c), a transcription factor, which in turn increases the expression of lipogenic genes such as Fatty acid synthase (FASN), Sterol-CoA Desaturase (SCD) and 3-Hydroxy-3-Methylglutaryl-CoA Reductase (HMGCR) to further increase lipid accumulation and hepatotoxicity [7].

Alternatively, in support of NAFLD playing a casual role in IR, a scarcity of data exists. A decade ago, Ibdah et al. in 2005, proposed that inhibition of mitochondrial β-oxidation might play a significant role

in the development of NAFLD and subsequent IR [15]. The authors elegantly showed that by inhibiting mitochondrial β-oxidation, fatty acids might cause the "first hit" in the onset of hepatic steatosis subsequently followed by IR [15]. More recent evidence also suggests that an influx of FFA due to overexpression of SREBP-1c in mice increases hepatic steatosis and subsequent IR [12]. Similarly, in a knock-down of carbohydrate responsive element-binding protein (ChREBP) in an ob/ob mouse model, liver-specific inhibition of ChREBP markedly improved hepatic steatosis, plasma triglycerides, and non-esterified fatty acid, while restoring insulin signaling in muscle and white adipose tissue [11]. A similar phenomenon was observed when mice, on a high-fat-diet, that constitutively express carnitine palmitoyl transferase (CPT1a), were found to be protected against the development of hepatic steatosis and systemic IR.

However, none of the mentioned findings was able to elaborate if NAFLD is a cause or consequence of IR that drives the cardiovascular pathology. Hence, to better understanding the conundrum that exists between NAFLD, IR and cardiovascular disease (CVD) this study will investigate whether NAFLD or muscle IR initiates the pathology that leads to the changes in cardiac structure and function, using a leptin-receptor-deficient (*Lepr*) diabetic (db/db) mice model.

2. Results

2.1. Morphometric analysis

Six- to fifteen-week-old db/db mice and their lean db/+ controls were fed a standard mouse chow diet for 10 weeks. Body weights and fasting blood glucose were recorded weekly. By 6 weeks body weights of db/db mice were significantly higher compared to db/+ (31.75 ± 0.71 compared to 20.50 ± 0.55, $p < 0.001$) and this remained significantly increased throughout (Fig.1A). Four-hour FBG levels of db/db mice were significantly raised by 8 weeks (65%) when compared to db/+ controls (13.27 ± 3.60 compared to 8.04 ± 2.14, $p < 0.05$). A further increase in FBG levels at 9 weeks was observed in db/db mice, with levels surging above 20 mmol/L (Fig. 1B). The degree of IR was estimated by using the Homeostasis Model of Assessment (HOMA-IR), this was only determined for 6 and 15 weeks, due to limited availability of serum. At 7 weeks no significance difference was observed between the db/db and db/+ group. However, at 15 weeks HOMA-IR was significant different between the two groups.

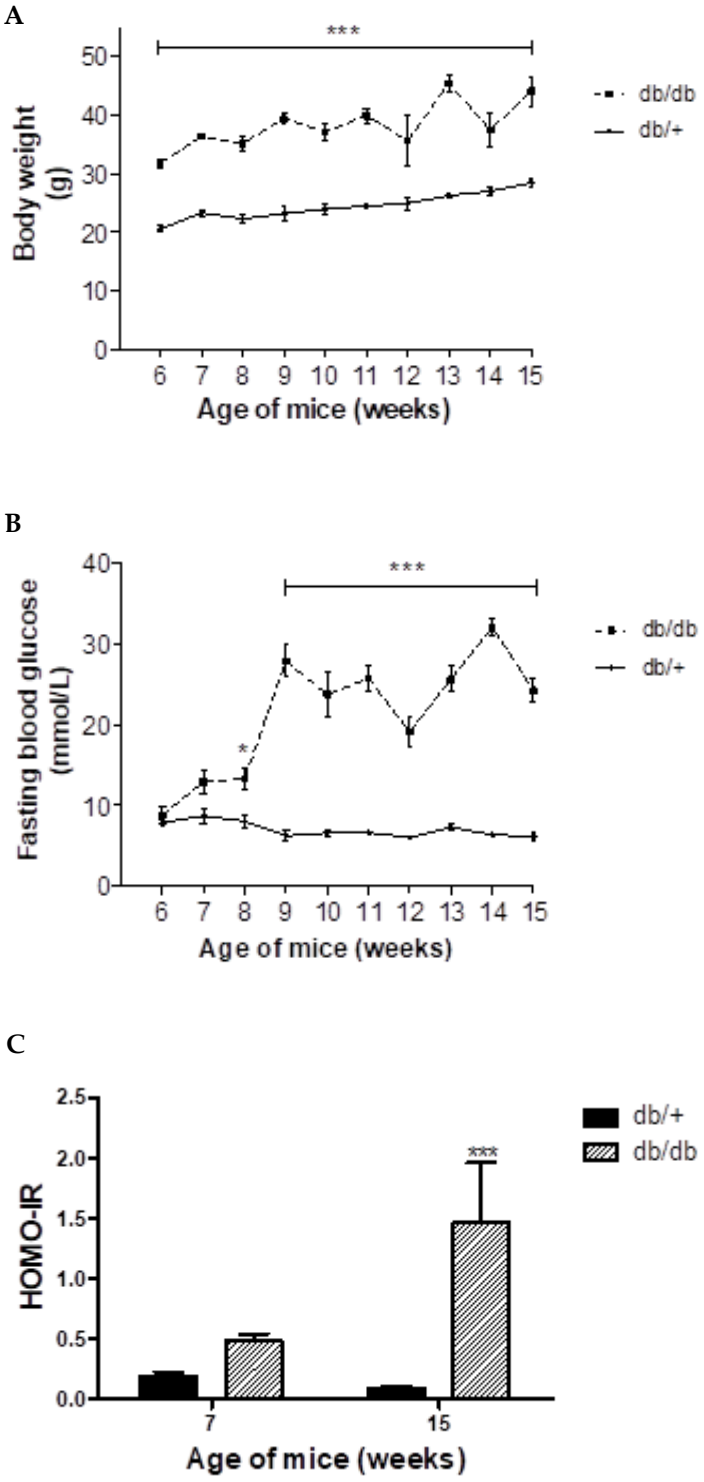

Figure 1: Body weights, fasting blood glucose levels and HOMA-IR. Body weights (A), four-hour fasting blood glucose levels (B), and HOMA-IR (C) were significantly different in leptin- receptor-deficient mice (*Lepr*$^{db/db}$) when compared to their age-matched heterozygous lean controls (*Lepr*$^{db/+}$). Results are presented as mean ± SEM of n=8 animals per group, * $p \leq 0.05$, ***$p \leq 0.001$ db/db versus age-matched db/+ control.

2.2. Echocardiography analysis

In the obese state, increased inflammation and oxidative stress result in structural and functional modifications to the myocardium leading to reduced cardiac contractility (EF<60%). As shown in Fig. 2, after 11 weeks of age, EF was significantly lower in db/db when compared to db/+ controls (Fig. 2).

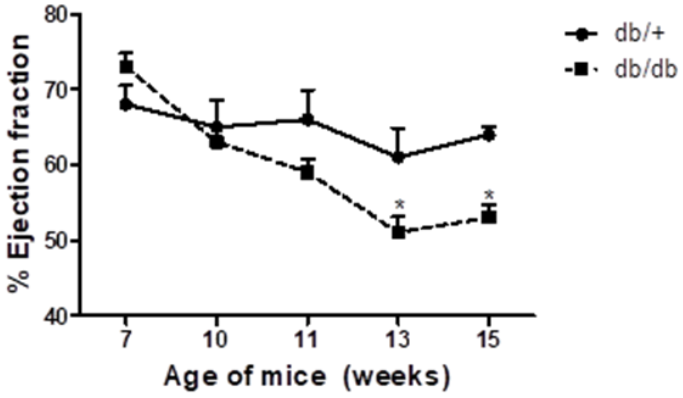

Figure 2: Echocardiography. After 11 weeks of age, left ventricle ejection fraction of leptin receptor deficient mice (*Lepr*$^{db/db}$) was significantly impaired when compared to both normal values (>60%) and heterozygous lean controls (*Lepr*$^{db/+}$). Results are presented as mean ± SEM of n= 8 animals per group, * $p \leq 0.05$ versus age-matched control.

2.3. Serum lipid profile as markers of cardiovascular risk

As an indication of dyslipidemia and a measure of metabolic risk, lipid profiles were performed in db/db mice and their heterozygous db/+ controls. At 7 weeks, triglyceride levels were significantly elevated in db/db mice when compared to the lean db/+ controls (2.43 mmol/L ± 0.11 compared to 0.84 mmol/L ± 0.08, $p < 0.001$), and levels remained raised throughout the experimental timeframe (Fig 3 A). Similarly, serum LDL levels were significantly elevated at 7 weeks in the db/db group when compared to the db/+ controls (0.55 mmol/L ± 0.03 compared to 0.30 mmol/L ± 0.004, $p < 0.01$) and this was evident until termination of the experimental conditions, though no significance was observed at 10 weeks (0.38 mmol/L ± 0.05 compared to 0.30 mmol/L ± 0.005) (Fig. 3B). Furthermore, at 7 weeks total cholesterol levels of db/db mice were significantly raised when compared to db/+ controls (3.90 mmol/L ± 0.14 compared to 1.90 mmol/L ± 0.04, $p < 0.001$) and remained elevated throughout the study (Fig. 3C).

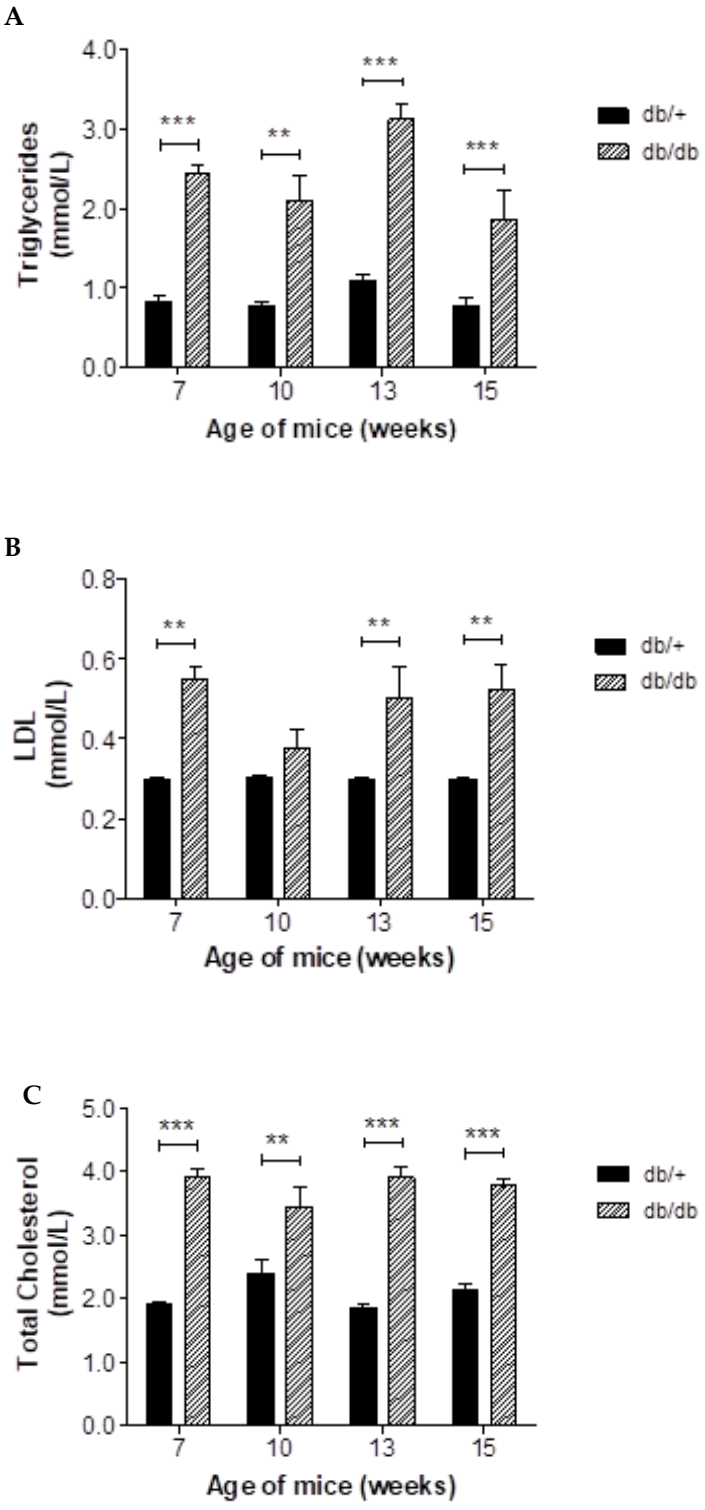

Figure 3. Serum lipid levels. Triglycerides (A), low-density lipoprotein (LDL) (B), and total cholesterol (C) were increased in leptin receptor-deficient mice (*Lepr*$^{db/db}$) when compared to heterozygous lean controls (*Lepr*$^{db/+}$) from 7 to 15 weeks of age. Results are presented as mean ± SEM of n=8 animals per group, ** $p \leq 0.01$, $^{***}p \leq 0.001$ versus age-matched control.

2.4. Liver toxicity

2.4.1 Liver enzymes as early markers of liver toxicity

Both AST and ALT are markers of liver injury. AST were significantly elevated at 13 weeks in db/db group when compared to db/+ controls (129 IU/L ± 29 versus 51 IU/L ± 1, respectively, $p < 0.01$) (Fig. 4A). Similarly, inflamed and injured liver cells usually leak increased levels of ALT into the bloodstream. With normal ALT levels being between 10-40 IU/L, db/db mice displayed significantly increased ALT levels as early as 7 weeks (> 50 IU/L) when compared to the db/+ control (<50 IU/L). This persisted throughout the experimental condition with results showing an increased in ALT at 13 and 15 weeks respectively, when compared to the aged matched db/+ control (165 IU/L ± 42 versus 33 IU/L ± 2, $p < 0.001$ and 159 IU/L ± 28 versus 43 IU/L ± 14, $p < 0.01$) (Fig. 4B). While AST and ALT can be used as a measure of liver damage, the ratio of AST/ALT provides an indication of the type of liver damage, with a high ratio (~ 2) associated with alcoholic liver disease, and a ratio lower than 1 associated with NAFLD [16]. The ratio of AST/ALT in db/db mice was less than 1 at 7 weeks (0.76 ± 0.07, $p<0.05$) and remained below 1 throughout (Fig. 4C), indicating the presence of hepatic steatosis.

2.4.2. Haematoxylin and Eosin stain of paraffin-embedded liver sections

While liver enzymes can be used as a marker of liver damage, histological analysis remains the gold standard confirming the onset of NAFLD. Haematoxylin and eosin stained liver sections indicated the presence of simple steatosis at 7 weeks. Additionally, results indicated that the severity of hepatic lipid accumulation increased with age. Microvesicular steatosis was identified at 7 weeks by the accumulation of multiple, small lipid droplets in hepatocytes, indicated by white arrows (Fig. 5B). At 10 weeks microvesicular steatosis persisted, with an increased number of hepatocytes displaying lipid accumulation. By 13 weeks, intracellular lipid accumulation in the db/db group (Fig, 5F) led to hypertrophy with the nucleus of some cells displaced to the side of the cell. This phenomenon worsened by 15 weeks of age (Fig. 5H), where the steatosis appeared to be progressing towards macrovesicular steatosis, and lipid droplets within the cell merge into one, whilst the nucleus completely disintegrate.

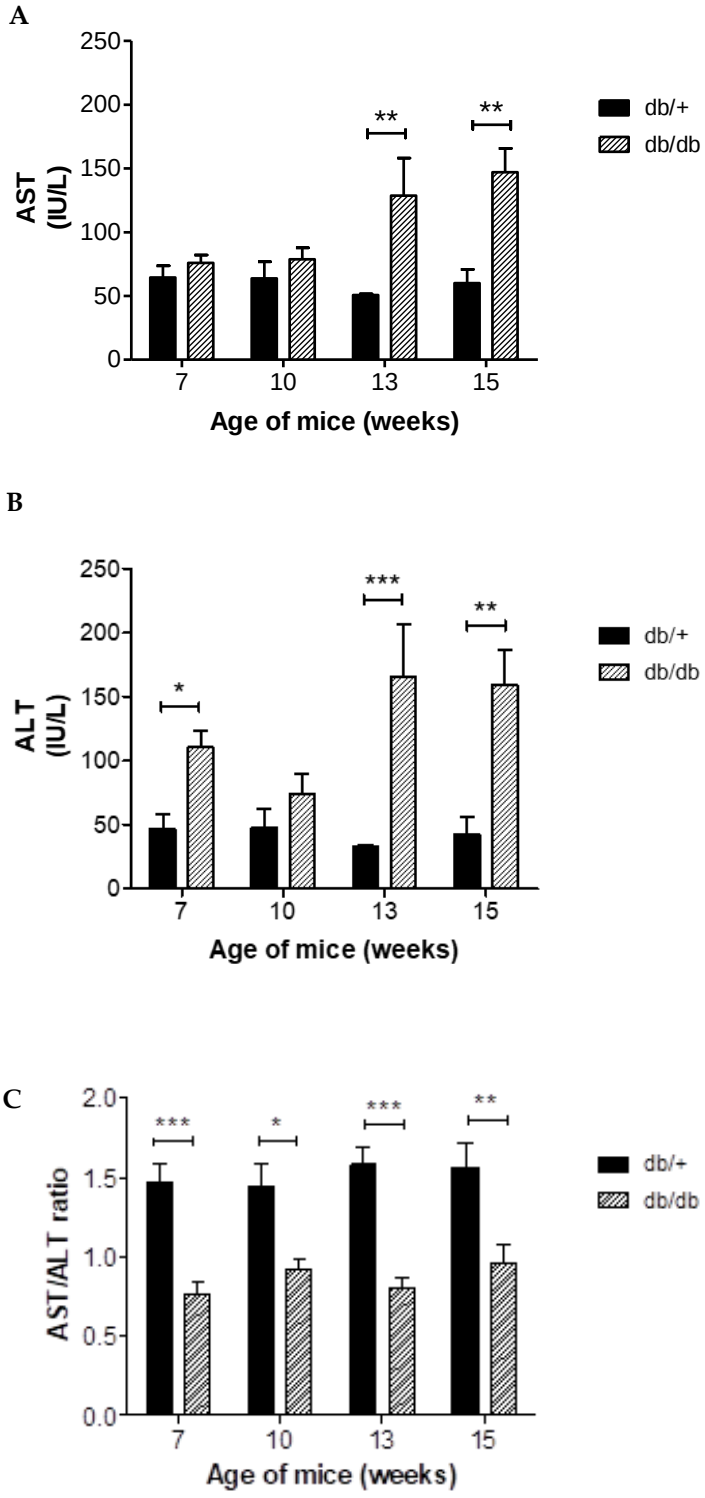

Figure 4: Aspartate Transaminase and Alanine Transaminase levels in serum. Levels of Aspartate Transaminase (AST) (A), Alanine Transaminase (ALT) (B), and AST/ALT ratio (C) in serum of leptin receptor deficient mice (*Lepr*$^{db/db}$) remained altered when compared to heterozygous lean controls (*Lepr*$^{db/+}$) from 7 to 15 weeks of age. Results are presented as mean ± SEM, * $p \leq 0.05$, ** $p \leq 0.01$, ***$p \leq 0.001$ db/db versus age-matched db/+ control.

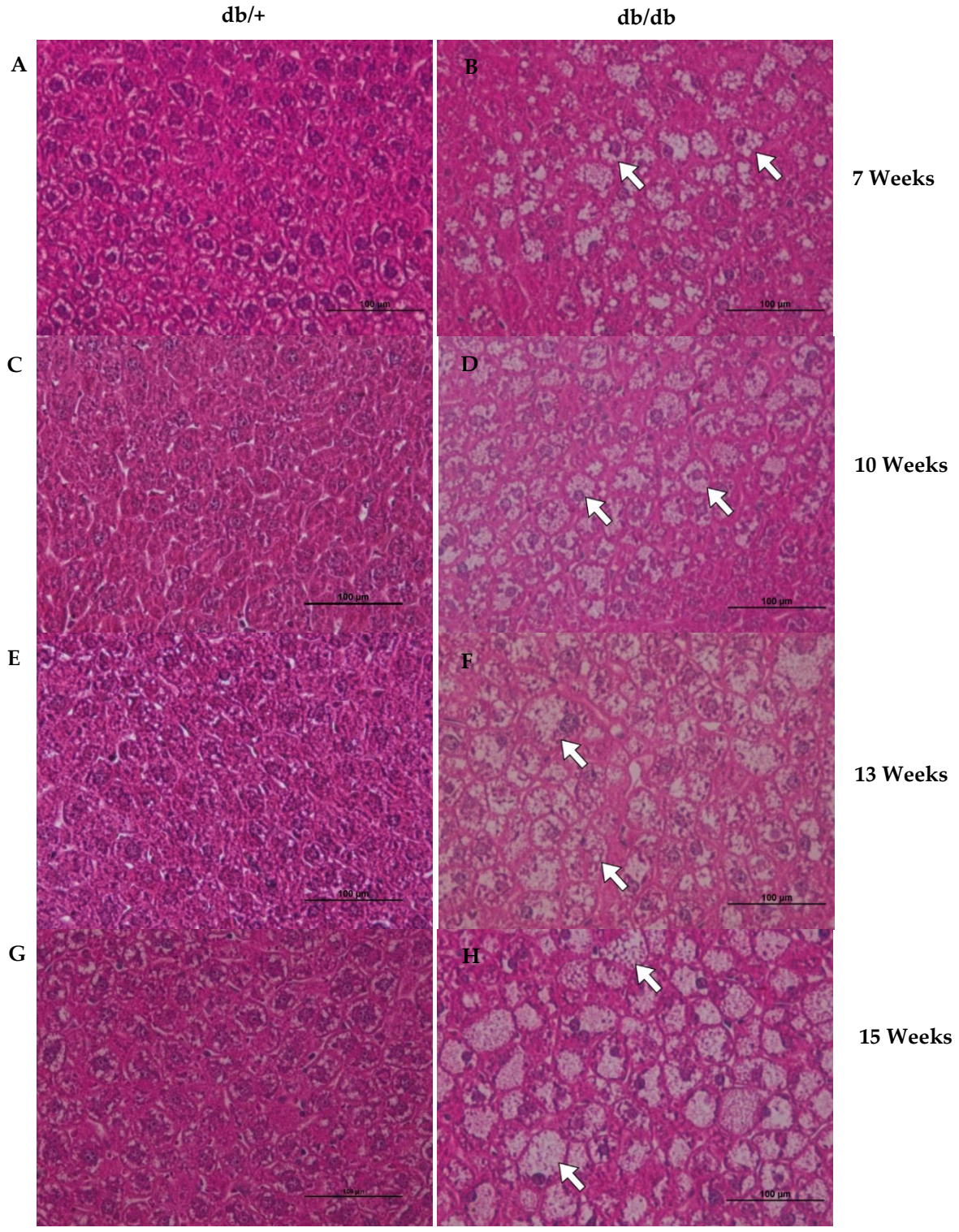

Figure 5: Haematoxylin and Eosin stained liver sections. Haematoxylin and Eosin stain on liver sections of lean (*Lepr*$^{db/+}$) and obese (*Lepr*$^{db/db}$) mice. Scale bar = 100 µm, white arrow = microvesicular steatosis.

2.5. Gene and Protein expression analysis

2.5.1.1 ***De novo* lipogenesis in liver**

Sterol regulatory element binding protein 1c is a transcription regulator associated with lipid metabolism and *de novo* lipid synthesis. Its main role as a transcriptional regulator is to regulate the expression of various hepatic lipid metabolism genes, including *FASN*, *SCD*, and *HMGCR*. In this study mRNA expression of *SREBF1*, was not significantly altered in db/db mice when compared to age-matched db/+ controls at any of the selected time points (Fig. 6A). Nonetheless, mRNA expression for *FASN*, the enzyme that catalyses fatty acid synthesis, was significantly increased at 7 weeks in db/db mice when compared to db/+ controls (1.16 ± 0.18 compared to 0.25 ± 0.05, $p < 0.01$) and remained elevated (Fig. 6B). Similarly, mRNA expression of *SCD1*, an enzyme involved in the synthesis of monounsaturated fatty acids, was also significantly increased by 7 weeks in db/db mice when compared to db/+ controls (1.03 ± 0.08 compared to 0.20 ± 0.05, $p < 0.001$) and remained raised (Fig. 6C). Hydroxyl-3-Methylglutaryl-CoA Reductase is a rate-controlling enzyme in cholesterol biosynthesis that is known to increase LDL clearance, of which *ApoB* is the main protein constituent. In this study mRNA expression of *HMGCR*, was significantly increased at 7, 13 and 15 weeks in the db/db group when compared to db/+ controls (1.23 ± 0.13 compared to 0.49 ± 0.08, $p < 0.001$ and 1.06 ± 0.09 compared to 0.72 ± 0.05, $p < 0.01$ and 0.786 ±1.047 compared to 0.04 ± 085, $p < 0.01$, respectively) (Fig. 6 D), while mRNA expression of *ApoB* remained the same (data not shown).

2.5.1.2. Hepatic fatty acid oxidation

Long-chain fatty acids, a known inducer of *CPT1A* modulate fatty acid β-oxidation through the activation of *PPARα*. In this study, the expression of *PPARα* was increased at 15 weeks, while *CPT1A* was decreased at 7 weeks when compared to db/+, no difference at any of the other time points was observed (Fig. 7A and B).

A

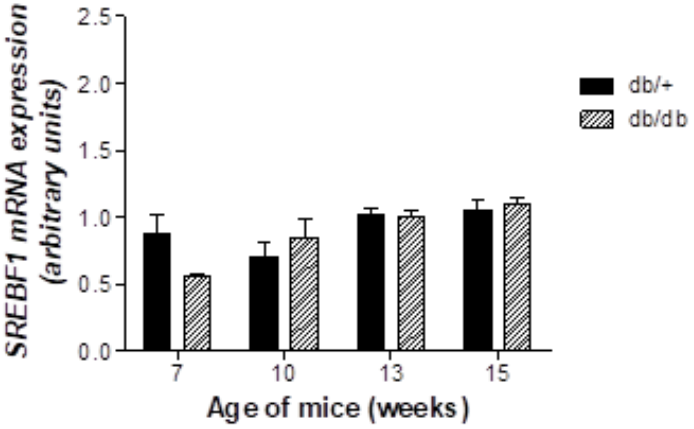

B

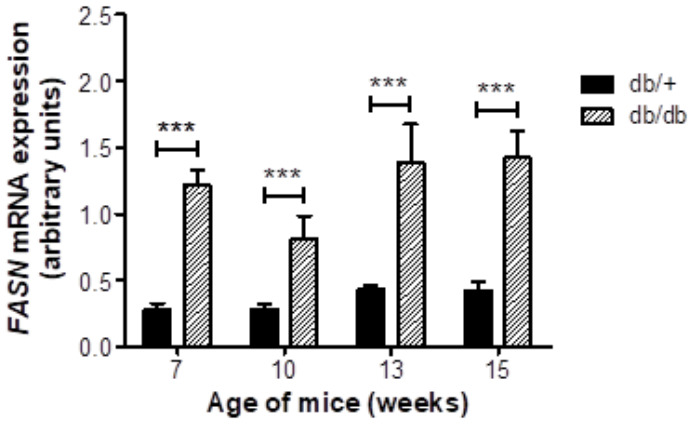

C

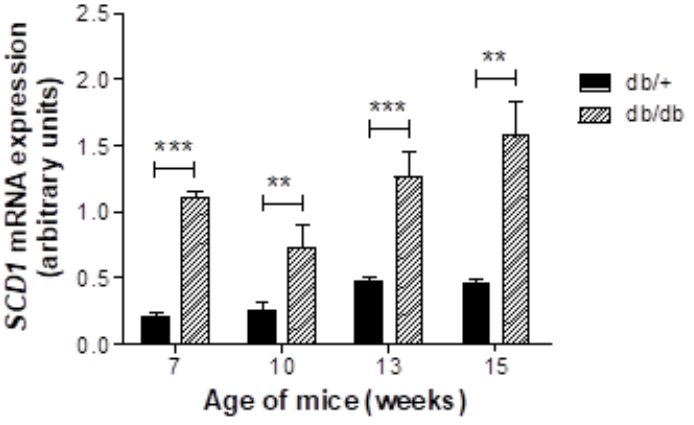

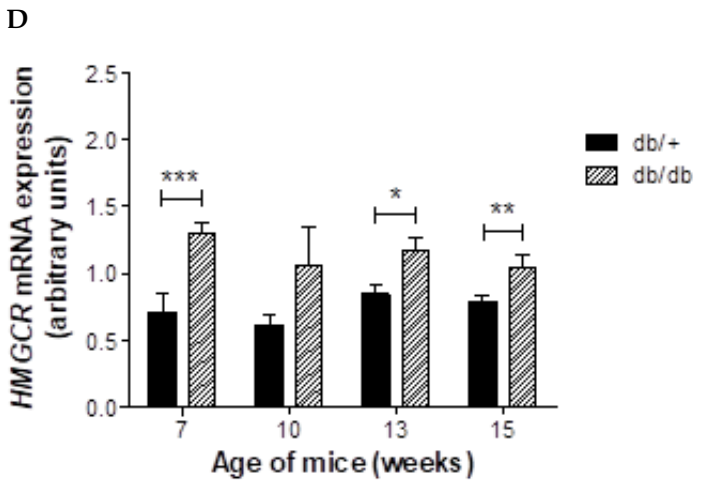

Figure 6: mRNA expression analysis of lipogenic genes in liver. mRNA epression analysis of Sterol regulatory element binding protein 1c (A), Fatty acid synthase (*FASN*) (B), Stearoyl-CoA Desaturas (*SCD*) (C) and 3-Hydroxy-3-Methylglutaryl-CoA Reductase (*HMGCR*) (D) in livers of leptin receptor deficient mice ($Lepr^{db/db}$) and heterozygous lean controls ($Lepr^{db/+}$) from 7 to 15 weeks of age. Results are presented as mean ± SEM of n=8 animals per group. * $p \leq 0.05$, ** $p \leq 0.01$, *** $p \leq 0.001$ compared to age-matched control.

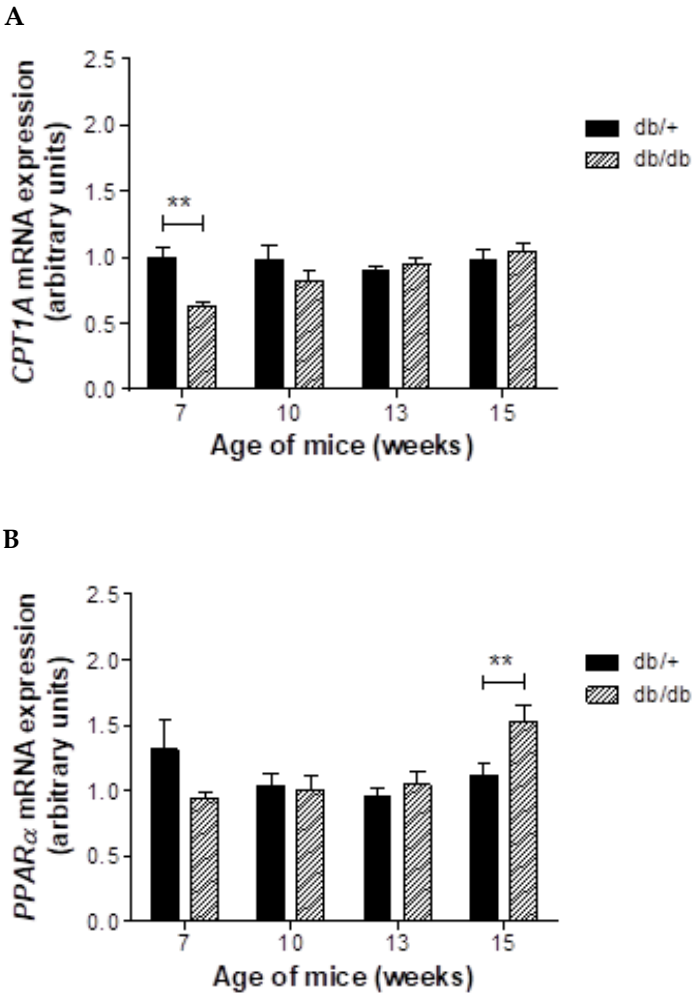

Figure 7: mRNA expression analysis of genes involved in β-Oxidation in liver. Relative mRNA expression of Peroxisome proliferator alpha (*PPARα*) (A), carnitine palmitoyl transferas (*CPT1A*) (B) of in livers of leptin receptor deficient mice ($Lepr^{db/db}$) and heterozygous lean controls ($Lepr^{db/+)}$ from 7 to 15 weeks of age. Results are presented as mean ± SEM of n=8 animals per group. * $p \leq 0.05$, ** $p \leq 0.01$, *** $p \leq 0.001$ compared to age-matched control.

2.5.2. Muscle insulin resistance

Insulin signalling regulates glucose and lipid energy homeostasis, mainly via its action on the liver, skeletal muscle, and adipose tissue. This effect is mediated through activation of either the insulin-dependent (PI3K/AKT) or insulin-independent (pAMPK) pathway. In this study, a significant increase in the ratio of pAKT/ tAKT ($p<0.01$) and pPI3K/tPi3K ($p<0.01$) was observed in db/db mice at 10 weeks when compared to the db/+ control (Fig. 8A and B). The expression of GLUT4 in the cytosolic fraction of skeletal muscle was increased at 15 weeks of age when compared to db/+ controls, though not significantly (Fig 8C). Protein expression of CPT1A, a marker of β-oxidation, was found to be is decreased at 10 and 13 weeks, though not significantly. However, at 15 weeks a significant reduction of CPT1A expression ($p<0.01$) was observed in the db/db group compared to the db/+ controls (Fig 8D).

2.5.3. Cardiac gene expression analysis

Obesity and insulin resistance are known inducers of glucolipotoxicity and has been positively correlated to oxidative stress, inflammation, fibrosis and apoptosis in cardiac cells. In this study, mRNA expression of NADPH Oxidase 4 (NOX4), a major source of oxidative stress, was increased in db/db mice when compared to db/+ controls, though not significantly (Fig. 9A). mRNA expression of NFκB, a transcription factor involved in inflammation and cell survival, was significantly increased from 10 weeks onwards, in the db/db group when compared to db/+ controls (1.68 ± 0.09 compared to 0.69 ± 0.04, $p < 0.001$) (Fig. 9B). Connective tissue growth factor (CTGF), a marker of fibrosis, also showed significantly increased mRNA expression in the obese db/db group when compared to db/+ controls (2.08 ± 0.39 compared to 0.98 ± 0.27, $p < 0.001$) at 15 weeks of age (Fig 9C). Similarly, Caspase 3 (CASP3), a known determinant of apoptosis was significantly increased in db/db mice when compared to db/+ controls (1.42 ± 0.10 compared to 1.06 ± 0.06, $p < 0.05$) at 10 weeks of age and remained elevated throughout the study (Fig. 9D).

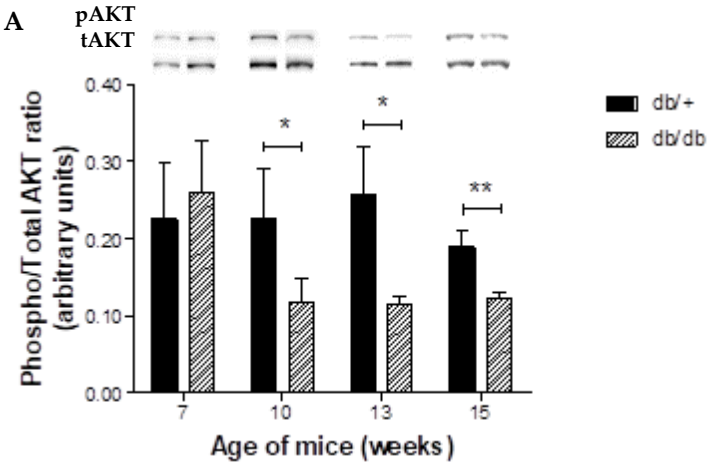

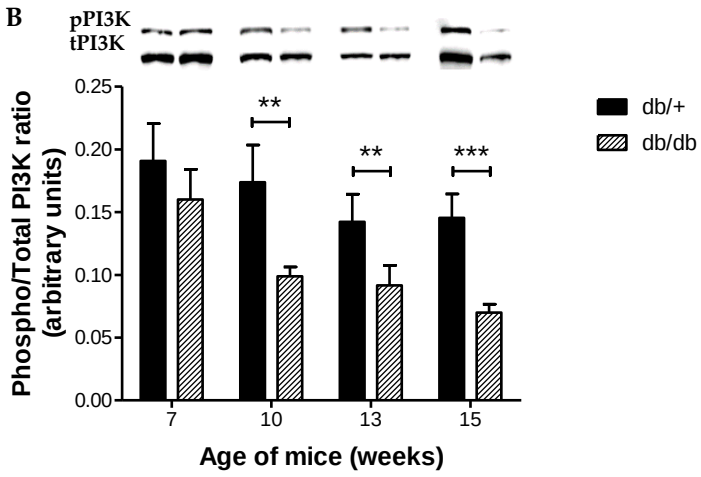

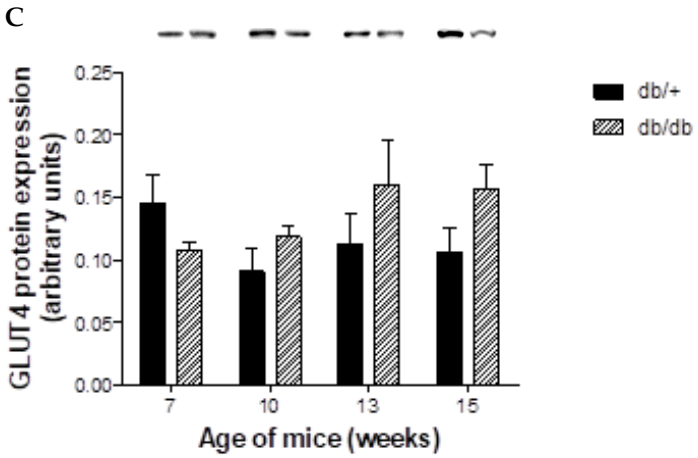

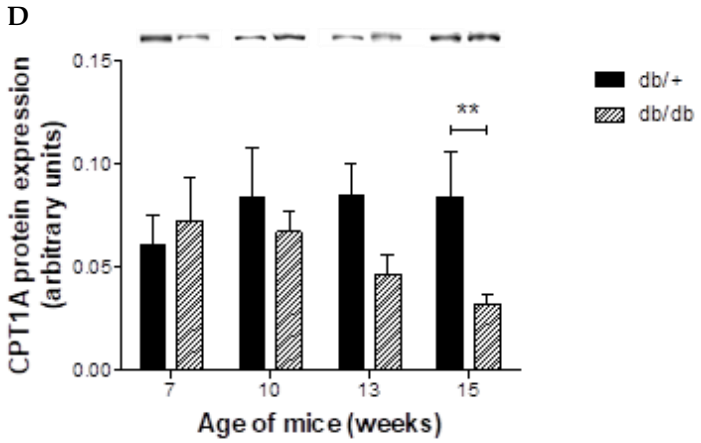

Figure 8: Protein expression in skeletal muscle. Ratio of phosphorylated to total protein expression of p/t AKT (A), p/tPI3K (B), cytosolic GLUT4 (C) and CPT1A (D) in skeletal muscle of leptin receptor deficient mice (*Lepr*$^{db/db}$) and heterozygous lean controls (*Lepr*$^{db/+}$) from 7 to 15 weeks of age, normalised to β-actin as a loading control. Results are presented as mean ± SEM of n=6 animals per group, ** $p \leq 0.01$ versus age-matched control.

A

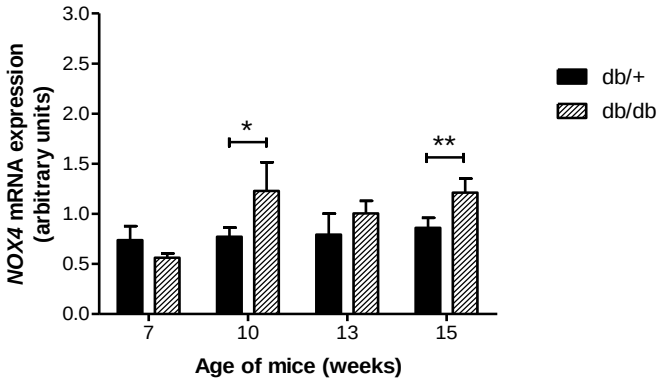

B

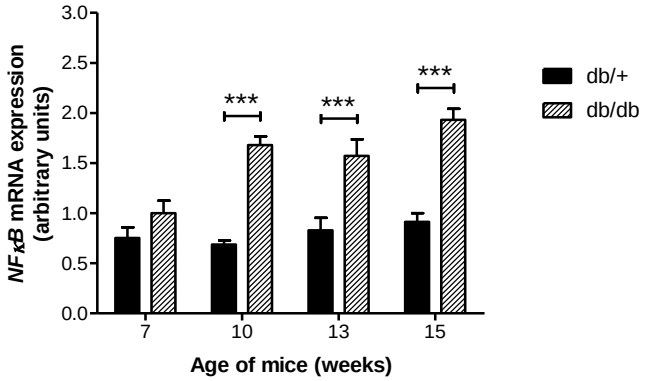

C

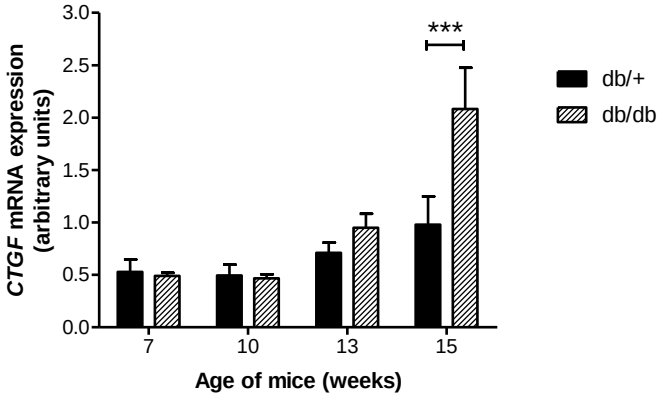

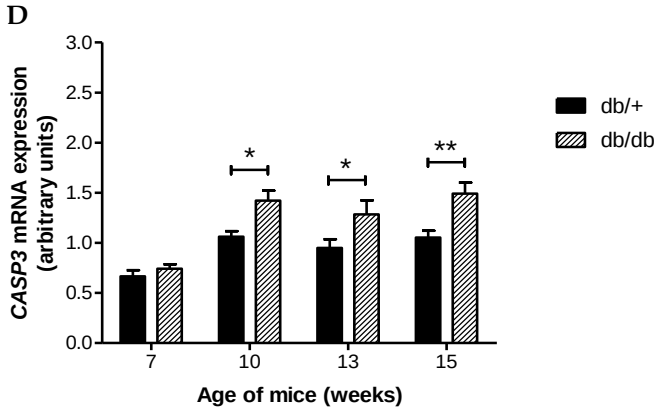

Figure 9: mRNA expression of known determinants of oxidative stress, inflammation, fibrosis, and apoptosis in heart tissue of db/db mice. Relative mRNA expression of Nox4 (A), NFKB (B), CTGF (C) and CASP (3) in the heart of leptin receptor deficient mice (*Lepr*$^{db/db}$) and heterozygous lean controls (*Lepr*$^{db/+}$) from 7 to 15 weeks of age. Results are presented as mean ± SEM of n=8 animals per group. $^{*}p \leq 0.05$, $^{**}p \leq 0.01$, $^{***}p \leq 0.001$ versus age-matched control.

3. Discussion

Glucolipotoxicity: Results from both epidemiological and physiological studies have demonstrated that "glucolipotoxicity is a clinical consequence of endogenous glucose and lipid dysregulation, of which obesity is the major driver [17]. Not only does this increase the risk for developing T2DM, but also, there is a strong association with macro and microvascular complications. Currently glucolipotoxicity is one of the leading medical complications of modern society. Insulin resistance and NAFLD, as the predecessor of T2DM and cardiovascular dysfunction, are the main metabolic inducers of the "glucolipotoxicity", which adversely affects the myocardium. The latter stems from the inability of insulin to inhibit lipolysis, thereby increasing FFA uptake into the hepatocytes. As a consequence, hepatic autoregulation is lost resulting in augmented hepatic *de novo* lipogenesis, inflammation, and gluconeogenesis, whilst concomitantly worsening peripheral IR. While it is well reported that IR causes hepatotoxicity, there is a paucity of data that supports the reverse. On the contrary, in this study we will present data that linked changes in body mass, FBG and augmented tryglecerides to hepatotoxicity, as the causality in the development of muscle IR and subsequent onset of CVD.

Hepatic lipotoxicity induces insulin resistance: To date various studies have linked NAFLD to a wide spectrum of cardio vascular abnormalities, however the exact mechanism remains to be explored [18-22]. In this study, a leptin receptor deficient mouse model was employed. The aforementioned is a well-established and translatable model in the development of T2DM, in which, db/db mice become grossly obese, hyperglycaemic and hyperlipidaemic as early as 7 weeks of age, while displaying left ventricular dysfunction at 12 weeks [23-26] . Furthermore, db/db mice are frequently used as a murine model in the study of NAFLD, with db/db mice displaying increased aminotransferases [27,28]. Our study confirms previous findings showing that db/db mice presented with elevated body weight as early as 6 weeks, while fasting blood glucose levels were significantly increased by 8 weeks. This was accompanied by the classical trio of augmented serum hypertriglyceridemia, cholesterolaemia and LDL, a paradox of metabolic syndrome that is said to revolve around the development of hepatic IR. Certainly, studies have shown that peripheral IR plays a casual role in the development of hepatic steatosis [29-31]. However, in our study we showed that lipotoxicity was observed at 7 weeks in the absence of peripheral IR and that this was accompanied by increased liver AST and ALT enzymes, which are early markers of hepatocellular damage and are used as predictive measures to evaluate an individual's risk for developing NAFLD and T2DM. Furthermore, hepatic steatosis due to increased alcohol consumption is frequently linked with an AST/ALT ratio >1, however in patients with NAFLD the AST/ALT ratio is <1, and this has been particularly observed in obese, insulin resistant patients, with increased risk for CVD [16,32,33]. In our study, we showed that except for 9 weeks, db/db mice displayed a AST/ALT ratio of <1, which is indicative of simple steatosis and correlated with liver damage being evident in hepatic tissue from 7 weeks. The former effect occurred concurrent with increased lipid profiles. While AST and ALT are widely used to screen for NAFLD, some individuals may present with normal levels of liver enzymes throughout the disease progression [34] and therefore histological analysis remains the gold standard for the conclusive diagnosis of NAFLD [35]. Mild NAFLD presents histologically as simple steatosis that develops into macrovesicular changes as the disease progresses ([35,36]. Data presented in this study confirm this phenomenon where mice from the obese group presented with evidence of simple steatosis in the form of microvesicular lipid accumulation by the age of 7 weeks.

Pathophysiology: NAFLD is considered as the hepatic manifestation of MetS and this has been associated with an enhanced expression of *de novo* lipogenic genes that activates a cascade of metabolic pathways that include the biosynthesis of saturated fatty acid, such as FASN and SCD-1 that is under the control of SREBF-1c. This was confirmed in the present study, where mice as early as 7 weeks presented with increased lipogenic genes.

Furthermore, increased β-oxidation in the liver has been associated with augmented CPT1A and PPAR-alpha (α) expression, which resulted in a decrease in triglycerides, aminotransferase, and liver steatosis. A study performed by Teng et al (2018) the author's showed that CPT1A was increased in db/db mice at 20 weeks of age [37]. In the current study, we found that PPARα expression was increased in the db/db mice by 15 weeks of age, though there was no increase in CPT1 expression. We propose that expression might have been increased at a later time point, which may indicate the activation of an adaptive mechanism to combat lipid accumulation as observed by Trak-Smayra et al (2011) [28]. Interestingly, at this, stage no evidence of muscle insulin resistance or cardiac dysfunction were present and therefore we speculate that in the current model NAFLD might be the main driver of muscle IR and subsequent CVD.

Onset of muscle insulin resistance: In support of the causal role, we further investigated muscle IR. In the obese state, dyslipidaemia causes chronic low-grade inflammation, which is accompanied by an increased release of FFA into the circulation including peripheral tissue. Augmented FFA uptake results in the generation of excess ceramide and diacylglycerol (DAG), which in turn activates PKCθ. Increased PKC promote the phosphorylation of IRS^{Ser307}. This results in the inhibition of pPI3K/pAKT complex to inhibit glycogen synthesis while increasing GLUT4 tranlocation to the plasma membrane. This was confirmed in a study done by Sharma et al (2015), who observed decreased phosphorylation of IRS, PI3K, and AKT, in db/db mice at 12 weeks [38], while Zheng et al (2015) demonstrated the presence of IR at 16 weeks [39]. In this study, we showed that muscle IR developed at 10 weeks as confirmed by phosphorylation of PI3K/AKT with concomitant increase in cytosolic GLUT4 expression.

Onset of cardiac dysfunction: With 425 million individuals living with diabetes and 1.6 million being obese, a reduced life expectancy is anticipated with a catastrophic rise in cardiovascular related deaths will occur within the next decade. This increase is directly associated with glucolipotoxicity that modulates key signal transduction genes associated with oxidative stress, inflammation, fibrosis, and apoptosis, with deleterious consequences to the myocardium. Glucolipotoxicity is worsened with the manifestation of NAFLD and IR, due to the inability of insulin to suppress endogenous hepatic glucose production and the failure of insulin to increase peripheral glucose uptake. These overarching changes in glucose and lipid metabolism, whether a cause or consequence of NAFLD, contribute towards the observed metabolic changes and accelerated cardiac phenotype present in diabetic individuals. In this study, we showed that hepatic lipotoxicity preceded muscle IR and that this deleterious action contributes towards an increased NADPH oxidase-dependant generation of ROS with an associated increase in the inflammatory response. It has been postulated that this metabolic pattern favours increased apoptosis, promotes collagen formation and augmented fibrosis with a reduced cardiac functional phenotype. In this study, we showed that an increased collagen cross-linking directly contributes towards a loss of myocardial contractility as demonstrated with increased CTGF expression and subsequent reduced ejection fraction at 13 weeks.

In conclusion, contradictory evidence still exists regarding the order of onset of NAFLD and IR. However, the current study provides strong evidence of the casual role NAFLD plays in the development of muscle IR, and subsequent time dependant onset of cardiac dysfunction. Nonetheless, we speculate that the observed effect is dependent on various factors, which include 1) the model under investigation and 2) genetics. In NAFLD, two phenotypes exist, "genetic" and "metabolic". We hypothesize that in a genetically modified model such as the db/db mouse model used in this study, IR is a consequence of NAFLD, whereas during a "metabolic insult," in the form of a "high-fat-high-sugar diet", IR will precede and contribute to the development of NAFLD. Although the latter feature was not investigated in the present study, we propose that the disease model used plays an imperative role

in delineating the order of onset, with the order of appearance of these risk factors being important and should be taken into consideration to develop effective therapeutics.

4. Materials and Methods:

4.1. Animals sample size and randomization

Four-week-old C57BLKS/J homozygous *Lepr*$^{db/db}$ mice (db/db) and their heterozygous *Lepr* nondiabetic lean controls (db/+) were obtained from Jackson's Laboratories (Sacramento, USA). Animals were housed at the Primate Unit and Delft Animal Centre (PUDAC) of the South African Medical Research Council (SAMRC) in a controlled environment with a 12 h light/dark cycle in a temperature range of 23-25ºC (relative humidity: ~50%). The mice received standard laboratory chow pellets (Afresh Vention, Cape Town, RSA) *ad libitum* and had free access to water. At 6 weeks, mice were divided into two groups based on their genetic background; db/+ (lean) (n=32) or db/db (obese) (n=32) group, each group was further divided into 4 subgroups (week 7, 10, 13, 15) with n=8 animals per group. For each subgroup, 4 hour fasting blood glucose (FBG), body weights and echocardiography analysis were performed at week 7, 10, 13, and 15. Upon termination after the allotted time, serum, heart and liver samples were collected for lipid profile, liver enzyme, as well as gene and protein expression analysis. Ethical clearance for the animal study was obtained from the South African Medical Research Council (SAMRC), Ethics Committee for Research on Animals (ECRA/05/15).

4.2. Echocardiography analysis

The mice were anaesthetised with 1.0-2.5% isoflurane and positioned in the supine position on a warming pad. Closed chest echocardiography was performed with a VEVO 2100 ultrasound system (Fujifilm, Visualsonics, Ontario, Canada) and a 30 MHz linear array transducer at the respective time intervals. Left ventricular ejection fraction (EF), as a measurement of cardiac dysfunction, was obtained from 2-dimensional and M-mode measurements at the mid-papillary level. All measurements were made off-line on the mean of at least three consecutive cardiac cycles with the software resident on the ultrasound system.

4.3. Lipid profile and liver enzyme analysis

After the predetermined experimental conditions, 4 hour fasted mice were weighed and anesthetized with halothane before blood was collected from the abdominal vena cava for subsequent lipid profile analysis. Blood was centrifuged at 4, 000 g at 4ºC for 15 min before the serum was removed and sent to PathCare Medical Diagnostic Laboratories (Cape Town, RSA) for total cholesterol, triglycerides, LDL, high-density lipoprotein (HDL) analyses as well as liver enzyme (Alanine aminotransferase (ALT) and Aspartate aminotransferase (AST)) analysis.

4.4. Histopathological analysis

Snap-frozen tissue were cut into 10 µm sections using a cryostat and attached to aminopropyltriethoxysilane coated glass slides (Sigma-Aldrich Corp., St. Louis) and then stained with hematoxylin and eosin stain (Merck-Millipore, Billerica, USA) to assess hepatic steatosis, as per manufacturer's instructions. For histopathological analysis, 5 random microscopic fields were captured and visualized using a Nikon Eclipse Ti inverted microscope (Tokyo, Japan).

4.5. Quantitative Real-Time polymerase chain reaction analysis (QRT-PCR)

Total RNA was extracted from rat heart tissue using TRrizol reagent (ThermoFisher Scientific, Inc., Waltham, MA, USA), while the Turbo DNase Kit (ThermoFisher Scientific, Inc.,Waltham, MA, USA) was used to remove genomic DNA, as per manufacturer's instructions. RNA integrity was determined using an Agilent 2100 Bioanalyser (Agilent Technologies, Inc., Palo Alto, CA, USA), according to manufacturer's instructions. First strand synthesis was done using a Superscript first strand cDNA

synthesis kit (ThermoFisher Scientific, Inc., Waltham, MA, USA), as per manufacturer's instructions. Predesigned and optimized TaqMan gene expression probes were used for differential gene expression (ThermoFisher Scientific, Inc., Waltham, MA, USA).

4.6. Western blot analysis

Proteins were extracted as previously described [40]. Twenty micrograms of protein lysate were denatured and loaded onto a 10% SDS-polyacrylamide gel and transferred to a polyvinylidene fluoride membrane. Nonspecific binding on the membranes was blocked, using 5% w/v low-fat milk in Tris-buffered saline with Tween-20. Subsequently, the membrane was incubated overnight at 4°C with Cell Signaling (Beverly, MA, USA) primary antibodies: Phosphatidylinositol-4,5-bisphosphate 3-kinase (anti-tPI3K; 1:1000 dilution), anti-pPI3K (1:1000), Protein kinase B (anti-tAKT; 1:1000), anti-pAKT (1:1000), 5' AMP-activated protein kinase (tAMPK; 1:1000), pAMPK(Thr^{172}) (1:1000), Glucose transporter type 4 (GLUT-4; 1:1000) and carnitine palmitoyltransferase (CPT1; 1:1000) (Sigma), with the relevant horseradish peroxidase-conjugated secondary antibodies applied the following day for 90 min at room temperature. β-Actin (1:2000) antibody was added as a loading control. Proteins were detected and quantified using a Chemidoc-XRS imager and Quantity One software (Bio-Rad Laboratories, Hercules, CA, USA).

4.7. Statistical Analysis

Data are expressed as the mean±standard error of the mean (SEM). Statistical analysis was performed using GraphPad Prism (Version 5.01, CA, USA). Groups of data were compared with a one-way analysis of variance (ANOVA) followed by Dunnet's Multiple Comparison tests. The unpaired, two-tailed student t-test was used when only two groups were compared. Values of $p<0.05$ were regarded as significant.

5. Author Contributions: Rabia Johnson was involved in the conceptualization, writing, editing and data analysis of article. Anel Boshoff performed and analyzed the experiments as well as edits the manuscript. Martin Cur and Sandrine Lecour performed TDI echocardiography and edit manuscript. Barbara Huisamen and Christo Muller review and edit the manuscript, while Johan acquired funding.

6. Funding: This research was funded by was funded in part by the National Research Foundation (NRF) Thuthuka Programme, grant number UID 107261 and South Africa Medical Research Council's Biomedical Research and Innovation Platform for baseline funding.

7. Acknowledgments: We would like to acknowledge Biomedical and Research Innovation technical staff.

8. Conflicts of Interest: The authors declare no conflict of interest. Authors declare that the funders did not have any role in the design of the study; in the collection, analyses or interpretation of data; in the writing of the manuscript, or in the decision to publish the results must be declared in this section.

9. Abbreviations

PPARα	Peroxisome proliferator alpha
IR	Insulin resistance
NAFLD	non-alcoholic fatty liver disease
$Lepr^{db/db}$	Leptin receptor-deficient diabetic
$Lepr^{db/+}$	Leptin receptor-deficient control
SREBP-1c	Sterol regulatory element binding protein 1c
ChREBP	Carbohydrate responsive element-binding protein
CPT1A	Carnitine palmitoyl transferasE
FBG	Fasting Blood Glucose
T2DM	Type 2 diabetes mellitus
FFA	Free fatty acid
FASN	Fatty acid synthase
SCD	Sterol-CoA Desaturase
HMGCR	Hydroxy-3-Methylglutaryl-CoA Reductase
HOMA-IR	Homeostasis Model of Assessment
EF	Ejection Fraction
β-Oxidation	Beta-Oxidation
CVD	Cardiovascular Disease
LDL	Low-density lipoprotein
HDL	High-density lipoprotein
ALT	Alanine aminotransferase
AST	Aspartate aminotransferase
QRT-PCR	Quantitative Real-Time polymerase chain reaction analysis

References

1. WHO. Cardiovascular diseases *World Health Organization Fact Sheet* **2018**.
2. CDC. *Global health-south africa fact sheet*; 9 April 2018, 2018.
3. WHO. Obesity and overweight. *World Health Organization Fact Sheet* **2018**
4. Vella, C.A.; Burgos, X.; Ellis, C.J.; Zubia, R.Y.; Ontiveros, D.; Reyes, H.; Lozano, C. Associations of insulin resistance with cardiovascular risk factors and inflammatory cytokines in normal-weight hispanic women. *Diabetes care* **2013**, *36*, 1377-1383.
5. Kitade, H.; Chen, G.; Ni, Y.; Ota, T. Nonalcoholic fatty liver disease and insulin resistance: New insights and potential new treatments. *Nutrients* **2017**, *9*.
6. Marchesini, G.; Brizi, M.; Morselli-Labate, A.M.; Bianchi, G.; Bugianesi, E.; McCullough, A.J.; Forlani, G.; Melchionda, N. Association of nonalcoholic fatty liver disease with insulin resistance. *Am J Med* **1999**, *107*, 450-455.
7. Biddinger, S.B.; Haas, J.T.; Yu, B.B.; Bezy, O.; Jing, E.; Zhang, W.; Unterman, T.G.; Carey, M.C.; Kahn, C.R. Hepatic insulin resistance directly promotes formation of cholesterol gallstones. *Nature medicine* **2008**, *14*, 778-782.
8. Porepa, L.; Ray, J.G.; Sanchez-Romeu, P.; Booth, G.L. Newly diagnosed diabetes mellitus as a risk factor for serious liver disease. *CMAJ : Canadian Medical Association journal = journal de l'Association medicale canadienne* **2010**, *182*, E526-531.
9. Ota, T.; Takamura, T.; Kurita, S.; Matsuzawa, N.; Kita, Y.; Uno, M.; Akahori, H.; Misu, H.; Sakurai, M.; Zen, Y., *et al.* Insulin resistance accelerates a dietary rat model of nonalcoholic steatohepatitis. *Gastroenterology* **2007**, *132*, 282-293.
10. Gruben, N.; Shiri-Sverdlov, R.; Koonen, D.P.; Hofker, M.H. Nonalcoholic fatty liver disease: A main driver of insulin resistance or a dangerous liaison? *Biochimica et biophysica acta* **2014**, *1842*, 2329-2343.
11. Dentin, R.; Benhamed, F.; Hainault, I.; Fauveau, V.; Foufelle, F.; Dyck, J.R.; Girard, J.; Postic, C. Liver-specific inhibition of chrebp improves hepatic steatosis and insulin resistance in ob/ob mice. *Diabetes* **2006**, *55*, 2159-2170.
12. Perla, F.M.; Prelati, M.; Lavorato, M.; Visicchio, D.; Anania, C. The role of lipid and lipoprotein metabolism in non-alcoholic fatty liver disease. *Children (Basel, Switzerland)* **2017**, *4*.
13. Liang, W.; Menke, A.L.; Driessen, A.; Koek, G.H.; Lindeman, J.H.; Stoop, R.; Havekes, L.M.; Kleemann, R.; van den Hoek, A.M. Establishment of a general nafld scoring system for rodent models and comparison to human liver pathology. *PloS one* **2014**, *9*, e115922.
14. Ahima, R.S. Insulin resistance: Cause or consequence of nonalcoholic steatohepatitis? *Gastroenterology* **2007**, *132*, 444-446.
15. Ibdah, J.A.; Perlegas, P.; Zhao, Y.; Angdisen, J.; Borgerink, H.; Shadoan, M.K.; Wagner, J.D.; Matern, D.; Rinaldo, P.; Cline, J.M. Mice heterozygous for a defect in mitochondrial trifunctional protein develop hepatic steatosis and insulin resistance. *Gastroenterology* **2005**, *128*, 1381-1390.
16. Sorbi, D.; Boynton, J.; Lindor, K.D. The ratio of aspartate aminotransferase to alanine aminotransferase: Potential value in differentiating nonalcoholic steatohepatitis from alcoholic liver disease. *The American journal of gastroenterology* **1999**, *94*, 1018-1022.
17. Toth, P.P.; Raghavan, V.A. Glucolipotoxicity and the heart. *Heart failure clinics* **2012**, *8*, xvii-xviii.
18. Gaudio, E.; Nobili, V.; Franchitto, A.; Onori, P.; Carpino, G. Nonalcoholic fatty liver disease and atherosclerosis. *Internal and emergency medicine* **2012**, *7 Suppl 3*, S297-305.
19. Valbusa, F.; Agnoletti, D.; Scala, L.; Grillo, C.; Arduini, P.; Bonapace, S.; Calabria, S.; Scaturro, G.; Mantovani, A.; Zoppini, G., *et al.* Non-alcoholic fatty liver disease and increased risk of all-cause mortality in elderly patients admitted for acute heart failure. *International journal of cardiology* **2018**, *265*, 162-168.

20. Anstee, Q.M.; Mantovani, A.; Tilg, H.; Targher, G. Risk of cardiomyopathy and cardiac arrhythmias in patients with nonalcoholic fatty liver disease. *Nature reviews. Gastroenterology & hepatology* **2018**, *15*, 425-439.
21. Chung, G.E.; Lee, J.H.; Lee, H.; Kim, M.K.; Yim, J.Y.; Choi, S.Y.; Kim, Y.J.; Yoon, J.H.; Kim, D. Nonalcoholic fatty liver disease and advanced fibrosis are associated with left ventricular diastolic dysfunction. *Atherosclerosis* **2018**, *272*, 137-144.
22. Takahashi, T.; Watanabe, T.; Shishido, T.; Watanabe, K.; Sugai, T.; Toshima, T.; Kinoshita, D.; Yokoyama, M.; Tamura, H.; Nishiyama, S., *et al.* The impact of non-alcoholic fatty liver disease fibrosis score on cardiac prognosis in patients with chronic heart failure. *Heart and vessels* **2018**, *33*, 733-739.
23. Dludla, P.V.; Essop, M.F.; Gabuza, K.B.; Muller, C.J.F.; Louw, J.; Johnson, R. Age-dependent development of left ventricular wall thickness in type 2 diabetic (db/db) mice is associated with elevated low-density lipoprotein and triglyceride serum levels. *Heart and vessels* **2017**, *32*, 1025-1031.
24. Kobayashi, K.; Forte, T.M.; Taniguchi, S.; Ishida, B.Y.; Oka, K.; Chan, L. The db/db mouse, a model for diabetic dyslipidemia: Molecular characterization and effects of western diet feeding. *Metabolism: clinical and experimental* **2000**, *49*, 22-31.
25. Pedersen, T.M.; Boardman, N.T.; Hafstad, A.D.; Aasum, E. Isolated perfused working hearts provide valuable additional information during phenotypic assessment of the diabetic mouse heart. *PloS one* **2018**, *13*, e0204843.
26. Faita, F.; Di Lascio, N.; Rossi, C.; Kusmic, C.; Solini, A. Ultrasonographic characterization of the db/db mouse: An animal model of metabolic abnormalities. *Journal of diabetes research* **2018**, *2018*, 4561309.
27. Liu, Q.; Li, X.; Li, C.; Zheng, Y.; Wang, F.; Li, H.; Peng, G. 1-deoxynojirimycin alleviates liver injury and improves hepatic glucose metabolism in db/db mice. *Molecules (Basel, Switzerland)* **2016**, *21*, 279.
28. Trak-Smayra, V.; Paradis, V.; Massart, J.; Nasser, S.; Jebara, V.; Fromenty, B. Pathology of the liver in obese and diabetic ob/ob and db/db mice fed a standard or high-calorie diet. *International journal of experimental pathology* **2011**, *92*, 413-421.
29. Prokopowicz, Z.; Malecka-Tendera, E.; Matusik, P. Predictive value of adiposity level, metabolic syndrome, and insulin resistance for the risk of nonalcoholic fatty liver disease diagnosis in obese children. *Canadian journal of gastroenterology & hepatology* **2018**, *2018*, 9465784.
30. Samuel, V.T.; Petersen, K.F.; Shulman, G.I. Lipid-induced insulin resistance: Unravelling the mechanism. *Lancet (London, England)* **2010**, *375*, 2267-2277.
31. Suresh, S.; Rajanbabu, B.; Veetil, V.M.; Hussain, A.; Veetil, J.N. A study on the altered glycemic and lipid parameters and prevalence of insulin resistance in nonalcoholic fatty liver disease. *Journal of family medicine and primary care* **2018**, *7*, 93-97.
32. Botros, M.; Sikaris, K.A. The de ritis ratio: The test of time. *The Clinical biochemist. Reviews* **2013**, *34*, 117-130.
33. Sattar, N.; Forrest, E.; Preiss, D. Non-alcoholic fatty liver disease. *BMJ (Clinical research ed.)* **2014**, *349*, g4596.
34. Mofrad, P.S.; Sanyal, A.J. Nonalcoholic fatty liver disease. *MedGenMed : Medscape general medicine* **2003**, *5*, 14.
35. Kleiner, D.E.; Makhlouf, H.R. Histology of nonalcoholic fatty liver disease and nonalcoholic steatohepatitis in adults and children. *Clinics in liver disease* **2016**, *20*, 293-312.
36. Birkenfeld, A.L.; Shulman, G.I. Nonalcoholic fatty liver disease, hepatic insulin resistance, and type 2 diabetes. *Hepatology (Baltimore, Md.)* **2014**, *59*, 713-723.

37. Teng, Y.; Li, D.; Guruvaiah, P.; Xu, N.; Xie, Z. Dietary supplement of large yellow tea ameliorates metabolic syndrome and attenuates hepatic steatosis in db/db mice. *Nutrients* **2018**, *10*.
38. Sharma, B.R.; Kim, H.J.; Rhyu, D.Y. Caulerpa lentillifera extract ameliorates insulin resistance and regulates glucose metabolism in c57bl/ksj-db/db mice via pi3k/akt signaling pathway in myocytes. *Journal of translational medicine* **2015**, *13*, 62.
39. Zheng, T.; Yang, X.; Wu, D.; Xing, S.; Bian, F.; Li, W.; Chi, J.; Bai, X.; Wu, G.; Chen, X., *et al.* Salidroside ameliorates insulin resistance through activation of a mitochondria-associated ampk/pi3k/akt/gsk3beta pathway. *British journal of pharmacology* **2015**, *172*, 3284-3301.
40. Johnson, R.; Beer, D.; Dludla, P.V.; Ferreira, D.; Muller, C.J.F.; Joubert, E. Aspalathin from rooibos (aspalathus linearis): A bioactive c-glucosyl dihydrochalcone with potential to target the metabolic syndrome. *Planta medica* **2018**, *84*, 568-583.